THE UNIVERSITY OF MICHIGAN
INDUSTRY PROGRAM OF THE COLLEGE OF ENGINEERING

Ultrasonic Field Effects on the Rate of Evaporation of Liquid Droplets at Their Terminal Velocity

William Mirsky

This dissertation was submitted in partial fulfillment of the requirements for the degree of Doctor of Philosophy in the University of Michigan.

May, 1956

IP-162

ACKNOWLEDGEMENT

We wish to express our appreciation to the author for permission to distribute this thesis under the Industry Program of the College of Engineering.

TABLE OF CONTENTS

LIST OF TABLES

LIST OF TABLES (cont.)

LIST OF FIGURES

LIST OF FIGURES (cont.)

LIST OF FIGURES (cont.)

LIST OF FIGURES (cont.)

NOMENCLATURE

$\mathscr{D}$ diffusion coefficient,

$\mathscr{m}$ molecular weight,

$\mathscr{R}$ gas constant.

A surface area of drop,

A_r surface area of sphere having radius r,

B transfer number due to Spalding,[31]

C constant,

$C = 2/f\ (Pr)^{1/3}\ (v/\nu)^{1/2}$,

C_D drag coefficient,

D diameter of drop,

D_f diameter of outer surface of equivalent thermal boundary layer,

D'_f diameter of outer surface of effective thermal boundary layer,

D_o initial drop diameter,

D_r diameter of sphere having radius r,

F factor in Equation (1.16) due to Kinzer and Gunn,[17]

$K = (z - y)/(y - x)$,

$K_{1,2}$ constants,

L latent heat of liquid drop,

M mass of drop,

T temperature,

T temperature of drop surface,

T_f temperature at outer surface of thermal boundary layers,

T_r temperature at surface of sphere having radius r,

V volume of drop,

X constant.

a general exponent,

b general exponent,

c general exponent,

c specific heat at constant pressure,

$f = 3 \sin \theta / 2Cf_1$,

f_1 proportionality factor,

f' wind factor due to Frössling,[5]

g gravitational acceleration,

h film heat-transfer coefficient,

i heating current required to maintain a constant hot-wire temperature,

i_o heating current required to maintain hot-wire temperature at zero velocity,

k thermal conductivity,

n exponent in evaporation equation,

n' measured values of n,

p pressure,

p_v vapor pressure,

q heat-transfer rate,

r radius of drop,

r_f radius to outer surface of equivalent thermal boundary layer,

r_o initial drop radius,

r_r radius of sphere,

t time,

t_t total time of evaporation,

t_t' arbitrary time such that $t_t' > t_t$,

v relative air velocity of free stream,

v_1 relative air velocity at outer surface of dynamic boundary layer,

$x = (t_t' - t_x)$
$y = (t_t' - t_y)$ see Figure 3
$z = (t_t' - t_z)$

$$\alpha = \frac{L}{c\,(T_f - T)} \ln \left[1 + \frac{c\,(T_f - T)}{L}\right],$$

$$\beta = -\frac{\pi k}{c} \ln \left[1 + \frac{c\,(T_f - T)}{L}\right],$$

δ thickness of dynamic boundary layer,

δ_t thickness of equivalent thermal boundary layer,

δ_t' thickness of effective thermal boundary layer,

θ angle measured from forward stagnation point,

λ evaporation constant,

μ absolute viscosity,

μ microns,

ν kinematic viscosity,

$\pi = 3.14159\ldots$,

ρ density of liquid drop,

ψ functional relationship,

$Nu = hD/k$, Nusselt number,

$Pr = c\mu/k$, Prandtl number

$Re = Dv/\nu$, Reynolds number,

$Sc = \nu/\mathcal{D}$, Schmidt number.

Subscripts

a air,

s drop surface,

v vapor.

INTRODUCTION

Interest in the evaporation and combustion processes of liquid fuel drops has increased considerably in recent years, due principally to the demands for increasing jet-engine performance. As a direct result numerous studies have been conducted in this country and abroad to investigate the combustion and associated evaporation processes of liquid drops under a variety of conditions. Because of the extremely complex nature of these processes as they exist in a burning-fuel spray, most investigators chose to study either the burning or evaporation process associated with a single isolated drop. Of these, some suspended drops from fine filaments and photographed the stationary drops as they evaporated or burned,[5,8,10,18,26] while others employed pseudo-drops such as flooded hollow spheres[30,31] and flooded porous spheres.[14,15] Still others studied drops falling at their terminal velocity[17,28,32] or injected at various velocities into hot furnace atmospheres.[13,29] Relatively few have investigated the evaporation or combustion processes in a spray.[1,4]

For a thorough study of drop evaporation or combustion, one should consider the effects of the fluid flow pattern around the drop at both the laminar and turbulent boundary layer regions; the internal liquid circulation within the drop and its effects on the boundary layer, drag, and internal heat transfer; conductive, convective, and radiant heat transfer between the drop and its surroundings; and, finally, the

effects of conductive and convective mass transfer of the liquid vapor, air, and products of combustion on the heat transfer process. Even for the seemingly relatively simple case of a spherical drop evaporating into an air stream having uniform motion, an exact solution to the analytical problem appears to be impossible at this time.

When initiating the present program of investigation, the evaporation of a single isolated drop in a moving-air stream was selected as the first step in the study of the more complicated processes involved in a burning-fuel spray. This selection was based on the opinion that combustion is essentially a high temperature evaporation process and that the evaporation study would permit the use of a simpler experimental procedure for investigating some aspects of the heat and mass transfer processes. In addition, better control of many of the variables affecting the process could be realized with the single-isolated evaporating drop.

The selection of the technique for conducting the experimental part of the study was based on the following considerations:

a. Actual drops would be preferred to pseudo drops, such as flooded-cork balls or hollow spheres, to approximate more closely the true nature of the process, to eliminate possible additional variables, to preserve the internal liquid circulation within the drop, and to obtain data for drops in the size range well below 1,000 microns.

b. Filament suspensions should not be used if possible because they distort the drop shape, the air flow pattern around the drop, and the internal liquid circulation within the drop; the actual effect of their presence on the heat

transfer processes would be difficult to predict accurately, especially if the flow pattern behind the drop were in the form of a turbulent wake; they would limit the minimum drop size to about 300 microns at best.

c. The investigation should consider the effect of relative air velocity on the evaporation rate, by studying either drops falling freely at their terminal velocity or drops suspended on filaments in moving-air streams of various constant velocities. The former would be more suitable than a possible third case of drops moving freely along some ballistic curve, as when thrown upward from a drop-generating device, for in this case the relationship between drop diameter and relative air velocity would be difficult to predict.

d. The ability to obtain continuous photographic records of relatively high magnification would be desirable, especially for freely-falling drops. In addition to supplying drop-size data, it would provide a means for detecting variations in drop shape during free fall and, possibly, the flow configuration around the drop.

As a result of these considerations, it was decided that an attempt should be made to devise a method by which a drop could be supported at a fixed position in space by means of air drag and other forces. The drop would then be at its terminal velocity with respect to the air stream and, in addition, would be fixed in space relative to the observer. This scheme would offer many obvious advantages with regard to data taking, length of equipment required, and time available for drop evaporation.

After several efforts, a method was devised by which drops actually could be maintained at a fixed position in space by means of air drag and ultrasonic forces. The development of this technique was primarily the work of Dr. John L. Wighton who, as a graduate student at the University of Michigan, worked with the author on the problem of obtaining "freely" suspended drops. Needless to say, the apparatus appeared extremely promising.

However, an inspection of the results obtained with this apparatus soon indicated that the effect of the ultrasonic field on the evaporation process could not be neglected and in some cases would actually be quite appreciable. Therefore, it became necessary to investigate the nature of this effect and to obtain quantitative data for all conditions that might arise in subsequent studies. The investigation was also intended to disclose methods for improving the technique by decreasing the ultrasonic effect, even though it was felt that in some applications the effect might actually be desirable.

It is this investigation that forms the basis for this dissertation.

The experimental investigation was carried out in four parts. These are:

1. The study of the evaporation of drops in the absence of an ultrasonic field while suspended on filaments in a moving air stream. These tests are similar to those made by Frössling[5] and others but were repeated as a check on the author's apparatus.

2. The determination of the effect of ultrasonic intensity on evaporation.

3. The determination of the effects on evaporation produced by ultrasonic fields of various frequencies.

4. The determination of the resultant effect by the ultrasonic field on the evaporation process for freely-suspended drops at their terminal velocity.

Cumene was used for the greater part of this study because of its suitable rate of evaporation and relatively low cost for the pure grade of liquid used (99 mole percent). Its evaporation rate was slow enough to permit good control of drop position by manual control of the relative air velocity and yet fast enough to avoid excessively long test runs.

CHAPTER I

BRIEF SUMMARY OF PREVIOUS WORKS ON DROP EVAPORATION

The problem of drop evaporation has been and is still being considered by many research workers from both the theoretical and experimental points of view. Their interest arises through several fields of application. It appears that the earlier workers were primarily interested in the meteorological aspects. Later, the process was used as an experimental method for finding values of diffusion coefficients. More recently, the problem has gained considerable interest because of its importance in the drying and evaporation processes of the chemical industries and in the combustion processes involved in diesel and turbo-jet engines.

The theoretical investigations are based on one of two similar processes, either that of mass transfer or heat transfer. In general, both analyses give similar results.

A. Previous Works

In 1918 Langmuir,[20] using the result he obtained from an investigation of heat transfer from small wires, derived the following expression for drops in still air,

$$-\frac{dM}{dt} = \frac{4\pi r \mathscr{D} p_v \mathcal{M}}{RT} = Cr \,, \qquad (1.1)$$

showing mass rate of evaporation to be proportional to drop radius.

Frössling[5] extended the theoretical and experimental investigations to include the effects of relative air velocity on the evaporation process. To account for the increased evaporation due to the velocity, the expression obtained by Langmuir was modified by a factor f' which Frössling called the "wind factor,"

$$-\frac{dM}{dt} = \frac{4\pi r \mathcal{D} \mathcal{M} p_v}{RT} f' \quad . \tag{1.2}$$

A theoretical analysis showed f' to be a function of the Schmidt number times Reynolds number raised to the one-half power, i.e.,

$$f' = \psi\,(Sc)(Re)^{1/2} \quad . \tag{1.3}$$

However, for Re = 0, it was obvious that Equation (1.2) must reduce to Equation (1.1) so that f' was given the form,

$$f' = 1 + \psi\,(Sc)(Re)^{1/2} \quad . \tag{1.4}$$

Using his experimental results obtained with 0.1 to 0.9 mm diameter drops suspended on fine glass filaments and thermocouples in a moving air stream at velocities from 0.2 to 7 meters/second, Frössling obtained the final form for the wind factor,

$$f' = 1 + 0.276\,(Sc)^{1/3}\,(Re)^{1/2} \quad , \tag{1.5}$$

giving the evaporation equation,

$$-\frac{dM}{dt} = \frac{4\pi r \mathcal{D} \mathcal{M} p_v}{RT}\,(1 + 0.276\,Sc^{1/3}\,Re^{1/2}) \quad . \tag{1.6}$$

Ranz and Marshall[26] performed similar experiments on suspended liquid drops having a range of diameters from 0.06 to 0.11 cm and at Reynolds numbers from 0-200. Variations in air temperature from 0-200°C was introduced as an additional variable.

The correlation of data was based entirely on Frössling's result by assuming

$$Nu = 2 + C\ Pr^{a}\ Re^{b} \tag{1.7}$$

for the heat-transfer process. This result was obtained directly from Frössling's equation for Nusselt's number for mass transfer,

$$Nu = 2 + 0.552\ Sc^{1/3}\ Re^{1/2}\ , \tag{1.8}$$

by simply replacing the Schmidt number with the Prandtl number.

The experimental data obtained by Ranz and Marshall was found to be correlated by the expression

$$Nu = 2 + 0.60\ Pr^{1/3}\ Re^{1/2}\ . \tag{1.9}$$

It is evident that the result agrees very well with that obtained by Frössling.

Godsave[7,8,9] and Kobayasi[19] studied the burning rates of stationary liquid-fuel drops. Godsave carried out his experiments at room temperature while Kobayasi did the greater part of his work at elevated furnace temperatures. Both investigators arrived at the same conclusion that the change of drop diameter can be expressed by the relationship,

$$D^2 = D_o^2 - \lambda t\ , \tag{1.10}$$

where, according to Godsave,

$$\lambda = \frac{8k}{\rho c}\left(\frac{Df}{D_f - D}\right) \ln\left[1 + \frac{c\ (Tf - T)}{L}\right]\ . \tag{1.11}$$

Ingebo[14] and Spalding[30,31] used a somewhat different experimental approach to the problem in that they used artificial or pseudo-drops rather than actual liquid drops.

Ingebo carried out evaporation tests with stationary flooded cork spheres, approximately 0.69 cm in diameter. Nine liquids having a range of latent heats from 50 to 500 gram-calories per gram were tested in air from 30 to 500°C. Reynolds number ranged from 1600 to 5700. From an assumed correlation having the form

$$Nu = \psi \left(\frac{k_a}{k_v}\right)^a (Re)^b (Sc)^c , \qquad (1.12)$$

where

k_a = thermal conductivity of air,

k_v = thermal conductivity of vapor,

Ingebo obtained the expression,

$$Nu = \left(\frac{k_a}{k_v}\right)^{0.5} [2 + 0.303 (Re\ Sc)^{0.6}] . \qquad (1.13)$$

In a later study of the pressure effects on vaporization Ingebo[15] modified the above result and obtained the following expression for the Nusselt number,

$$Nu = 2 + 2.58 \times 10^6 \left(Re\ Sc \frac{gl}{\bar{c}^2}\right)^{0.6} \left(\frac{k_a}{k_v}\right)^{0.5} \qquad (1.14)$$

where

g = gravitational acceleration,

l = mean-free-molecular path of air,

$\bar{c}$ = root-mean-square molecular velocity of air.

Spalding performed his combustion tests with stationary, flooded, hollow metal spheres ranging from 1/2 to 1-1/2 inches in diameter. Fuel was made to pass up through the hollow sphere and spill out over its outside surface through a hole at the top. Any excess fuel that did not burn was collected by a trough at the base of the sphere.

For a sphere evaporating into a stagnant medium, Spalding gives the result in terms of a dimensionless factor B which he names the transfer number. The result is,

$$\dot{m}D\,\frac{c}{k} = 2\ln(1+B)\,, \tag{1.15}$$

where

$\dot{m}$ = mass rate of evaporation per unit area,

$B = (h_\infty - h_s)/L$,

h_∞ = enthalpy of the surrounding air,

h_s = enthalpy of the vapor at the drop surface.

Kinzer and Gunn[17] measured the evaporation rates of freely-suspended water drops by three different techniques: freely-falling electrified drops, drops floated in a tapered tube, and drops supported by a vertical air flow. They were thus able to cover the wide range of drop sizes from 0.0016 to 0.42 cm. The result of their theoretical and experimental study is given by,

$$\frac{dM}{dt} = -2\pi kD\,\frac{T_f - T}{L}\,[1 + 0.24F\,Re^{1/2}]\,, \tag{1.16}$$

where F is an experimentally-determined factor. The values obtained for F were found to be dependent upon the Reynolds number, indicating that the evaporation rate is not a linear function of $Re^{1/2}$ as found by Frössling. See Equation (1.6).

CHAPTER II

ANALYSIS OF THE DROP-EVAPORATION PROCESS

The precise analytical solution to any heat-transfer problem in which there is fluid flow around a bluff body becomes very difficult because of the nature of the flow pattern around the body and its effects on the heat-transfer processes. When mass transfer is also present, as in the case of an evaporating drop, the problem becomes even more complicated. To alleviate the predicament with which the engineer is faced in trying to gain some usable information about this type of process, use is made of an experimentally-determined heat-transfer factor which is used to correlate experimental data obtained for cases that are similar to one another, thus eliminating the need for a critical examination of the processes involved.

For the case of an evaporating drop in a moving air stream, the experimental heat-transfer data is well correlated by the Nusselt number as modified by mass transfer and expressed in terms of the Reynolds and Prandtl numbers. This forms the basis for the analysis that follows.

A. Derivation of the Evaporation Equations

1. Film Concept of the Nusselt Number

An examination of the temperature profile in the laminar airflow region at the surface of an evaporating drop would show that the total change in temperature is confined to a thin thermal-boundary layer or film of thickness δ_t. For the solution of heat transfer problems the

conventional procedure is to replace the actual thermal boundary layer with an "effective" layer of thickness δ_t' in which the temperature gradient is assumed to be constant and equal to the gradient at the drop surface in the actual film.[3] Heat transfer can then be assumed to take place through the effective film by conduction alone under the driving action of the constant-temperature gradient.

By equating the heat transfer to the drop given in terms of the heat-transfer coefficient for convection h,

$$q = hA\,(T_f - T)\,, \tag{2.1}$$

to that given in terms of the effective thermal boundary-layer thickness, δ_t',

$$q = kA\left(\frac{dT_r}{dr_r}\right)_s = kA\,\frac{T_f - T}{\delta_t'}\,, \tag{2.2}$$

where heat transferred to the drop is taken as positive, we obtain the result that

$$h = \frac{k}{\delta_t'}\,. \tag{2.3}$$

Since the Nusselt number is defined as

$$Nu = \frac{hD}{k}\,, \tag{2.4}$$

it becomes equal to

$$Nu = \frac{D}{\delta_t'} \tag{2.5}$$

in terms of the effective thermal boundary-layer thickness. It is apparent that the Nusselt number defined in this manner gives the ratio between a characteristic length of the system, in this case the drop diameter, and the effective thermal boundary-layer thickness.

The presence of mass transfer in the boundary layer changes the temperature profile near the drop surface and, therefore, the temperature

gradient at the surface. This causes a change in the thickness of the effective boundary layer and thereby affects the Nusselt number. The Nusselt number is then said to be modified by the mass-transfer rate.

2. Mass Rate of Evaporation Expressed in Terms of the Nusselt Number

The heat transferred through the surface of a drop is used as latent heat to evaporate the liquid at the surface temperature and as sensible heat to raise the liquid temperature from the inner drop temperature to the surface temperature. If we let L be equal to the latent plus sensible heats for the liquid drop, the heat balance at the drop surface can be written as,

$$q = -L\frac{dM}{dt} = kA\left(\frac{dT_r}{dr_r}\right)_s = k\pi D^2\left(\frac{dT_r}{dr_r}\right)_s \qquad (2.6)$$

where M is the mass of the drop. By introducing the film concept of the Nusselt number as given by (2.5), the above expression becomes,

$$-L\frac{dM}{dt} = k\pi D\frac{D}{\delta_t'}(T_f - T)\,, \qquad (2.7)$$

or

$$\frac{dM}{dt} = -k\pi D\,(Nu)\frac{T_f - T}{L}\,. \qquad (2.8)$$

3. Mass Rate of Evaporation Based on Heat Transfer through the Thermal Boundary Layer

For the case of a drop evaporating into a moving-air stream the isothermal surfaces surrounding the drop certainly do not form concentric spheres except for those that are extremely close to the drop. At the outer edge of the thermal boundary film there is an isothermal surface whose temperature is very close to that of the surrounding air stream.

For the analysis that follows it is assumed that this outer isothermal surface can be replaced by an "equivalent" spherical one at the same temperature, concentric with the drop, and having radius r_f. The temperature gradient at this surface is assumed equal to the average value for the original surface and the radius r_f chosen to given an equal area. In this manner the same rate of total heat transfer to the interior as provided by the original non-spherical surface is maintained.

Consider an intermediate sphere of radius r_r, where $r_f > r_r > r$, concentric with the drop. The heat balance across the surface of this sphere is given by

$$- [L + c\ (T_r - T)] \frac{dM}{dt} = kA_r \left(\frac{dT_r}{dr_r}\right)_{r_r} \qquad (2.9)$$

where c is the specific heat at constant pressure for the vapor. Substituting for the spherical area, separating variables, and writing the equation in integral form between the proper limits, we get,

$$\frac{dM}{dt} \int_r^{r_f} \frac{dr_r}{r_r^2} = - \frac{4\pi k}{c} \int_T^{T_f} \frac{c\,dT_r}{[L + c\ (T_r - T)]} \qquad (2.10)$$

When integrated, this becomes,

$$\frac{dM}{dt} \left(\frac{1}{r} - \frac{1}{r_f}\right) = - \frac{4\pi k}{c} \ln \left[1 + \frac{c\ (T_f - T)}{L}\right] \qquad (2.11)$$

or

$$\frac{dM}{dt} = - \frac{4\pi k}{c} \left(\frac{r\ r_f}{r_f - r}\right) \ln \left[1 + \frac{c\ (T_f - T)}{L}\right] . \qquad (2.12)$$

In this equation r_f is the radius to the outer edge of the equivalent thermal boundary layer of thickness δ_t, where the film temperature

first becomes essentially equal to that of the ambient air stream. In terms of diameters, the above equation becomes,

$$\frac{dM}{dt} = -\frac{\pi k D}{c}\left(\frac{2}{1 - D/D_f}\right) \ln\left[1 + \frac{c\,(T_f - T)}{L}\right] \qquad (2.13)$$

where D/D_f is the ratio between the diameters of the drop and the outer edge of the equivalent spherical thermal boundary layer.

It is interesting to note that Equation (2.11) was obtained by Godsave[8] for a single burning drop by the more complicated procedure of first solving for the temperature distribution through the thermal layer.

4. Expressions for Nu in Terms of D/D_f

Equating the two expressions (2.8) and (2.13) for the mass rate of evaporation, we get,

$$-k\pi D\,(Nu)\,\frac{(T_f - T)}{L} = -\frac{\pi k D}{c}\left(\frac{2}{1 - D/D_f}\right) \ln\left[1 + \frac{c\,(T_f - T)}{L}\right] \qquad (2.14)$$

so that the expression for Nu in the presence of evaporation is given by,

$$Nu = \frac{L}{c\,(T_f - T)}\left(\frac{2}{1 - D/D_f}\right) \ln\left[1 + \frac{c\,(T_f - T)}{L}\right]. \qquad (2.15)$$

From an inspection of Equations (2.8) and (2.15) it is apparent that for given temperatures and liquid, the evaporation will affect Nusselt's number through the factor D/D_f.

A first-order approximation of Equation (2.15) is obtained by expanding the ln term according to the following rule:

$$\ln(1 + X) = \left[X - \frac{X^2}{2} + \frac{X^3}{3} - \frac{X^4}{4} + \ldots\right] \quad \text{for } (-1 < X < 1) \qquad (2.16)$$

which gives,

$$\ln \left[1 + \frac{c\,\Delta T}{L}\right] = \left[\frac{c\,\Delta T}{L} - \frac{1}{2}\left(\frac{c\,\Delta T}{L}\right)^2 + \frac{1}{3}\left(\frac{c\,\Delta T}{L}\right)^3 - \ldots\right] \quad (2.17)$$

where $\Delta T = (T_f - T)$.

Since the series converges very rapidly for the values of c, ΔT, and L encountered in low temperature evaporation, the series can be approximated to a high degree of accuracy by use of the first term alone. If this is done in Equation (2.15), we are left with

$$Nu = \left(\frac{2}{1 - D/D_f}\right) . \quad (2.18)$$

In the limiting case where Reynolds number approaches zero, the ratio D/D_f also approaches zero with the result that,

$$Nu \rightarrow 2 \quad (2.19)$$

as predicted by others.[25]

5. Evaporation Equation in Terms of Drop Diameter

If ρ and V are the density and volume of a liquid drop, the mass rate of evaporation can be written as,

$$\frac{dM}{dt} = \frac{d}{dt}(\rho V) . \quad (2.20)$$

Since $V = \pi D^3/6$,

$$\frac{dM}{dt} = \frac{\pi\rho}{6}\frac{d}{dt}(D^3) = \frac{\pi\rho}{2} D^2 \frac{d}{dt}(D) . \quad (2.21)$$

Equating this expression for mass rate of evaporation to that given by Equation (2.13), we obtain,

$$\frac{\pi\rho}{2} D^2 \frac{d}{dt}(D) = -\frac{\pi k D}{c}\left(\frac{2}{1 - D/D_f}\right) \ln\left[1 + \frac{c\,(T_f - T)}{L}\right] . \quad (2.22)$$

Separating variables and writing the resulting equation in integral form between the proper limits the equation becomes,

$$\int_{D_o}^{D} (D - \frac{D^2}{D_f})\, d\ D = -\frac{4k}{\rho c} \ln [1 + \frac{c\ (T_f - T)}{L}] \int_{o}^{t} dt \qquad (2.23)$$

which, when integrated, gives,

$$[D^2 - D_o^2] - 2 \int_{D_o}^{D} (\frac{D^2}{D_f})\, d\ D = -\frac{8k}{\rho c} \ln [1 + \frac{c\ (T_f - T)}{L}]\ t. \qquad (2.24)$$

It is obvious that for a complete solution we must know the functional dependence of D_f upon D.

If we follow the assumption made by Godsave that D/D_f is constant, the above equation can be written in the integrable form,

$$[D^2 - D_o^2] - 2\ (\frac{D}{D_f}) \int_{D_o}^{D} D d\ D = -\frac{8k}{\rho c} \ln [1 + \frac{c\ (T_f - T)}{L}]\ t \qquad (2.25)$$

which becomes after the integration,

$$(1 - \frac{D}{D_f})[D^2 - D_o^2] = -\frac{8k}{\rho c} \ln [1 + \frac{c\ (T_f - T)}{L}]\ t \qquad (2.26)$$

or

$$D^2 - D_o^2 = -\frac{8k}{\rho c} (\frac{D_f}{D_f - D}) \ln [1 + \frac{c\ (T_f - T)}{L}]\ t\ . \qquad (2.27)$$

Letting

$$\frac{8k}{\rho c} (\frac{D_f}{D_f - D}) \ln [1 + \frac{c\ (T_f - T)}{L}] = \lambda \qquad (2.28)$$

then Equations (2.27) and (2.28) are the results obtained by Godsave[8] by a different method, where he defines λ as the evaporation constant. It must be remembered that these results are based upon the assumption that D/D_f is constant throughout the evaporation process of a single

drop. However, in the next section this ratio is shown to be a function of the Reynolds and Prandtl numbers.

6. Expression for $[2/(1 - D/D_f)]$ obtained from Boundary-Layer Theory

For the theoretical dynamic boundary layer around a solid sphere in a moving air stream, Goldstein[11] gives,

$$v_1 = \frac{3}{2} v \sin \theta \tag{2.29}$$

and for the velocity distribution obtained from pressure distribution measurements at Reynolds numbers just below the critical range,

$$\frac{v_1 \delta}{\nu} = C \left(\frac{vD}{\nu}\right)^{1/2} \tag{2.30}$$

where C is a constant depending on the value of θ. The angle θ is measured between the drop radii to the forward stagnation point and any other point on the drop surface. If the first of these equations is substituted in the second, the following expression is obtained for the dynamic boundary layer,

$$\delta = \frac{2}{3} \frac{C}{\sin \theta} \left(\frac{\nu D}{v}\right)^{1/2} . \tag{2.31}$$

Eckert[3] shows for a flat plate heated over its entire length that the thermal boundary layer is related to the dynamic boundary layer by the relation

$$\frac{\delta_t}{\delta} = (Pr)^{-1/3} . \tag{2.32}$$

Assuming that the same form of expression also holds for an evaporating drop, i.e., that the ratio of equivalent thermal boundary-layer thickness to dynamic boundary-layer thickness is proportional to $(Pr)^{-1/3}$, we can write

$$\frac{\delta_t}{\delta} = f_1 (Pr)^{-1/3} \tag{2.33}$$

where f_1 is the proportionality factor. Combining Equations (2.31) and (2.33), the following expression is obtained for the equivalent thermal boundary-layer thickness,

$$\delta_t = \frac{2}{3} \frac{C}{\sin \theta} f_1 (Pr)^{-1/3} \left(\frac{vD}{v}\right)^{1/2} . \tag{2.34}$$

Substituting the above expression for δ_t in the following,

$$\frac{2}{1 - D/D_f} = \frac{2 (D + 2\delta_t)}{2\delta_t} = 2 \left[1 + \frac{D}{2\delta_t} \right] , \tag{2.35}$$

where $D_f = D + 2\delta_t$, we obtain the result

$$\frac{2}{1 - D/D_f} = 2 + f (Pr)^{1/3} (Re)^{1/2} \tag{2.36}$$

where

$$f = \frac{1}{\frac{2}{3} \frac{C}{\sin \theta} f_1} . \tag{2.37}$$

7. Evaporation Equations Based on the Results of the Boundary Layer Theory

Having obtained an expression for $[2/(1 - D/D_f)]$ in the more useful form in terms of Re, Pr, and f, we can substitute this expression in the evaporation equations which have been derived in the previous sections.

A. If we substitute for $[2/(1 - D/D_f)]$ in Equation (2.13) we get,

$$\frac{dM}{dt} = - \frac{\pi k D}{c} [2 + f (Pr)^{1/3} (Re)^{1/2}] \ln \left[1 + \frac{c (T_f - T)}{L}\right]. \tag{2.38}$$

Letting

$$-\frac{\pi k}{c} \ln \left[1 + \frac{c\,(T_f - T)}{L}\right] = \beta\,, \tag{2.39}$$

the mass rate of evaporation becomes,

$$\frac{dM}{dt} = \left[2 + f\,(Pr)^{1/3}\,(Re)^{1/2}\right] \beta D \tag{2.40}$$

so that

$2\beta D$ = evaporation rate in stagnant air,

$f\,(Pr)^{1/3}\,(Re)^{1/2}\,\beta D$ = increase in rate of evaporation due to forced convection.

B. If we substitute for $[2/(1 - D/D_f)]$ in Equation (2.15) for the Nusselt number, we obtain

$$Nu = \left[2 + f\,(Pr)^{1/3}\,(Re)^{1/2}\right] \frac{L}{c\,(T_f - T)} \ln \left[1 + \frac{c\,(T_f - T)}{L}\right]. \tag{2.41}$$

Letting

$$\frac{L}{c\,(T_f - T)} \ln \left[1 + \frac{c\,(T_f - T)}{L}\right] = \alpha, \tag{2.42}$$

the expression for Nusselt's number becomes,

$$Nu = \alpha \left[2 + f\,(Pr)^{1/3}\,(Re)^{1/2}\right]. \tag{2.43}$$

Equation (2.43) shows that Nusselt's number is a function of $(Pr)^{1/3}$, $(Re)^{1/2}$, the factor f which must be determined experimentally, and the function α of the fuel properties and temperature difference.

8. Evaporation Equation for Fixed Drops Suspended in a Constant Velocity Air Stream

The ratio D/D_f, instead of being constant as was assumed for Equation (2.25), was shown by Equation (2.36) to be a function of Re, Pr, and f. Solution of this equation for D/D_f gives,

$$\frac{D}{D_f} = \frac{D^{1/2}}{\left[D^{1/2} + \frac{2}{f\ (Pr)^{1/3} \left(\frac{V}{\nu}\right)^{1/2}}\right]} \tag{2.44}$$

For evaporation at constant air velocity, it is assumed that

$$f\ (Pr)^{1/3}\ \left(\frac{V}{\nu}\right)^{1/2} = \text{constant}, \quad \text{say } \frac{2}{C}\ , \tag{2.45}$$

so that Equation (2.44) becomes

$$\frac{D}{D_f} = \frac{D^{1/2}}{D^{1/2} + C}\ . \tag{2.46}$$

The integral in Equation (2.24) can then be written as,

$$2 \int_{D_o}^{D} \frac{D^2}{D_f}\ dD = 2 \int_{D_o}^{D} \frac{D^{3/2}}{D^{1/2} + C}\ dD\ , \tag{2.47}$$

which can be integrated by the method of substitution. Letting

$$D = y^2$$

$$dD = 2y\,dy$$

we obtain the transformed integral

$$2 \int_{D_o}^{D} \left(\frac{D^{3/2}}{D^{1/2} + C}\right) dD = 2 \int_{D_o^{1/2}}^{D^{1/2}} \left(\frac{y^3}{y + C}\right) 2y\ dy \tag{2.48}$$

where the integrand can be expanded as,

$$\frac{4y^4}{y + C} = 4\ (y^3 - Cy^2 + C^2y - C^3 + \frac{C^4}{y + C})\ . \tag{2.49}$$

Substituting in (2.48) and integrating gives,

$$2\int_{D_o}^{D}\left(\frac{D^2}{D_f}\right)dD = (D^2 - D_o^2) - \frac{4C}{3}(D^{3/2} - D_o^{3/2})$$

$$+ 2C^2(D - D_o) - 4C^3(D^{1/2} - D^{1/2}) + 4C^4 \ln\left\{\frac{D^{1/2} + C}{D_o^{1/2} + C}\right\}. \tag{2.50}$$

This result, when used in Equation (2.24), leads to the equation for drop evaporation at constant relative air velocity. It is given by

$$(D_o^{3/2} - D^{3/2}) - \frac{3}{2}C(D_o - D) + 3C^2(D_o^{1/2} - D^{1/2}) - 3C^3 \ln\left(\frac{D_o^{1/2}+C}{D^{1/2}+C}\right)$$

$$= \frac{6k}{C\rho c} \ln\left[1 + \frac{c(T_f - T)}{L}\right] t. \tag{2.51}$$

It should be recalled that the equation normally found in the literature for this type of evaporation is given by,

$$D^2 - D_o^2 = -\lambda t \tag{2.52}$$

which differs quite markedly in form from that given by (2.51).

CHAPTER III

EXPERIMENTAL RESULTS

Experimental data for evaporating drops were obtained from silhouette photographs taken with a 16-mm motion picture camera. In one series of tests the drops were suspended on a fine glass filament, approximately sixty microns in diameter, in constant velocity air streams. Tests were made at several velocities and sound field intensities. A typical sequence of frames from a test run is shown in Figure 1.

The second series of tests was made with freely-suspended drops falling at their terminal velocity with respect to the air stream. The drops were actually maintained at a fixed position in space by the combined effects of air drag and ultrasonic forces. A sequence of photographs of a free drop of n-butyl alcohol is shown in Figure 2. The greater reduction in size and lower drop-shape distortion than that obtained with drops on filaments is clearly illustrated.

A. Reduction of Data--Fixed Drops

1. Determination of Exponent n from Experimental Data

Because of the reports by many other investigators[8,12,18] on similar studies that the total time of life of an evaporating drop could be expressed in the form

$$t_t = CD_o^n , \qquad (3.1)$$

it was assumed for comparative purposes that the relationship between drop diameter and elapsed time of evaporation could be described by an equation such as,

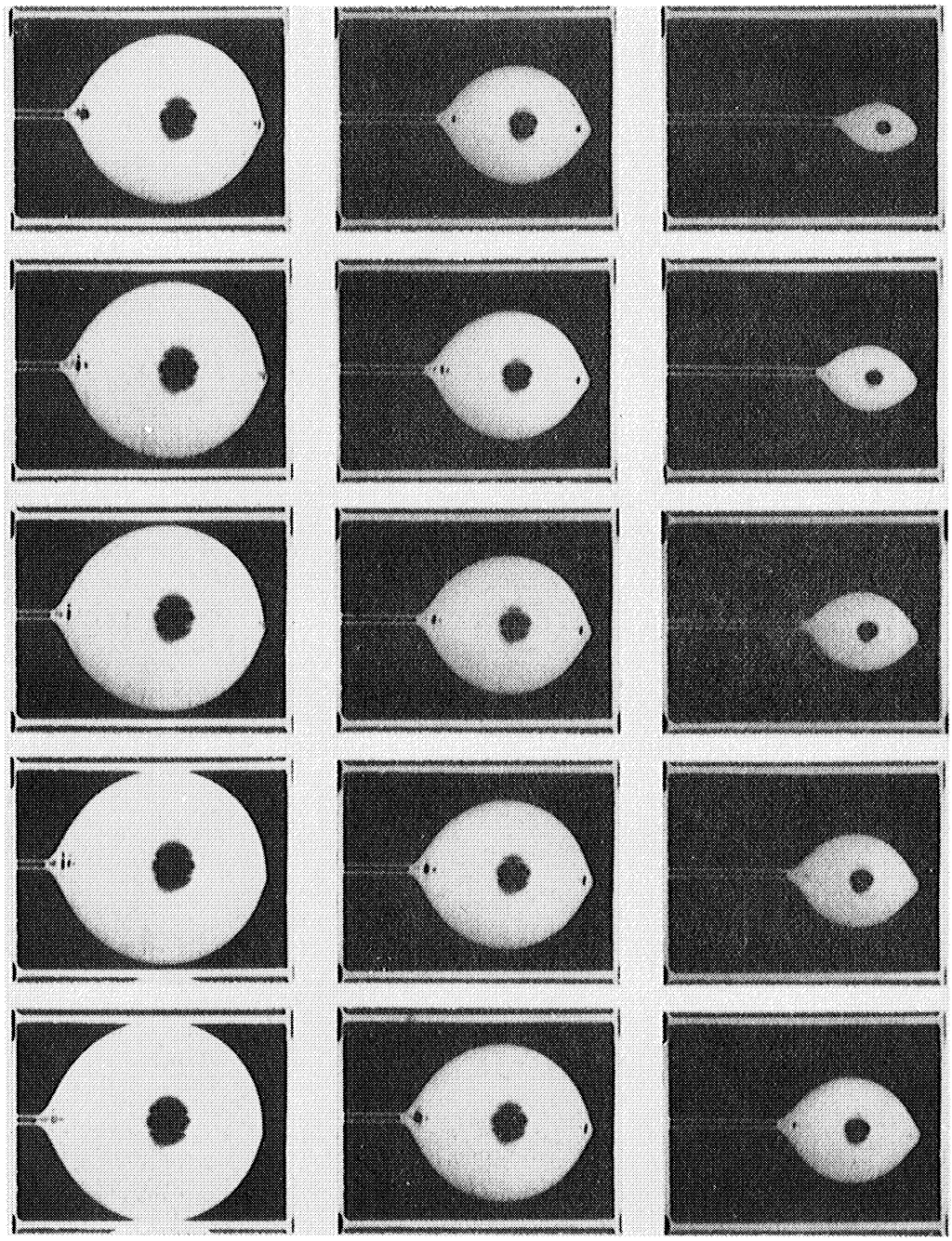

FIG. 1 SEQUENCE PHOTOGRAPHS OF A FIXED EVAPORATING DROP OF CUMENE, RUN 5-4. D_o = 1112 MICRONS.

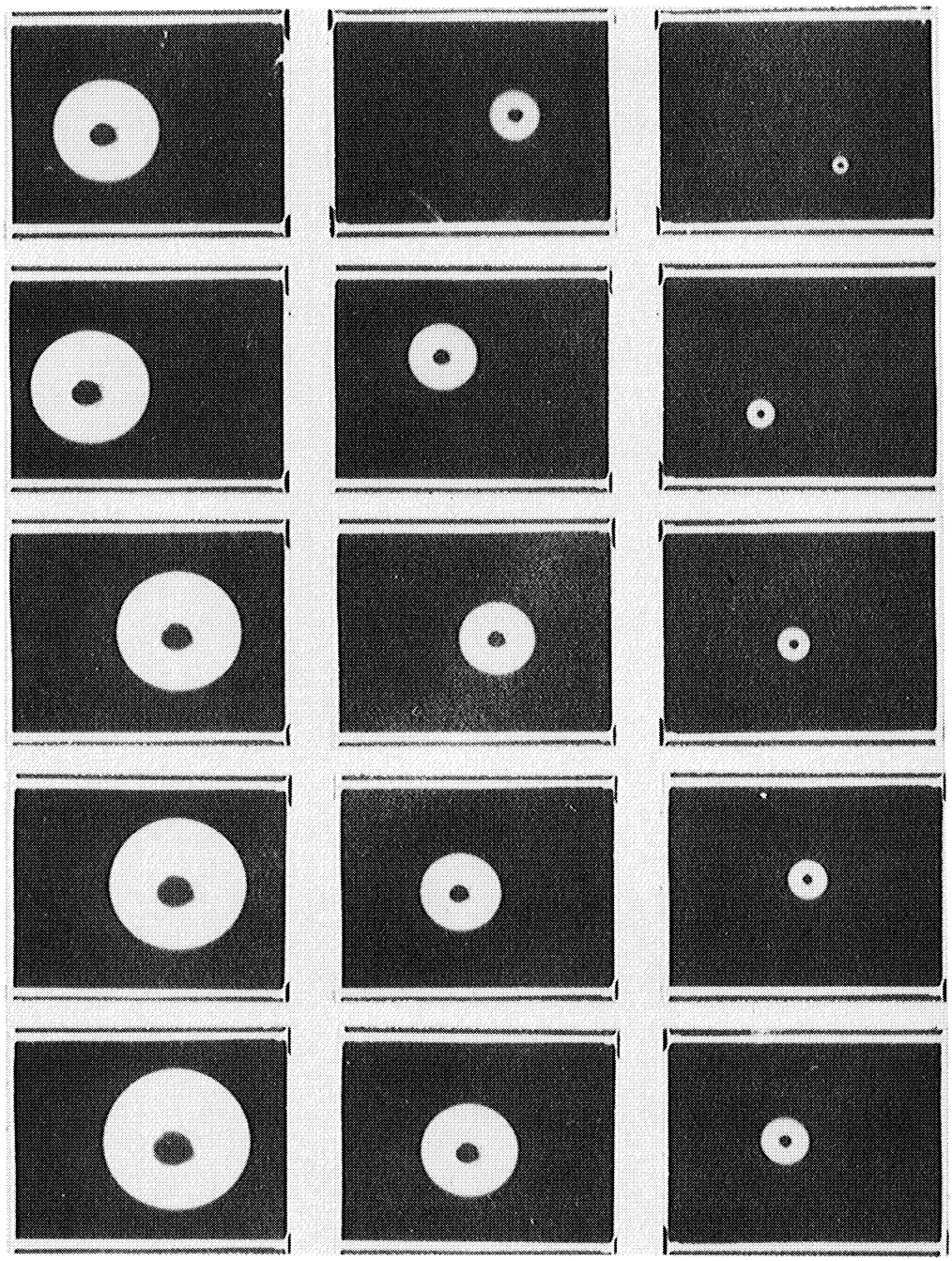

FIG. 2 SEQUENCE PHOTOGRAPHS OF A FREE EVAPORATING DROP OF n-BUTYL ALCOHOL. D_o = 1178 MICRONS.

$$D^n = D_o^n - \lambda t \qquad (3.2)$$

To determine the exponent n from the experimental data for fixed drops, drop diameters computed from measurements of magnified drop images (approx. 140X) were plotted against elapsed time of evaporation. In most cases more than ten measurements were made for each drop, and the smoothness of the resulting curves indicated that additional measurements were unnecessary. A typical curve is shown in Figure 3.

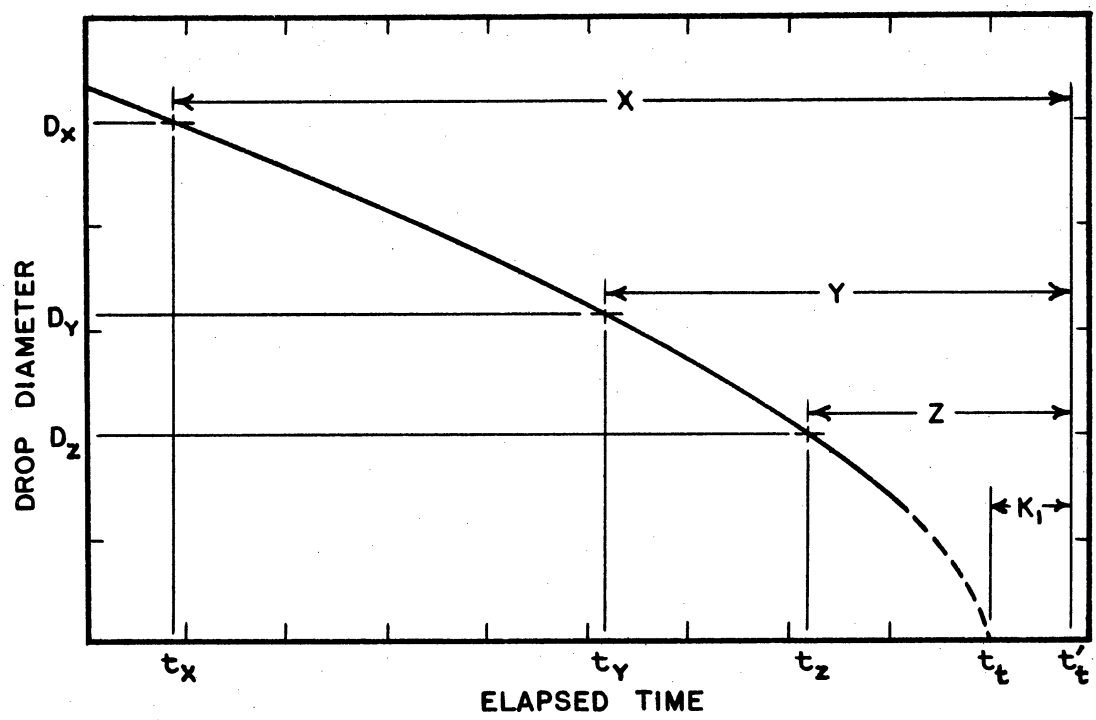

FIG. 3 EVAPORATION CURVE — SHOWING MEASUREMENTS USED FOR FINDING EXPONENT n

If the assumption given by Equation (3.2) is valid, the curves can be described equally well by the equation,

$$t'_t - t = K_1 + K_2 D^n \qquad (3.3)$$

where t'_t is some arbitrarily selected time such that $t'_t > t_t$, the total time for evaporation, and K_1 and K_2 are constants. The above equation was solved for three positions on the evaporation curve in terms of three measured quantities x, y, and z, where

$$x = t'_t - t_x ,$$

$$y = t'_t - t_y ,$$

$$z = t'_t - t_z .$$

These are illustrated graphically in Figure 3.

The complete solution is given in Appendix A and shows that if the diameters D_x, D_y, and D_z are selected so that

$$\frac{D_z}{D_x} = \left(\frac{D_y}{D_x}\right)^2 , \tag{3.4}$$

the exponent n will be given by the simple expression

$$n = \frac{\log K}{\log (D_y / D_x)} , \tag{3.5}$$

where

$$K = \frac{z - y}{y - x} . \tag{3.6}$$

For the test data, the following drop diameters were selected:

$$D_x = 400 \text{ microns}$$

$$D_z = 1000 \text{ microns}$$

so that from Equation (3.4)

$$D_y = 632.5 \text{ microns}$$

and

$$n = \frac{\log K}{0.199} . \tag{3.7}$$

Using this result, measurements were taken from curves for drops evaporating in air streams of different velocities. The data and resulting exponents n' are given in Table I.

TABLE I

EXPERIMENTAL DATA FOR CUMENE GIVING EXPONENT n
AS A FUNCTION OF RELATIVE AIR VELOCITY

Run	x (sec)	y (sec)	z (sec)	K	log K	n'	n	v (ft/sec)
4-2	1.60	5.78	15.67	2.368	0.3744	1.88	1.88	0
4-3	1.78	6.69	17.37	2.176	0.3377	1.70	1.69	0.82
4-4	1.05	5.66	15.48	2.132	0.3288	1.65	1.65	1.16
4-5	1.62	5.71	14.22	2.081	0.3183	1.60	1.63	2.01
4-6	1.07	4.82	12.80	2.127	0.3278	1.65	1.625	2.48
4-7	1.55	4.97	12.15	2.098	0.3218	1.62	1.62	3.51
4-8	1.13	4.32	11.15	2.140	0.3304	1.66	1.60	4.29
4-9	2.20	5.27	11.62	2.067	0.3153	1.58	1.60	4.96
4-10	0.82	3.73	9.70	2.053	0.3124	1.57	1.58	6.07
4-11	0.83	3.57	9.27	2.080	0.3181	1.60	1.57	7.00
4-12	2.45	5.09	10.35	2.000	0.3010	1.51	1.53	7.84
4-13	1.32	4.00	9.27	1.967	0.2938	1.47	1.47	8.59

These data are plotted in Figure 4 giving n' as a function of relative air velocity. The values of the exponent obtained from the smooth curve are given in Table I as n and are the values used in the subsequent analysis for the corresponding relative air velocities.

2. Measurement of the Evaporation Constant λ

A series of evaporation tests were made with fixed drops at various relative air velocities and ultrasonic field intensities. Twelve velocities from 0 to 8.59 feet per second and six ultrasonic field "intensities" from 0 to 25 volts were used. The drop diameters measured for each run were then raised to the proper exponential power n determined in the previous section, depending on the velocity at which the

test was made. The exponent n was assumed to be a function of relative air velocity only.

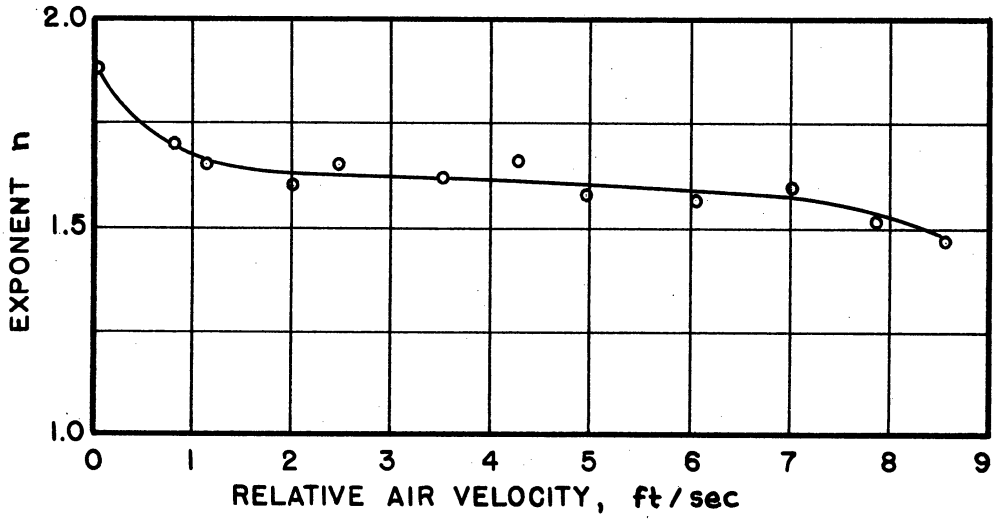

FIG. 4 VARIATION OF EXPONENT n WITH RELATIVE AIR VELOCITY

Data obtained from these runs are given in Tables IX through XXIII in Appendix B. The set of experimental curves for this series of tests, giving D^n as a function of elapsed time of evaporation, are shown in Figures 29 through 54, also in Appendix B.

The positive values of the slopes of these curves, measured in $(\text{microns} \times 10^{-2})^n/\text{second}$, give the values for the evaporation constant λ.

Measured values of λ for runs made under several combinations of relative air velocity and ultrasonic field intensity are listed in Table II.

To illustrate more clearly the relationship between λ and n in determining evaporation rates, $\log \lambda t_t$ is plotted in Figure 5 as a function of $\log (D_o/100)^n$ for several values of the exponent n. The result shows that for a given evaporation constant and initial drop diameter

TABLE II

VALUES OF THE EVAPORATION CONSTANT λ FOR FIXED DROPS
OF CUMENE AT VARIOUS COMBINATIONS
OF ULTRASONIC FIELD INTENSITIES AND RELATIVE AIR VELOCITIES

Voltage	0		2.5		5		10		20		25	
Velocity	Run	λ*	Run	λ*	Run	λ*	Run	λ*	Run	λ*	Run	λ*
	1-3	.254	2-9	.295	3-3	.240	3-15	.249	8-13	.310	8-14	.365
	1-12	.221	5-2	.238	5-15	.237	6-13	.226			9-6	.366
	4-2	.222	5-14	.231								
0	4-14	.223										
(ft/sec)	Avg.	.230		.255		.238		.237		.310		.365
	1-13	.229	5-3	.253	3-4	.254	3-16	.247	8-2	.292	8-15	.398
0.82	2-3	.278	2-10	.290								
	4-3	.248										
	Avg.	.252		.271		.254		.247		.292		.398
	2-4	.275	2-11	.276	3-5	.251	3-17	.245	8-3	.282	8-16	.336
1.16	4-4	.241	5-4	.255								
	Avg.	.258		.265		.251		.245		.282		.336
	4-5	.262	2-12	.310	3-7	.268	6-4	.258	8-4	.298	8-17	.343
2.01			5-5	.280			3-18	.274				
	Avg.	.262		.295		.268		.266		.298		.343
	1-5	.292	2-13	.320	3-8	.292	6-5	.275	8-5	.317	8-18	.329
2.48	4-6	.280	5-6	.293								
	Avg.	.286		.306		.292		.275		.317		.329
	1-6	.312	2-14	.352	3-9	.309	6-6	.302	8-6	.336	8-19	.344
3.51	4-7	.307	5-7	.323								
	Avg.	.309		.337		.309		.302		.336		.344
	1-7	.316	2-15	.365	3-10	.311	6-7	.302	8-7	.338	8-20	.337
4.29	4-8	.306	5-8	.327							8-21	.363
	Avg.	.311		.346		.311		.302		.338		.350
	4-9	.325	2-16	.370	3-11	.328	6-8	.324	8-8	.340	8-22	.363
4.96			5-9	.331								
	Avg.	.325		.350		.328		.324		.340		.363
	1-9	.314	5-10	.342	3-12	.331	6-9	.326	8-9	.319	8-23	.356
6.07	4-10	.329									9-2	.374
	Avg.	.321		.342		.331		.326		.319		.365
	1-10	.341	2-18	.398	3-13	.340	6-10	.331	8-10	.342	9-3	.374
7.00	4-11	.339	5-11	.343								
	Avg.	.340		.370		.340		.331		.342		.374
	1-11	.321	3-2	.331	3-14	.320	6-11	.311	8-11	.311	9-4	.319
7.84	4-12	.325	5-12	.328	6-2	.326						
	Avg.	.323		.329		.323		.311		.311		.319
8.59	4-13	.277	5-13	.292	6-13	.230	6-12	.278	8-12	.282	9-5	.255

*λ = (microns x 10^{-2})^n/sec.

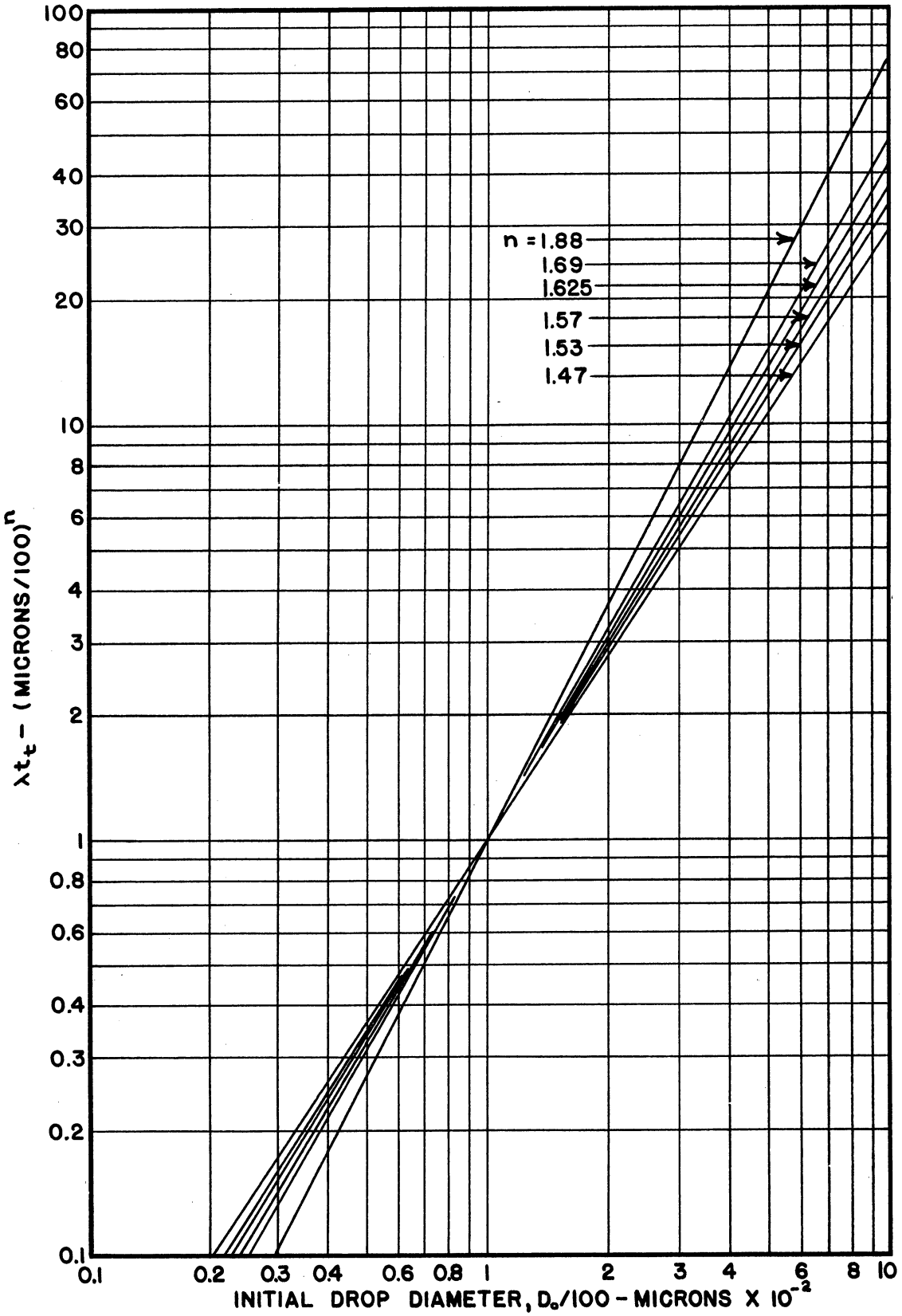

FIG.5 RELATIONSHIP BETWEEN INITIAL DROP DIAMETER AND TOTAL TIME OF EVAPORATION AS A FUNCTION OF λ AND n - FIXED DROPS

the total time of life will be dependent upon the exponent n, so that λ alone does not give a true indication of evaporation rate.

3. Effect of Ultrasonic Field Intensity on the Evaporation Constant

The evaporation constants found in the previous section are plotted against ultrasonic field intensity in Figures 6 and 7. Separate curves are used for the different velocities to eliminate the effect of variations in n with velocity.

The resulting curves clearly indicate a definite pattern for the effect of ultrasonic field intensity on the evaporation rate.

4. Effect of Ultrasonic Field Frequency on the Evaporation Constant

A series of tests were made with fixed drops in constant velocity air streams and at various ultrasonic frequencies. Results at two velocities were measured. These are given in Table III and are plotted in Figure 8.

TABLE III

DATA SHOWING THE VARIATION OF λ WITH ULTRASONIC FREQUENCY AT CONSTANT AIR VELOCITY--CUMENE DROPS

v = 2.48 (ft/sec)				v = 4.29 (ft/sec)	
Frequency (cps)	λ $(\frac{\mu}{100})^n$/sec	Frequency (cps)	λ $(\frac{\mu}{100})^n$/sec	Frequency (cps)	λ $(\frac{\mu}{100})^n$/sec
35,260	0.260	35,329	0.304	35,245	0.291
35,280	0.258	35,343	0.345	35,266	0.295
35,301	0.271	35,343	0.357	35,286	0.361
35,310	0.289	35,365	0.278	35,307	0.305
35,317	0.291	35,384	0.264	35,326	0.286
35,321	0.301	35,404	0.265	35,347	0.285
35,324	0.304				

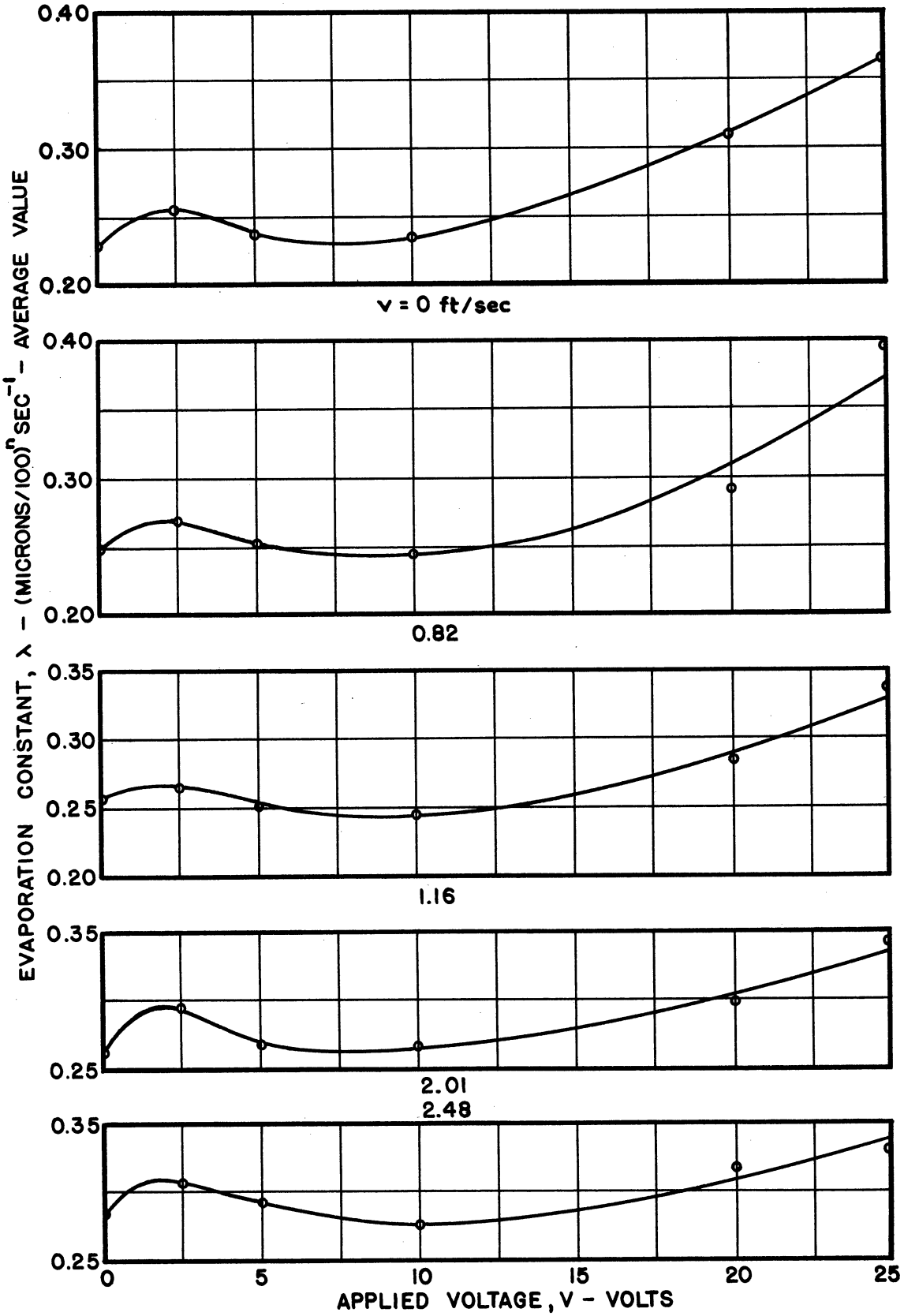

FIG. 6 EFFECT OF FIELD INTENSITY ON EVAPORATION CONSTANT

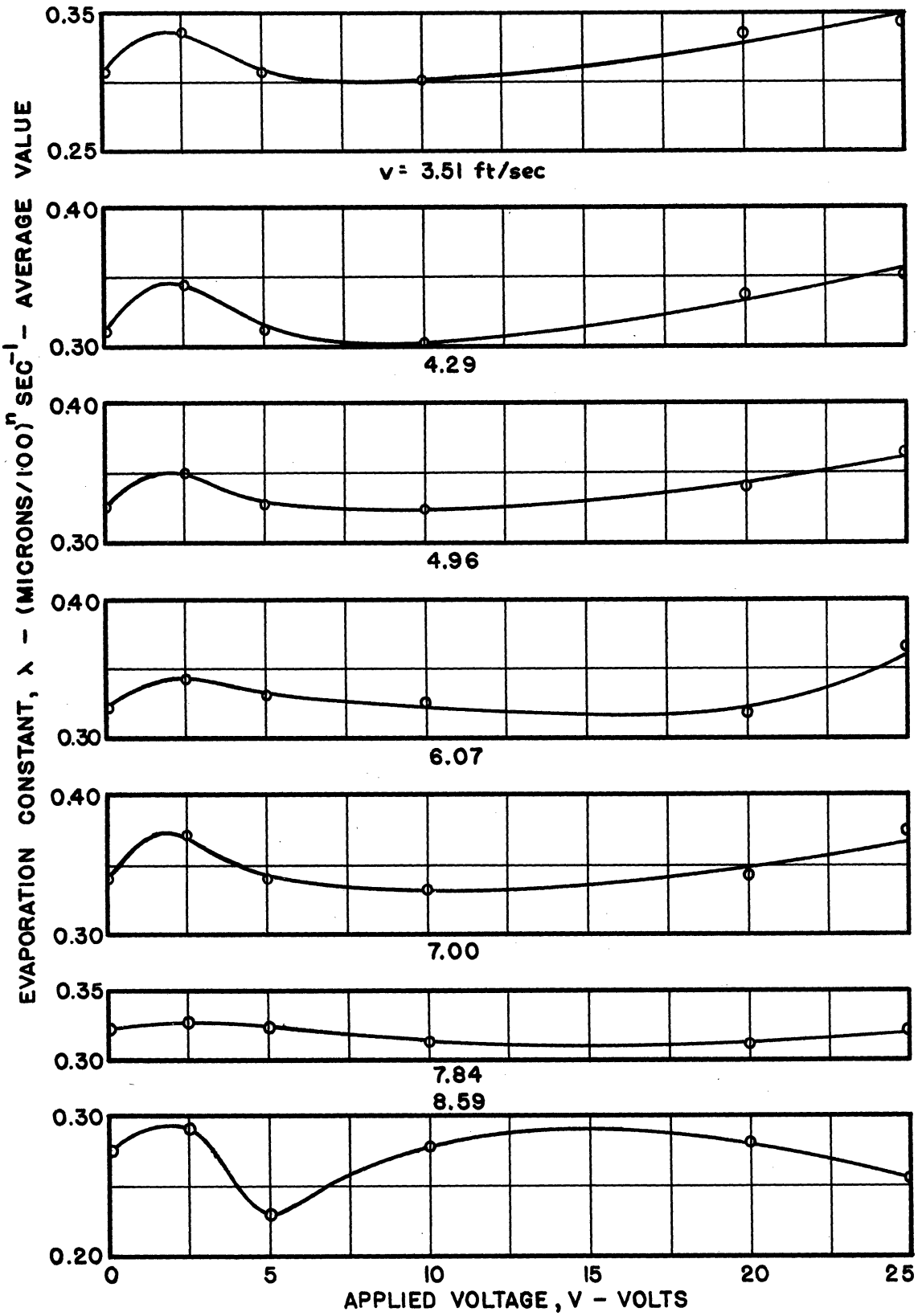

FIG.7 EFFECT OF FIELD INTENSITY ON EVAPORATION CONSTANT

Values of the evaporation constants obtained for zero ultrasonic field are indicated by broken horizontal lines drawn through the curves. The frequencies at which the maximum evaporation constants occur are designated in the text as the critical frequencies.

5. Variation of Critical Frequency with Relative Air Velocity

Drops that evaporate while freely suspended, as shown in Figure 2, would be doing so in an air stream having a velocity equal to the drop terminal velocity. As indicated in Figure 8 the critical frequency was affected by a change in relative velocity, so a series of tests were made to measure the change in critical frequency over the range of velocities likely to be encountered in tests with free drops.

Results are given in Table IV and are plotted in Figure 9. The two points obtained from Figure 8 are also shown.

TABLE IV

DATA SHOWING THE VARIATION OF ULTRASONIC CRITICAL FREQUENCY WITH CHANGES IN RELATIVE AIR VELOCITY

Velocity (ft/sec)	Critical Frequency--(cps)	
	Increasing Velocity	Decreasing Velocity
0	35,504	35,421
0.82	35,655	35,561
1.16	35,633	35,537
2.01	35,535	35,439
2.48	35,475	35,398
3.51	35,410	35,351
4.29	35,373	35,328
4.96	35,330	35,298
6.07	35,293	35,282
7.00	35,282	35,257
7.84	35,260	35,256
8.59	35,236	35,244

A large hysteresis effect is clearly illustrated in the figure.

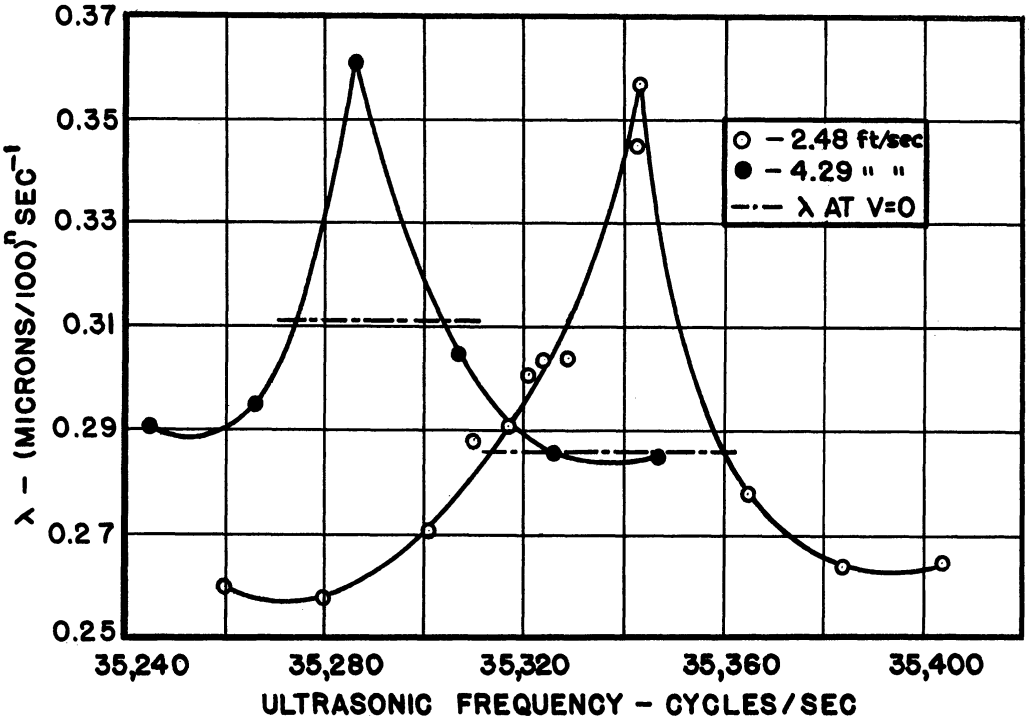

FIG.8 EFFECT OF ULTRASONIC FREQUENCY ON EVAPORATION CONSTANT AT CONSTANT VELOCITY AND VOLTAGE (20 VOLTS)

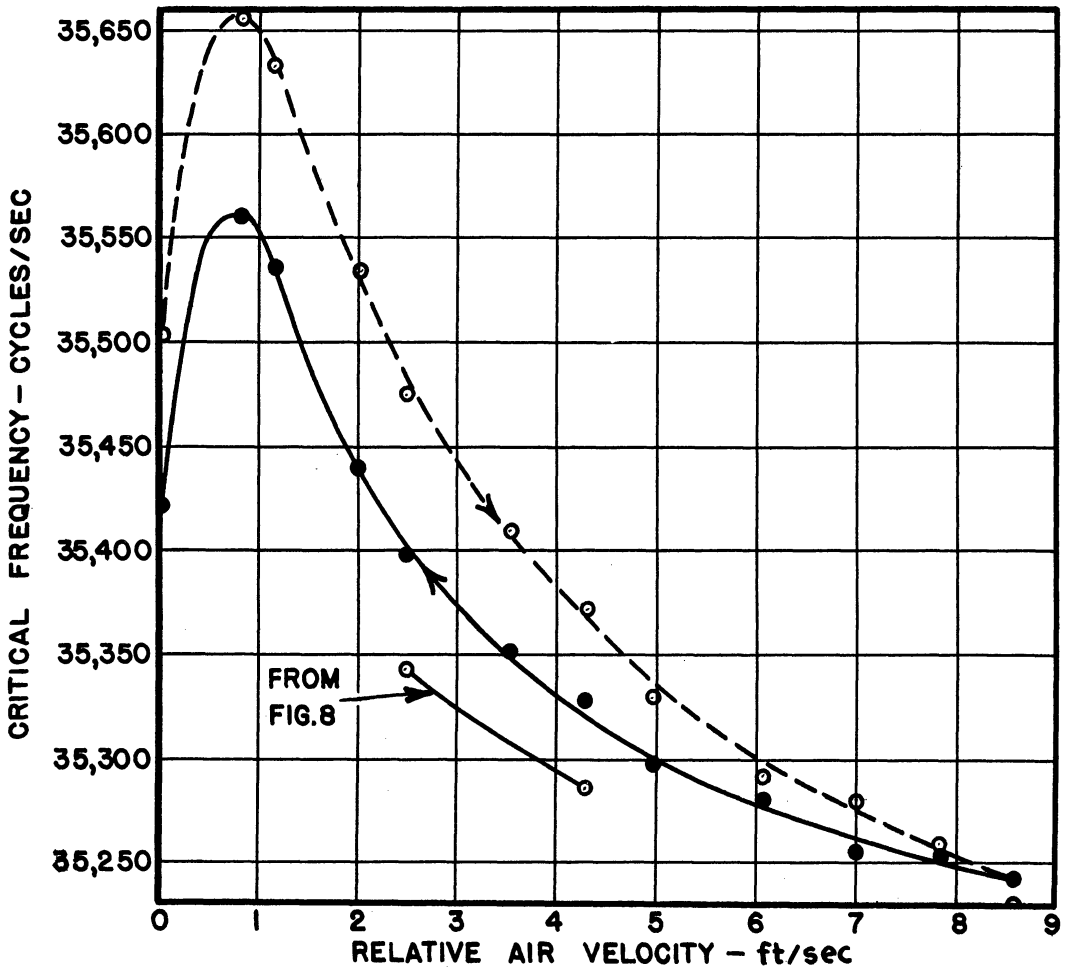

FIG.9 VARIATION OF CRITICAL FREQUENCY WITH RELATIVE AIR VELOCITY

6. Reduction of Data for Fixed Drops, Based on the Evaporation Equation (2.51)

The evaporation equation (2.51) was derived for the case of a single drop evaporating in a constant velocity air stream in the absence of an ultrasonic field. Repeated here for convenience, it was shown to be

$$(D_o^{3/2} - D^{3/2}) - \frac{3}{2} C (D_o - D) + 3C^2 (D_o^{1/2} - D^{1/2}) - 3C^3 \ln \left(\frac{D_o^{1/2} + C}{D^{1/2} + C}\right) = \frac{6k}{C\rho c} \left[1 + \frac{c (T_f - T)}{L}\right] t \qquad (3.8)$$

where

$$C = \frac{2}{f (Pr)^{1/3} \left(\frac{v}{\nu}\right)^{1/2}} \qquad (3.9)$$

All independent variables are known except for the quantity f which must be determined from the experimental data.

Using the values for the physical properties given in Appendix C and the average values of the temperatures measured in the tests, the following expressions were obtained,

$$C = \frac{2.96}{f v^{1/2}} \qquad (3.10)$$

and

$$\frac{6k}{C\rho c} \left[1 + \frac{c (T_f - T)}{L}\right] = 3.29 \times 10^{-7} f v^{1/2} . \qquad (3.11)$$

Substituting these in the evaporation equation and modifying the result to express D in microns x 10^{-2}, the evaporation equation for stationary cumene drops in a constant velocity air stream whose temperature is 83°F (the test conditions) becomes

$$\left.\begin{aligned} &\frac{18.1}{fv^{1/2}}\left(D_o^{3/2} - D^{3/2}\right) - \frac{44.3}{f^2 v}\left(D_o - D\right) + \frac{145}{f^3 v^{3/2}}\left(D_o^{1/2} - D^{1/2}\right) \\ &- \frac{236}{f^4 v^2} \ln\left[\frac{fv^{1/2} D_o^{1/2} + 1.63}{fv^{1/2} D^{1/2} + 1.63}\right] = t \,. \end{aligned}\right\} \quad (3.12)$$

To solve this equation for f, a point on the evaporation curve is selected and the corresponding values for D and t substituted in the equation. The values for D_o and v are the initial drop diameter and relative air velocity for the particular test run. The values of f computed for several relative air velocities are shown in Table V below.

TABLE V

VALUES OF f FOR SEVERAL AIR VELOCITIES

Air Velocity (fps)	f
0.82	2.31
2.01	1.96
4.29	1.74
7.00	1.69
8.59	1.66

B. Reduction of Data--Free Drops

Figures 10, 11, and 12, plotted from the experimental data given in Tables XXIV - XXVI in Appendix B, show the results of evaporation tests with freely-suspended drops of fourteen pure liquids and kerosene. The drops were supported in the air stream at their terminal velocities by means of air drag and ultrasonic forces. A typical sequence of photographs from one of the runs is shown in Figure 2.

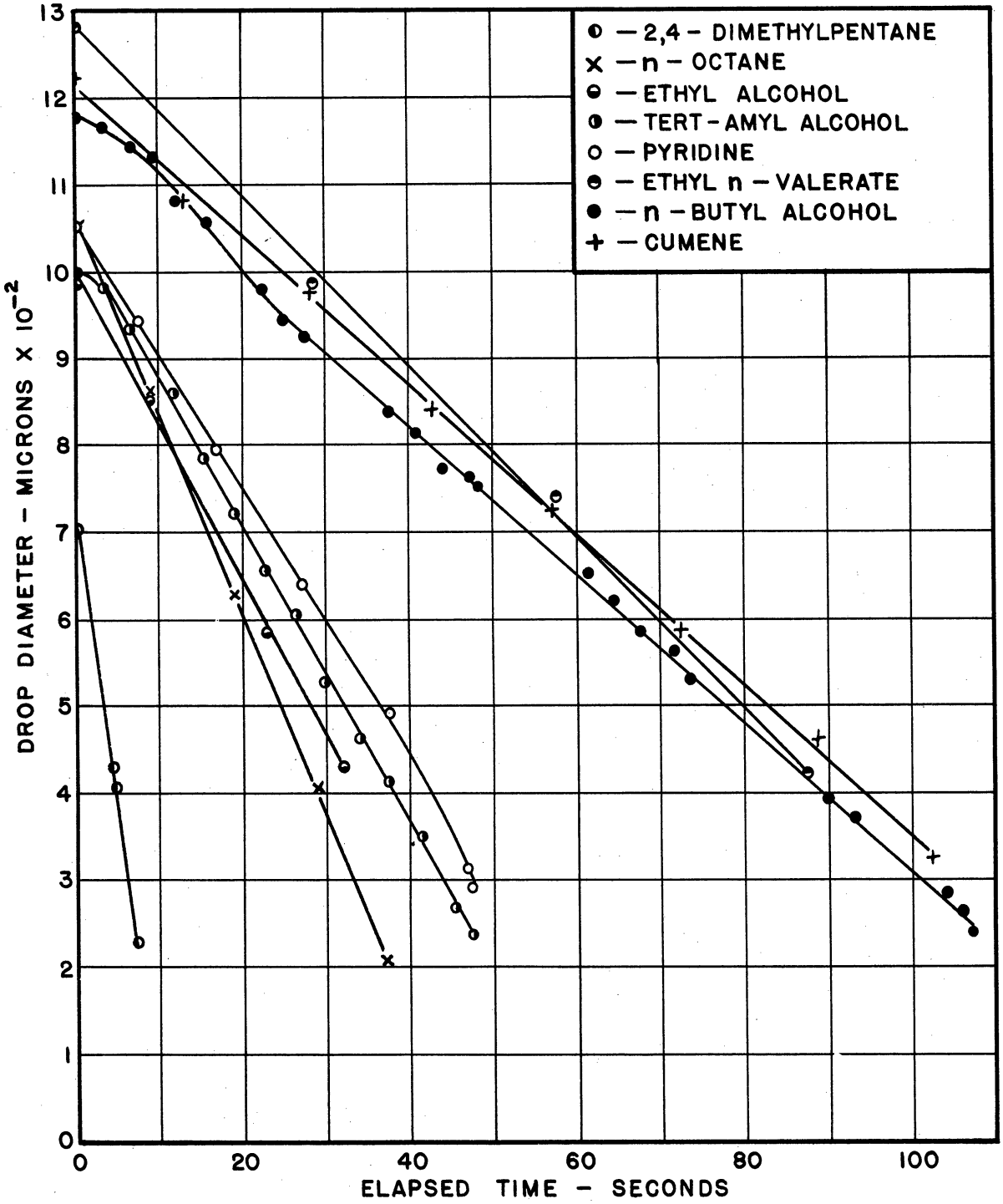

FIG. 10 EVAPORATION CURVES FOR SOME PURE LIQUIDS - FREE DROPS

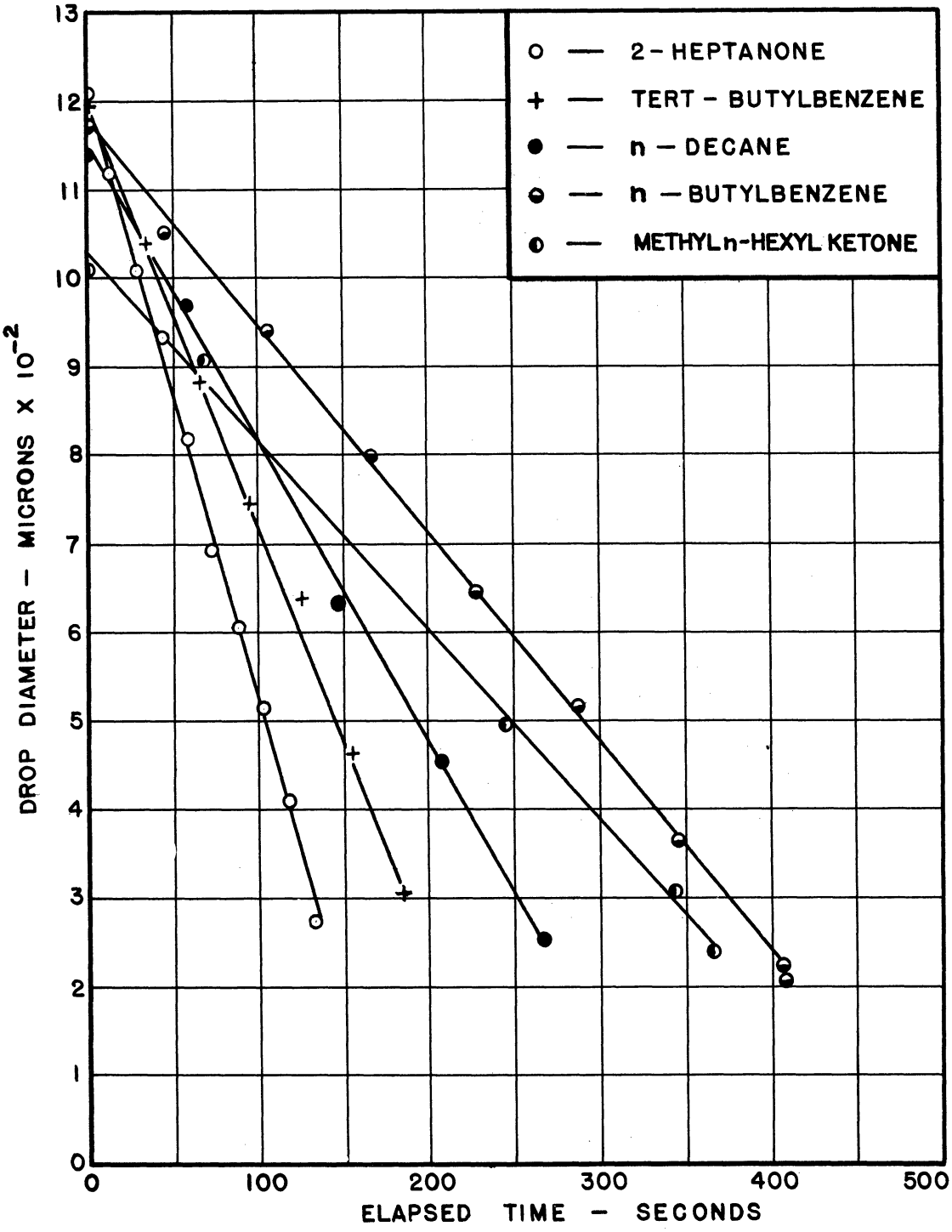

FIG. 11 EVAPORATION CURVES FOR SOME PURE LIQUIDS - FREE DROPS

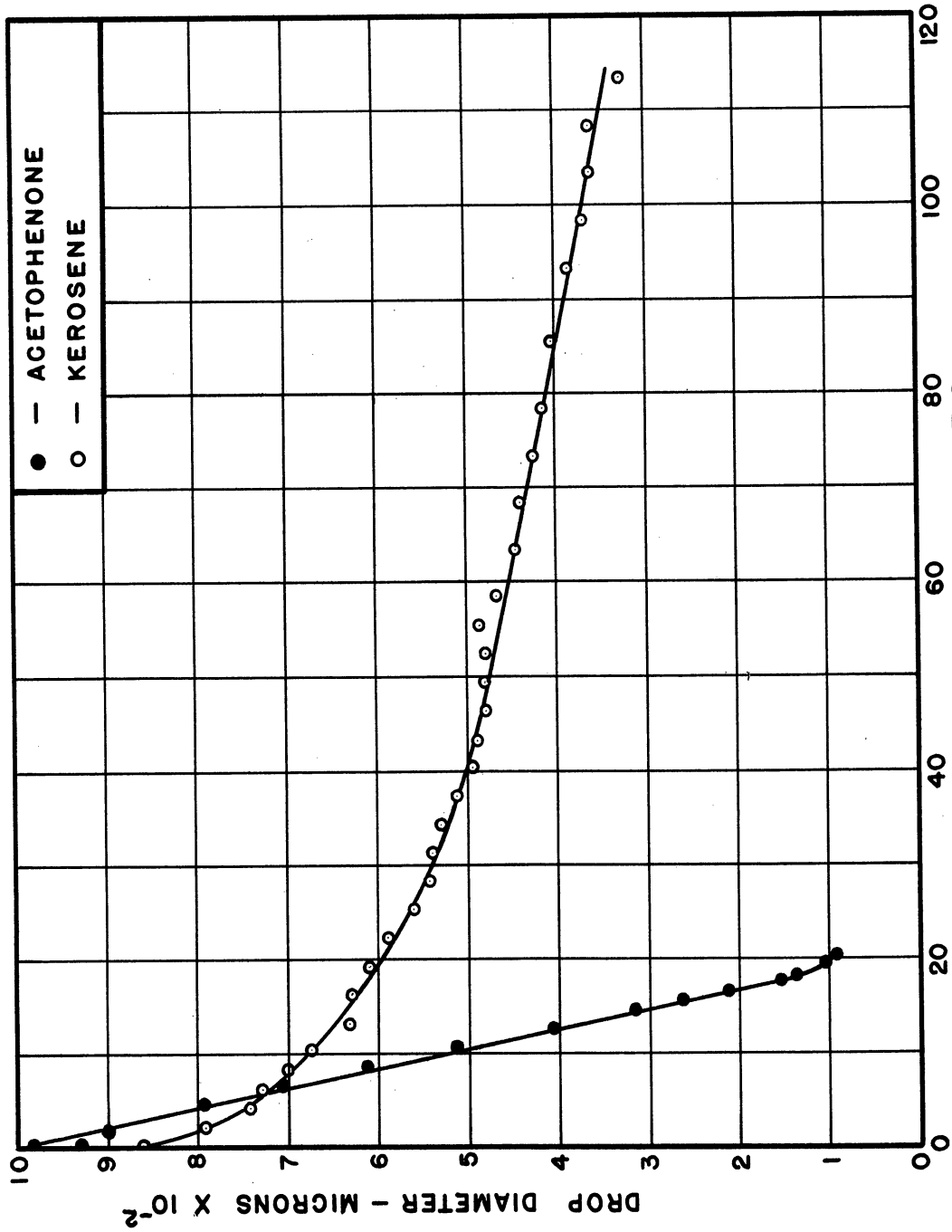

FIG. 12 EVAPORATION CURVES FOR ACETOPHENONE AND KEROSENE – FREE DROPS

When evaporating in this manner, and in a constant frequency field, drop diameter for the pure liquids was found to be a linear function of elapsed time of evaporation. The measured slopes, in microns per second, are listed in Table VI below.

TABLE VI

EVAPORATION RATES FOR FREE DROPS
OF SOME PURE LIQUIDS IN A STATIONARY ULTRASONIC FIELD

Liquid	Evaporation Rate (microns/sec)
2,4-Dimethylpentane	66.7
n-Octane	22.7
Ethyl Alcohol	17.6
Tert-Amyl Alcohol	17.0
Pyridine	15.2
Ethyl n-Valerate	9.90
n-Butyl Alcohol	8.55
Cumene	8.55
2-Heptanone	6.75
Tert-Butylbenzene	4.80
n-Decane	3.39
n-Butylbenzene	2.39
Methyl n-Hexyl Ketone	2.20
Acetophenone	0.81

For kerosene, the evaporation rate is seen to decrease with an increase in elapsed time of evaporation.

CHAPTER IV

EXPERIMENTAL EQUIPMENT

The experimental-test equipment is composed of four main functional systems, each being somewhat independent of the others. These are classified as follows:

1) air flow system,

2) ultrasonic field generation system,

3) photographic recording system,

4) instrumentation and accessories.

These form the complete apparatus shown in Figure 13. A somewhat clearer understanding of the manner in which these are related can be obtained from the schematic diagram given in Figure 14.

The basic operation of the apparatus is as follows. The air system produces a vertical flow of air with little turbulence. This flow is made to pass through a ceramic cylinder of barium titanate, the piezoelectric transducer which produces a standing wave ultrasonic field in the air within the tube. The ultrasonic field, when stationary, i.e., when the sound nodes are fixed, introduces lateral forces on the drop within the tube which hold the drop in a fixed horizontal position. At the same time, the action of the air stream on the drop creates an upward drag force which opposes the downward vertical force of gravity. By varying the velocity of the air stream, the drag force on the drop can be controlled to just balance out the gravitational force, so that the drop is held in a fixed position in space. By adjusting the air velocity

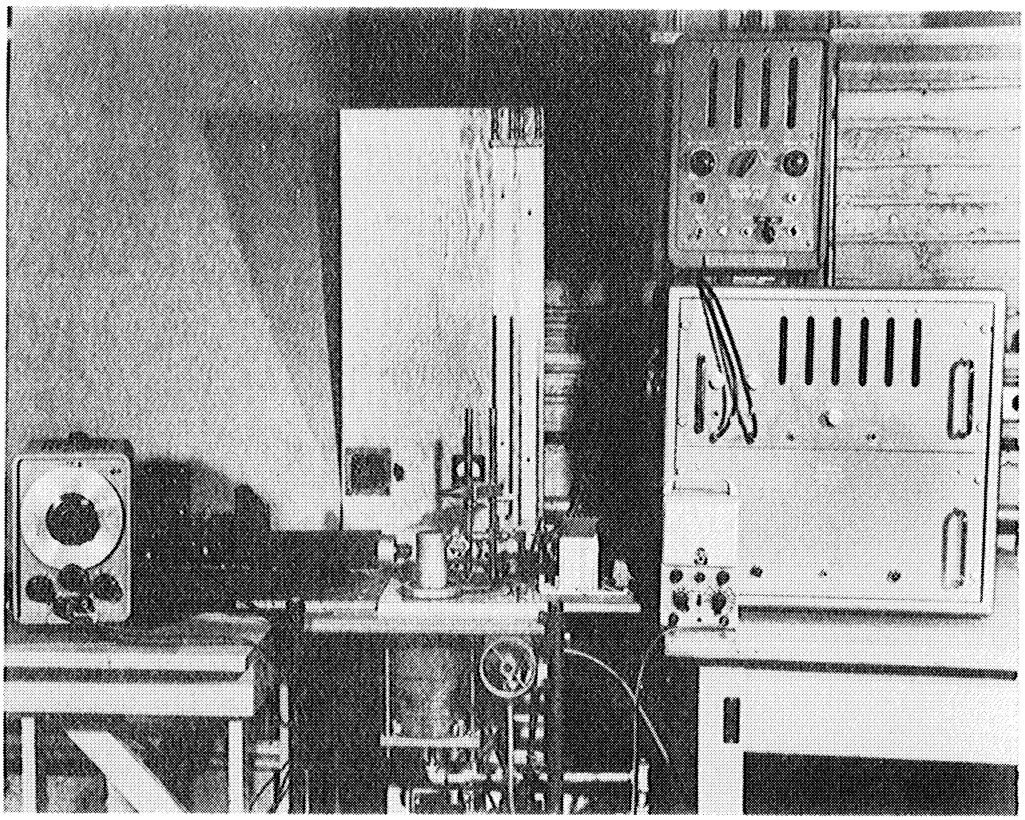

FIG. 13 PHOTOGRAPH OF EXPERIMENTAL EQUIPMENT

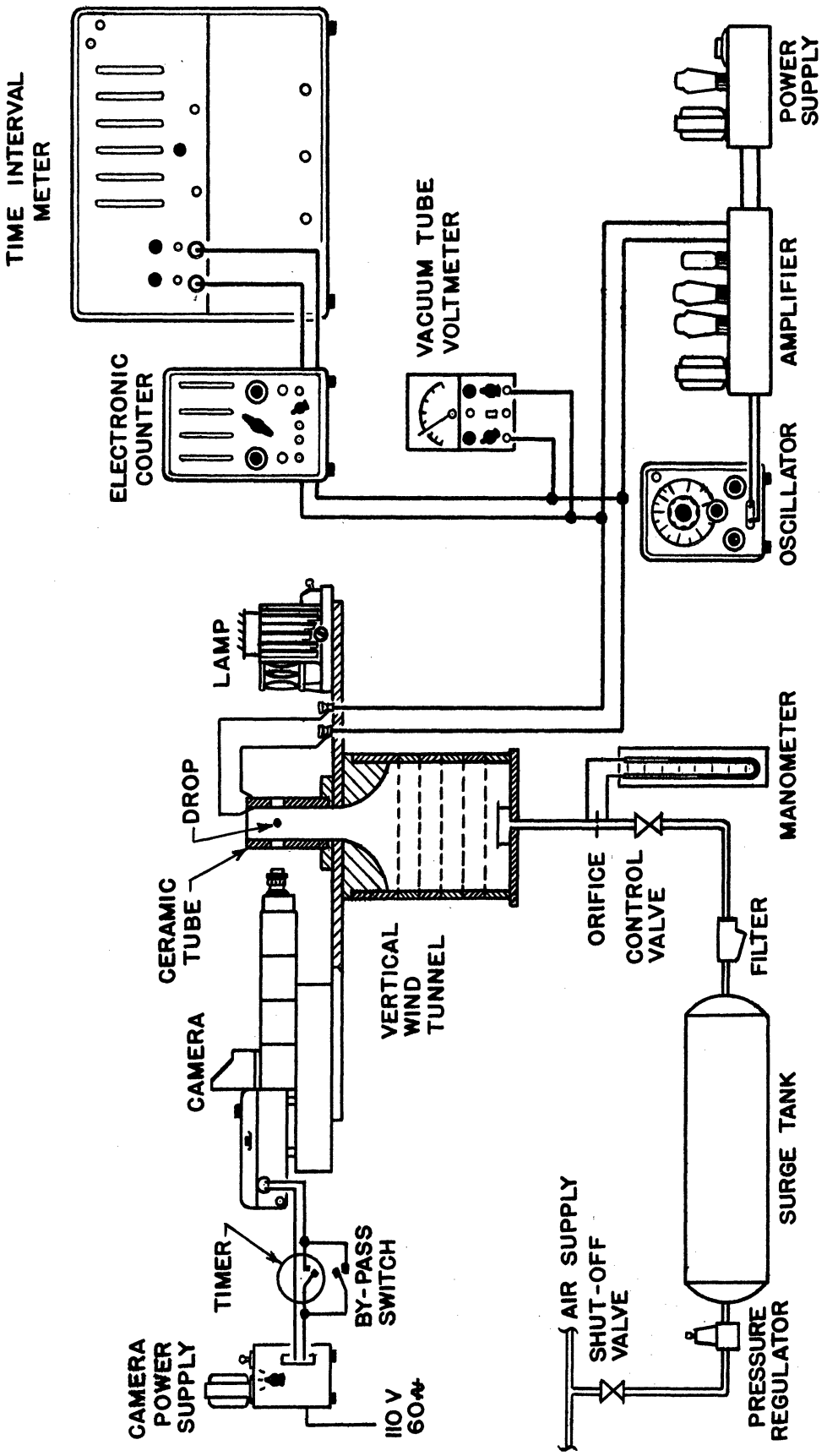

FIG. 14 SCHEMATIC DIAGRAM OF EXPERIMENTAL EQUIPMENT

it becomes possible to hold the drop in this position as it evaporates. Motion pictures of the drop were taken at known time intervals to get drop diameter as a function of time.

A. Air Flow System

1. Vertical Wind Tunnel

The low turbulence air stream is formed by a small wind tunnel, approximately six in. in diameter and 7-3/4 in. long. See Figure 15. The body of the wind tunnel is made of six sections of six in. steel tubing. Screens, which reduce the scale of turbulence in the air stream, are soldered to each of the five botton sections. When assembled, the sections are positioned so that the screen mesh sizes decrease as the exit nozzle is approached, except for the 100 mesh bottom screen.

A wooden convergent nozzle, used to give the exit air stream a flat velocity profile, provide a smooth approach to the barium titanate tube, and compress the turbulence scale, is fitted into the top section. One-eighth inch pipe couplings provide connections to two small holes in the side of this section and serve as thermocouple holes.

Four bolts attach the bottom section to a bottom plate. Air is allowed to enter the wind tunnel through a hole in the center of this plate, while a baffle mounted directly over this hole reduces the velocity of the incoming air and creates a more uniform pressure in the bottom section of the tunnel. Figure 15 clearly shows the individual sections with their turbulence screens, the exit nozzle, and entrance baffle.

All sections, properly aligned with each other, are clamped between two plates by four long bolts running along the outside of the

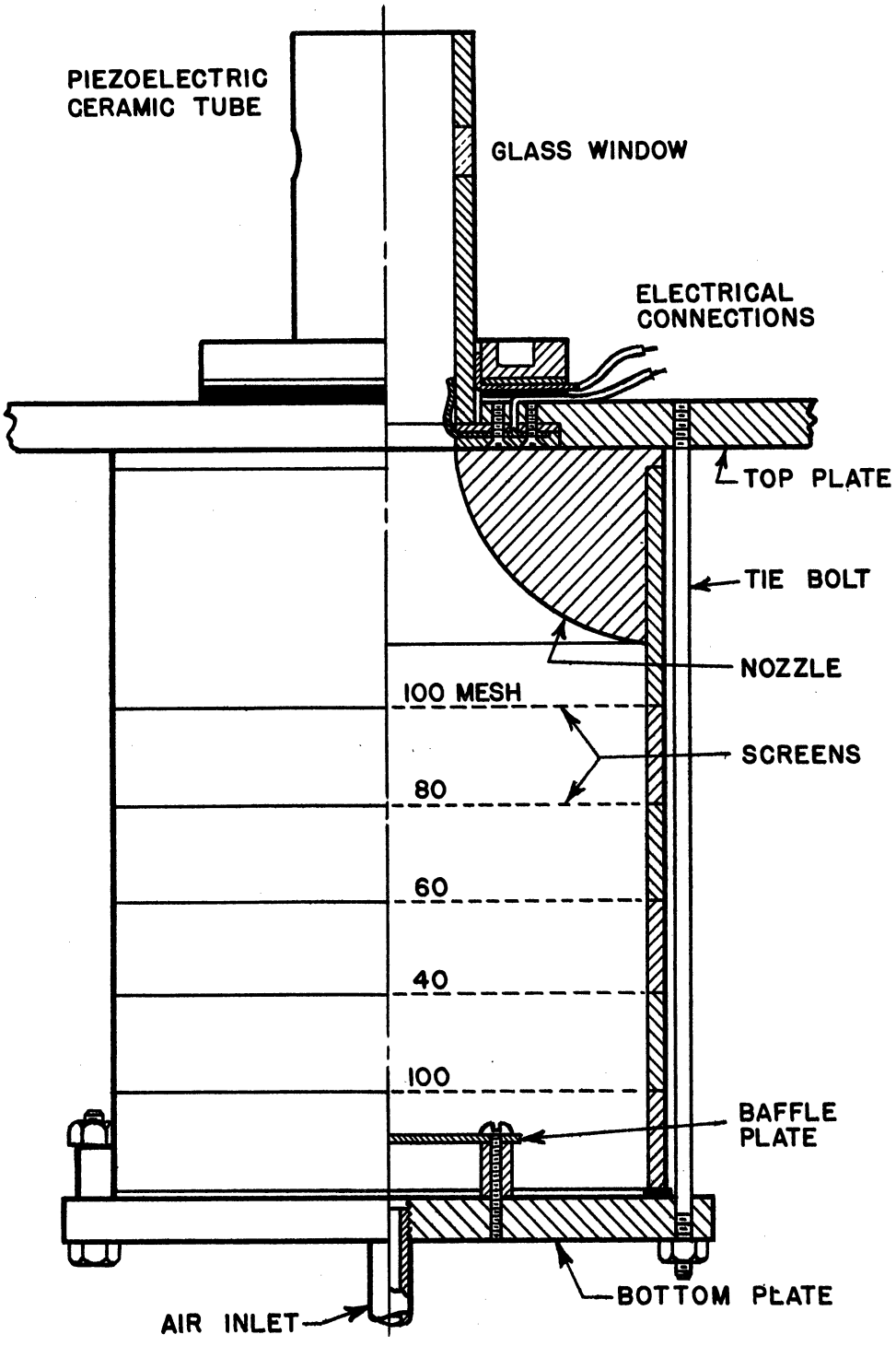

FIG. 15 SECTIONAL VIEW OF VERTICAL WIND TUNNEL

tunnel. The top plate serves as a mount for the barium titanate tube and contains spring contactors used to make electrical connection to the transducer. One of the contactors is insulated while the other is grounded to the top plate. Details are shown in Figure 15.

The top plate also carries insulated binding posts for external electrical connections and an adjustable holder for the glass filament used for suspending drops.

2. Air Supply

Air is obtained from a building supply header at about 95 psig and 83°F and fed to a surge tank through a shutoff valve and small pressure regulator. A hot-water tank rated at 150 psig continuous duty was selected for the surge tank and has served quite well in diminishing the adverse effects due to slight pressure variations in the main line.

Leaving the surge tank, the air is made to pass through a filter, control valve, and flow metering orifice before entering the wind tunnel.

B. Ultrasonic Field Generation System

The ultrasonic field is generated by a cylindrical barium titanate transducer which is excited by a source of high frequency sinusoidal voltage. The transducer and source comprise the field-generating system.

1. Barium Titanate Transducer

A transducer is an element that converts energy from one form to another. In the apparatus used in these tests the transducer converts a sinusoidally-varying electrical voltage at a fixed frequency into

acoustic energy at the same frequency. Since a cylindrical transducer is used the acoustic energy is radiated as cylindrical sound waves concentric to the walls of the tube. Only the waves directed toward the center of the tube were of use in these tests.

Under certain conditions, the waves within the cylinder combine to form a standing-wave sound field, that is, a sound field having stationary nodes. Different patterns are possible depending on the mode of vibration; however, only the field having concentric cylindrical nodes was used for these tests. When a drop or small solid particle is introduced into the field it is forced to take a position in one of the nodes.

The particular transducer used in these experiments is a cylinder cast from a barium titanate which the manufacturer designates as ceramic "A". It has a safe working temperature of 100°C. Dimensions of the cylinder are two in. O.D. x 1-5/8 in. I.D. x four in. long. The corresponding operating frequency is limited to a very narrow frequency band around the resonant frequency of about 35,500 cycles per second. Several basic piezoelectric elements are shown in Figure 16.

Very thin layers of silver are plated on both inner and outer surfaces to within 1/16 in. of both the top and bottom of the tube and serve as electrodes for the element. Maximum safe operating voltage specified by the manufacturer is 100 volts rms. However, all tests were made below 45 volts. The voltage is applied between the inner and outer plated surfaces.

Before the element could be used, it was necessary to cut holes on diametrically-opposite sides of the tube and install windows for the purpose of viewing the suspended drops.

FIG. 16 BASIC PIEZOELECTRIC CERAMIC ELEMENTS

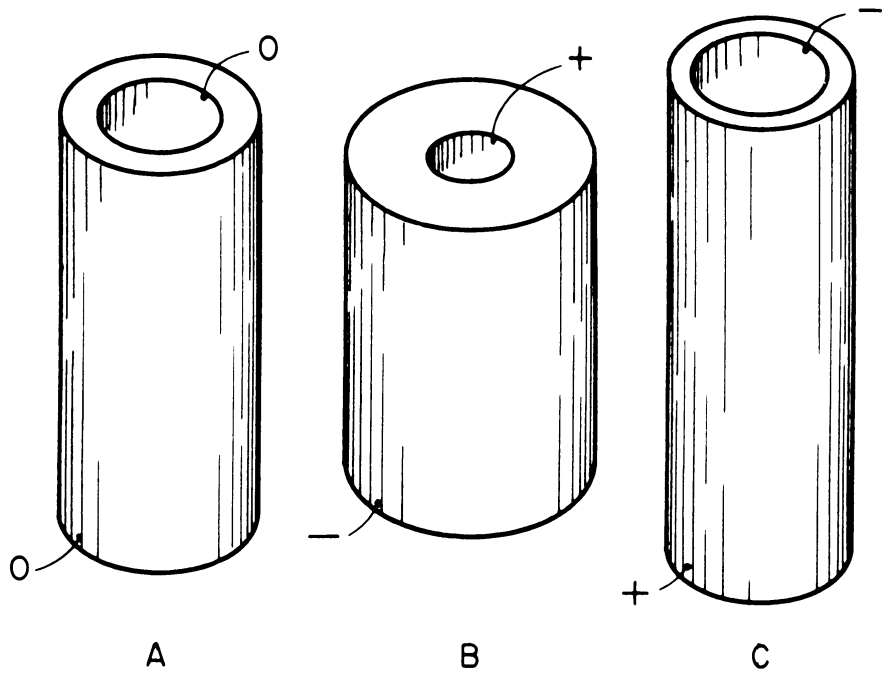

FIG. 17 ACTION OF THE PIEZOELECTRIC CERAMIC TUBE DUE TO CHANGES IN POLARITY OF APPLIED VOLTAGE

The operation of the ceramic element is a result of the piezoelectric effect. The effect is such that if the crystal is strained under an applied stress, electric charges of opposite polarity appear on the two opposite faces of the wall, causing it to become electrically polarized. The opposite effect also occurs. That is, when the two plated surfaces are connected to a source of voltage, so that the ceramic lies in an electric field, it will suffer a strain and either expand or contract.

When an alternating voltage is applied to the ceramic such that the frequency is equal to the resonant frequency of the element, the amplitude of mechanical deformation of the tube wall becomes quite large and results in the generation of an ultrasonic sound wave. This action is illustrated in Figure 17. One polarity causes the wall to increase in thickness and decrease in length, thereby generating a radial compression wave within the tube. The opposite polarity causes the opposite effect and generates a radial rarefaction wave. As the wall alternately increases and decreases in thickness it generates a sound field in the radial direction.

The action of two waves originating at diametrically opposite sides of the tube is illustrated in Figure 18 to show how they combine to form a standing-wave sound field in the form of concentric cylindrical nodes. The pattern is easily made visible with lycopodium powder sprinkled on a flat horizontal sheet held within the tube.

Figure 19 shows a small cork sphere suspended in air in one of the nodes of the ultrasonic field.

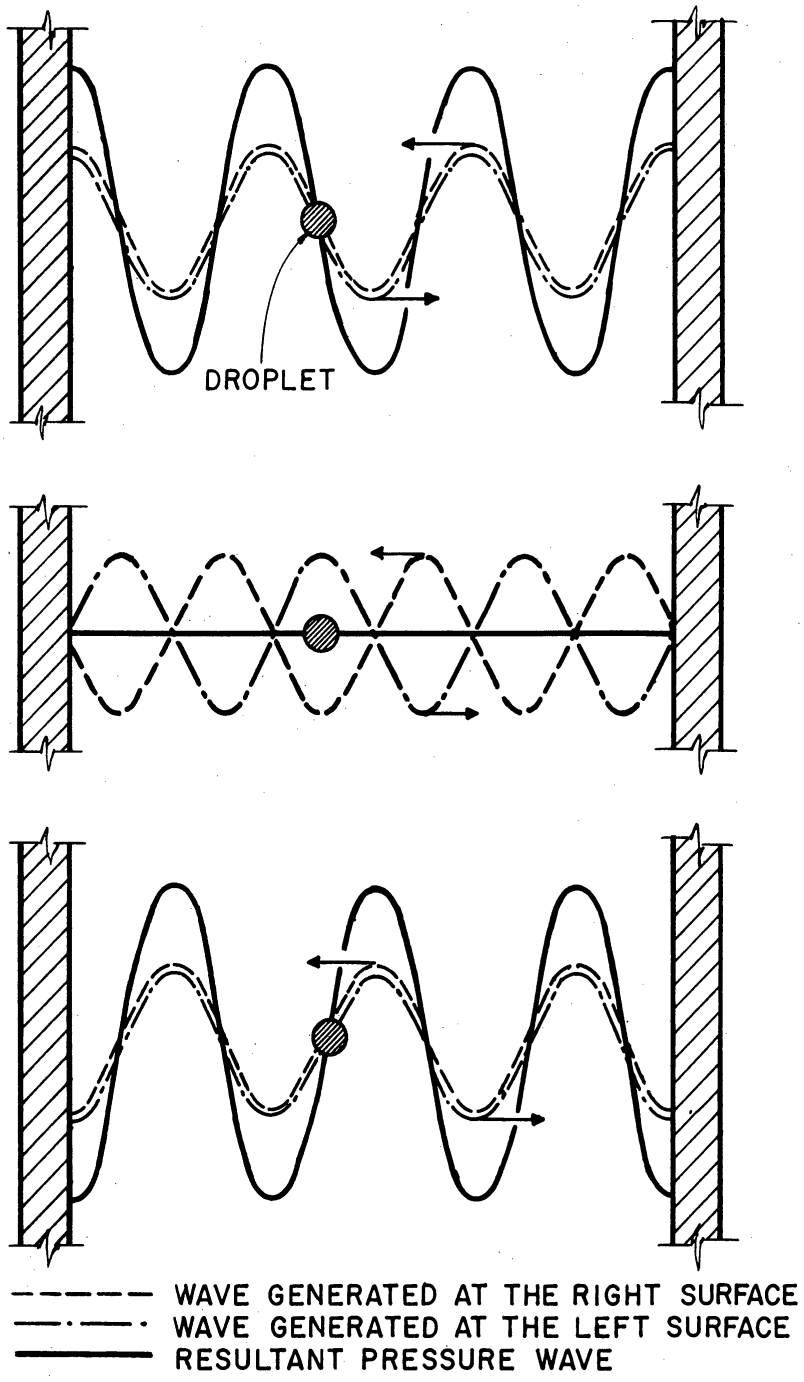

FIG. 18 GENERATION OF A STANDING SOUND WAVE BY THE PIEZOELECTRIC TUBE

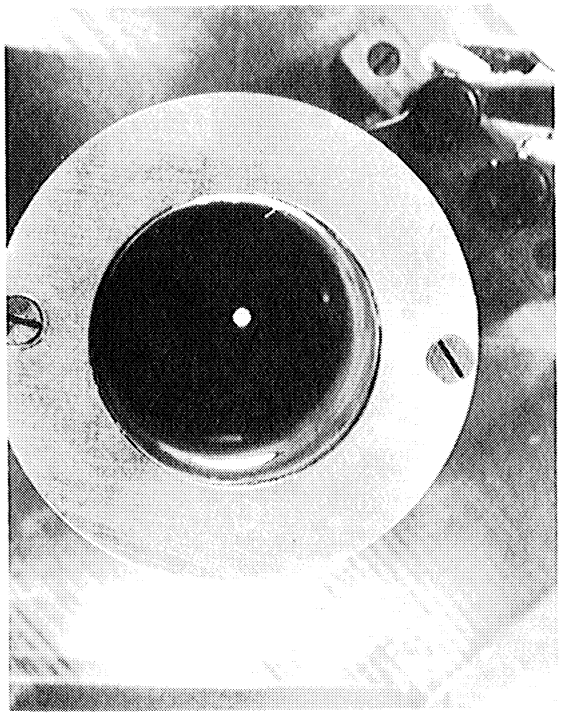

FIG. 19 CORK SPHERE SHOWN SUSPENDED WITHIN THE CERAMIC TUBE

2. Ultrasonic Field Detection

A simple and convenient device for detecting the presence of a stationary field is a needle attached to the end of a fine thread. The needle is suspended in the tube while the frequency is varied around the resonant frequency. When the resonant frequency is reached, the needle is "grasped" by the field and held in a fixed position in one of the nodes. A fair amount of movement of the thread will not dislodge the needle from the node.

The field intensity can be changed by varying the voltage applied to the tube. This voltage, when measured by a vacuum tube volt meter, also serves as an indication of the relative field intensity.

This method was used throughout the test for the initial frequency setting and will detect a "tuned" field adequate enough to suspend drops.

When a drop has been suspended, a more critical indication of the tuning is obtained by observing the motion of light reflected from the surface of the drop and appearing on the inside surface of the tube. The change in angle at which the light is reflected is due to distortion in drop shape. The distortion occurs as a result of field forces acting on the drop, and at high field intensities the drop sphere is considerably flattened, depending on the value of the applied voltage and the tuning of the tube. At the resonant frequency, which will be referred to as the critical frequency, the strongest field action occurs and creates the maximum drop distortion. Therefore, when tuning for the critical frequency, the deflection of the reflected light beam increases as the critical frequency is approached from either direction and reaches a maximum at this frequency.

The drop distortion was also viewed with a pocket microscope. A small light was placed inside the wind tunnel to provide backlighting as the drop was viewed from above. At high field intensity and critical frequency the distortion was quite pronounced, giving the drop the appearance of a rounded, well-flattened disk.

An alternate method used for detecting and exploring the sound field was the hot wire technique. Although not as convenient to use for field detection, it is capable of providing more information and was used to a limited extent for this purpose.

3. Ultrasonic Frequency Voltage Supply

The high frequency voltage supply consists of a voltage step-down transformer, oscillator, power supply and amplifier. These are shown in the schematic diagram, Figure 14.

A voltage step-down transformer was used to decrease the building 220 volt, 60 cycle supply to 110 volts, since the 110 volt building supply was heavily loaded at times by other equipment in the building. The resulting large voltage surges caused erratic operation of the equipment and loss of stabilizing action on freely-suspended droplets. After the change to the 220-volt supply, no further difficulties of this nature were experienced.

The high frequency voltage signal is obtained with a Hewlett-Packard Model 200 AB variable frequency oscillator. The output signal is fed directly to the input of a 45-watt amplifier which serves to amplify the voltage, provide sufficient power to drive the ceramic tube, and to improve the impedance match between the voltage supply and ceramic tube.

A separate B+ supply is used to provide some of the power to the amplifier. Schematic diagrams for both the amplifier and B+ supply are given in Figure 20.

C. Photographic Recording System

Photographic records of evaporating drops were taken at fixed time intervals to get drop diameter as a function of elapsed time of evaporation. Enlarged drop images were obtained with a modified 16 mm motion picture camera. The timing device was calibrated with a stop watch during each run.

1. Motion Picture Camera

A 16 mm U.S. Army Air Force Type N-6 gun camera, with speeds of 16, 32, and 64 frames per second, was used to photograph the

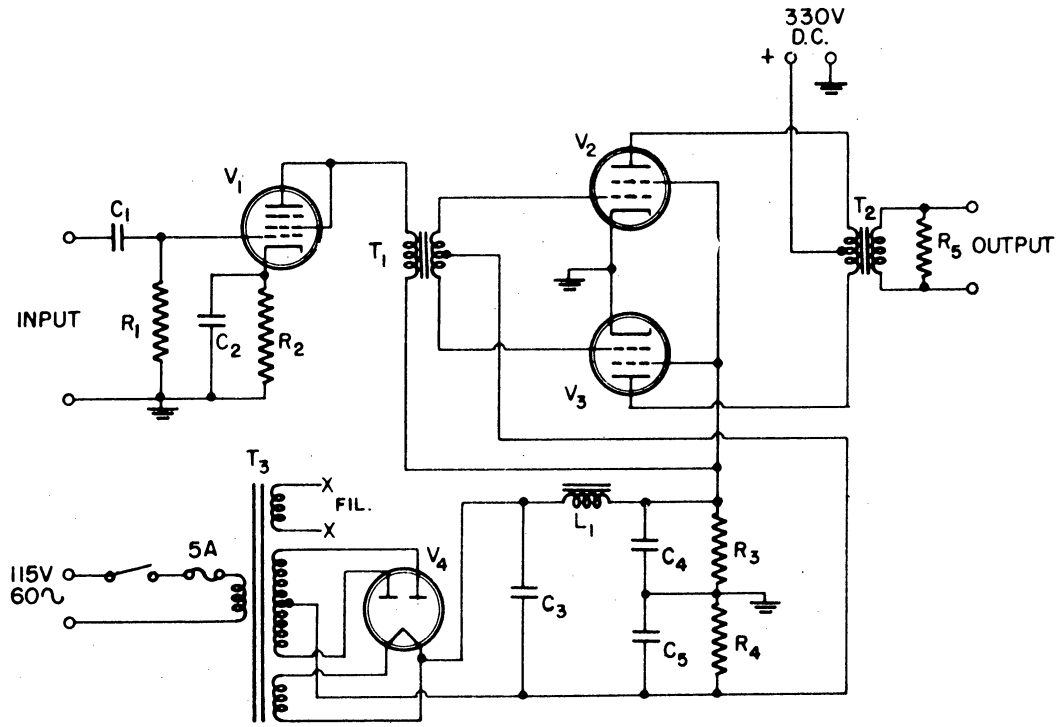

V_1 = 6F6

V_2, V_3 = 6L6

V_4 = 5U4G

R_1 = 0.5MEG., 1/2W

R_2 = 1700, 1/2W

R_3 = 5.1K, 30W

R_4 = 200, 10W

R_5 = 2250, 25W

C_1 = 10mmfd., MICA

C_2, C_5 = 25mfd, 25V.

C_3, C_4 = 4mfd., 400V.

L_1 = 4H AT 130ma., 100 Ohms

T_1 = DRIVER TRANSFORMER, TURNS RATIO, PRI–1/2 SEC.=4:1

T_2 = OUTPUT TRANSFORMER 3800 OHM PRIMARY TO 500 OHM SECONDARY

T_3 = POWER TRANSFORMER 375-375 VOLTS AT 150 ma. D.C.

FIG. 20 SCHEMATIC DIAGRAM OF AMPLIFIER

evaporating drops. Before the camera could be used, it was necessary to provide the camera with a sliding mount for rough focusing, a combination lens extension tube and reflex viewer, and a focusing screen adaptor. Figure 21 gives a close-up of the modified camera mounted in position.

The sliding mount is nothing more than a pair of slotted pieces of thin metal plate, each attached to a wooden support by means of soft rubber grommets. The camera mounting bolts fit into the slots, allowing the camera limited motion in one direction only. Adjustments for rough focusing are made with a focusing screw.

The lens extension tube and reflex viewer unit consists of five sections. These are the threaded aluminum lens mount, three extension tube sections, and the reflex viewer housing. Various factors of magnification can be obtained by varying both the number of sections used and the focal length of the lens. Figure 22 shows the assembled unit mounted to the camera.

Most of the results were obtained with the original camera lens, a 35 mm, f/3.5 Wollensak, providing a magnification factor of about 7X when used with all extension tube sections. To increase image sharpness, the lens was mounted backwards in the lens mount, i.e., the front lens element faced the film instead of the drop.

The inside of the extension tube is lined with black velvetine and a black paper diaphragm was inserted in the tube to cut down light reflections from the tube wall. At the camera end of the tube, an image-splitting block reflects part of the incoming light and forms a second image on a ground glass viewing screen directly above the block, while the

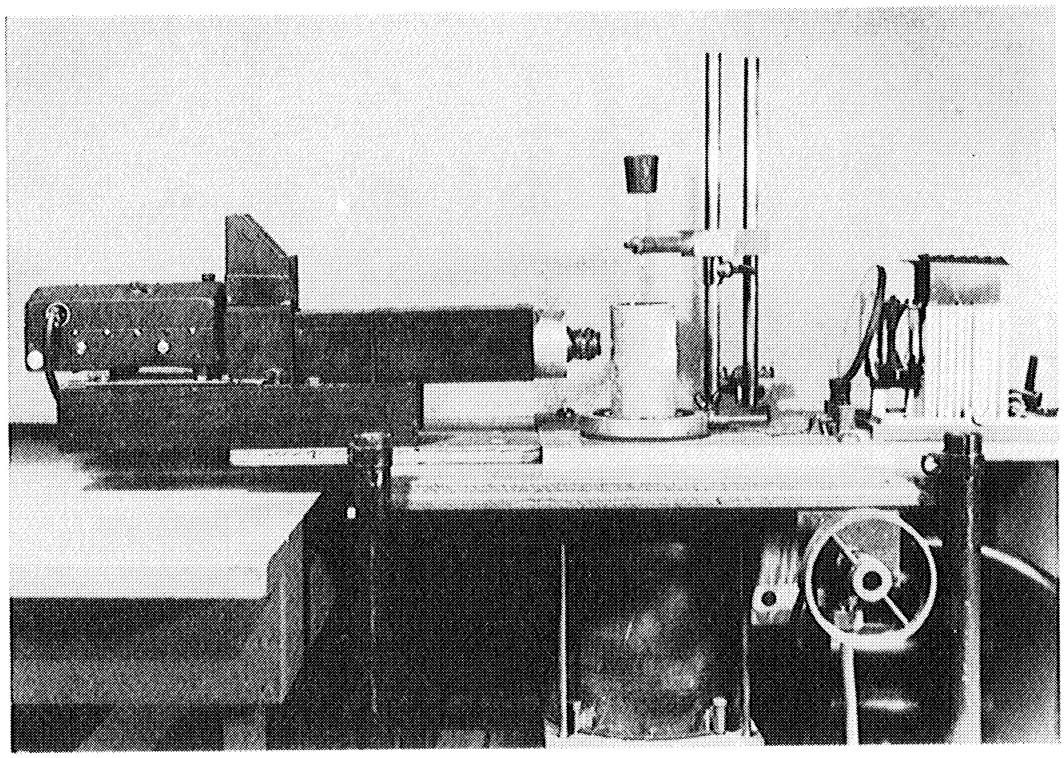

FIG. 21 CLOSE-UP PHOTOGRAPH OF VERTICAL WIND TUNNEL, CAMERA, AND LAMP

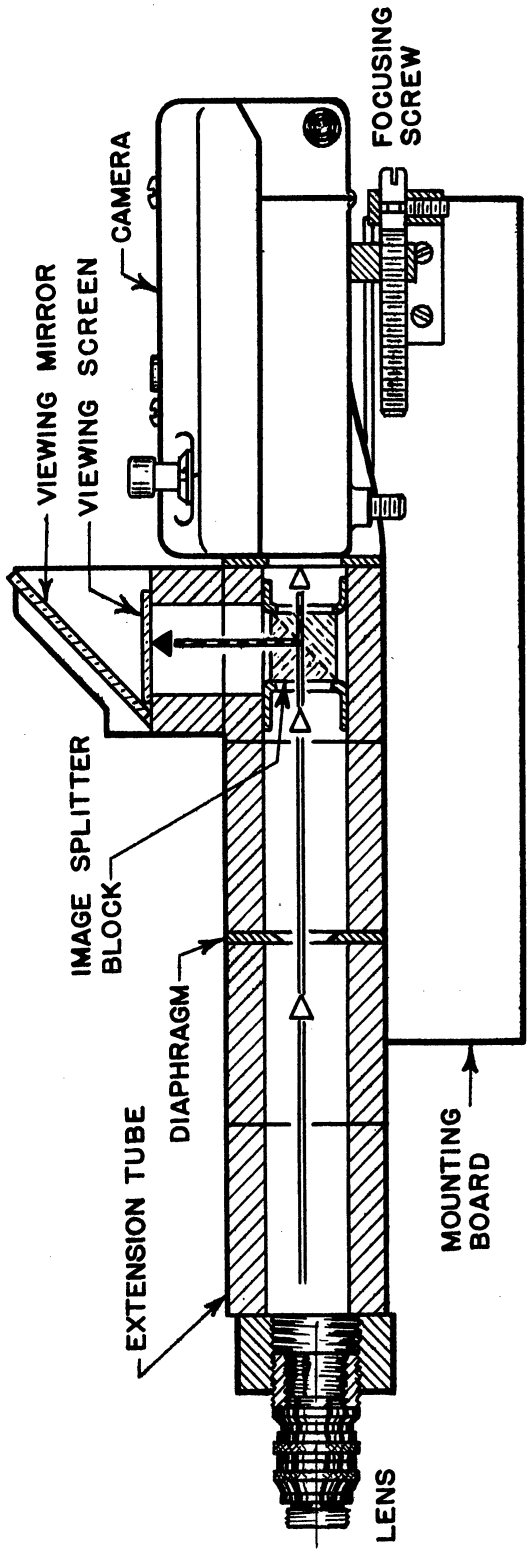

FIG. 22 SECTIONAL VIEW OF LENS EXTENSION TUBE - SHOWN MOUNTED TO CAMERA

transmitted image appears on the 16-mm film. Transparent Scotch Tape is used to frame the field of view of the camera on the viewing screen.

Two right-angle prisms were used to make the image splitter. The hypotenuse of one was half-silvered, then cemented to the hypotenuse of the other, forming a rectangular block. Images produced by the block are much cleaner than those from a simple half-silvered mirror since ghost reflections from the non-silvered surface of the plane mirror are eliminated.

With this arrangement, the drop can be observed in the reflex viewer as it is being photographed, making it possible to control drop position during evaporation.

For critical focusing, a piece of fine ground glass was placed at the plane of focus in a discarded film magazine. The drop image appearing on the ground surface is inspected with a pocket microscope for best focus while turning the lens in its screw mount.

When the camera was first operated, considerable camera vibration developed. It was especially severe during starting periods. Because of the high image magnification used, even slight vibrations resulted in badly-blurred images, making accurate measurements impossible. The problem was solved to a satisfactory degree by altering the camera mount by the addition of soft rubber grommets and loading the camera and extension tube with steel blocks. This lowered the resonant frequency of the system to a point well below the vibration frequency. The decrease in vibration amplitude resulted in satisfactory operation.

2. Photographic Accessories

These include the camera control and power supply box, timer, and background lamp.

A circuit diagram for the camera control box is shown in Figure 23. The control box is used to convert 115-volt, 60 cycle building supply to 25-volts D.C. for camera operation. This is accomplished with a 115:26 step-down transformer and full-wave rectifier. Various switches are used to control the power to the camera, timer, and background lamp.

The timer is an Air Force Camera Intervalometer, type B-5A. This unit can be adjusted to give repetitive time intervals of from zero to 60 seconds in 1/2 second intervals. At the end of each time interval, a short pulse of D.C. power is allowed to pass to the camera, causing it to operate for the duration of the pulse. At a camera speed of 16 frames per second, about eleven frames were exposed during the pulse. Therefore, the timing operation is semi-automatic in that it must be started and stopped. A timer by-pass switch is provided so that the camera can be operated manually, if desired.

Background illumination for the drop is provided by the lamphouse of an Argus 35 mm projector. A 100-watt projection lamp provides more than enough illumination so that good control of light intensity is obtained with a 5-ampere Variac. A piece of heat absorbent glass placed in front of the lamp reduces the radiant heat passing to the ceramic tube. This was felt necessary to protect the tube from overheating. In addition, a red "A" filter placed between the lamp and ceramic tube further reduces the light intensity and decreases the effect of chromatic aberration in the camera lens.

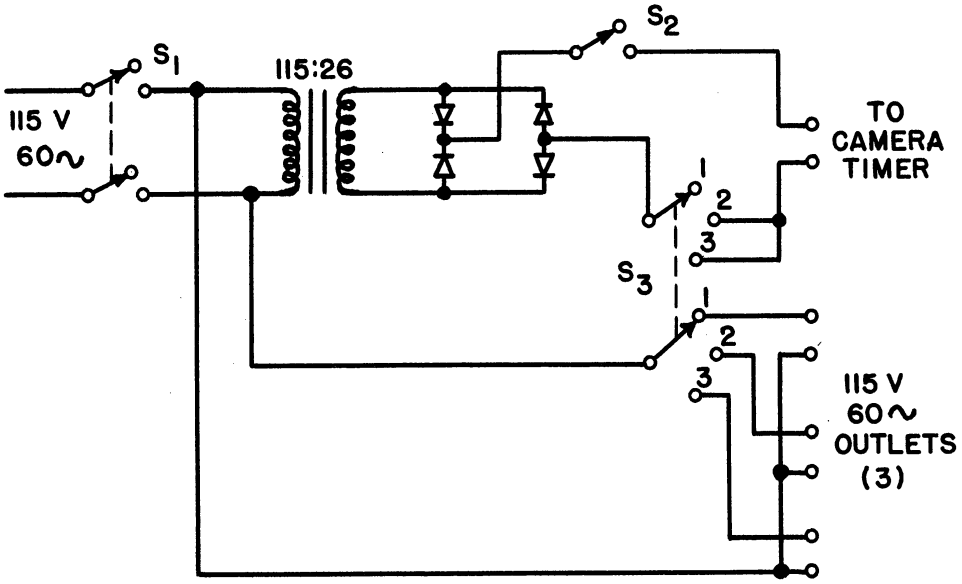

FIG. 23 SCHEMATIC DIAGRAM OF CAMERA POWER SUPPLY

D. Instrumentation and Accessories

The instrumentation and accessories comprise the equipment for measuring ultrasonic frequency, air velocity, and temperature, and the miscellaneous small accessories.

Accurate frequency measurements were made with a Hewlett-Packard electronic counter, Model 521-A, used in conjunction with a Berkley time-interval-meter, Model 5120. The output signal of the variable frequency oscillator, used for driving the barium titanate tube, was also applied to the input of the electronic counter. This instrument counts the events, in this case the voltage oscillations, in a given time interval. However, the time interval used in the counter is based on 60-cycle line frequency and was not accurate enough for use in this case. Therefore, the pulses of both the first and six-thousandth oscillations were fed from the counter to the start and stop connections respectively of the Berkley time-interval-meter. This instrument measures the time interval between two events to within one one-millionth of a second, the timing being based on an accurately-controlled crystal oscillator. The time required for the 5999 oscillations was easily converted to ultrasonic frequency in cycles per second.

Air-flow measurements made with a sharp-edged orifice were used to compute relative air velocities. Orifice and inside pipe diameters are 0.150 in. and 0.375 in. respectively. The pressure drop across the orifice was measured with one of two U-tube manometers, a mercury-filled manometer for large flow rates and one filled with acetylene tetrabromide, s.g. = 2.964, for low flow rates. The latter was used only for

steady-state operations because of the adhesion of the fluid to the tube walls.

Calibration of the orifice by means of suspended drops is described in the next chapter.

A hot-wire anemometer probe, made from a length of ceramic thermocouple-wire shielding, two steel sewing needles, and 0.0005 in. platinum wire, was used for checking the shape of the velocity calibration curve. When used in the bridge circuit shown in Figure 28 the probe provided data for determining velocity variations in accordance with the following equation derived by King,[16]

$$i^2 = i_o^2 + K (\rho_a v)^{1/2} . \qquad (4.1)$$

Air and drop temperature measurements were made with an ordinary copper-constantan thermocouple and precision-type potentiometer. For air measurements, the unshielded thermocouple was placed in the air stream at the exit of the ceramic tube. Drop temperature measurements were made by suspending the drops on a fine thermocouple in air streams of known velocities.

The filament for suspending drops was made by drawing a 7/32 in. glass rod into a fine thread, breaking the thread at a convenient length, and reheating the end to form a slightly bulbous tip. This slight enlargement provided better support for the large drops. A rubber stopper pressed on the rod end of the filament was used to store the unit in a glass tube when not in use, providing protection against breakage.

When in use, the glass filament was supported in the adjustable holder shown in Figure 21. Besides giving lateral and vertical adjustments for drop position, it also provides a rapid means for withdrawing the filament from the tube for cleaning or drop reloading, and repositioning within the tube. The structure also serves as a mount for the thermocouple and filter holders.

A Heathkit vacuum-tube-voltmeter, used for measuring the voltage impressed across the ceramic tube, and an ordinary pocket stopwatch, used for checking the timing of the camera intervalometer, complete the accessories.

CHAPTER V

EXPERIMENTAL TEST PROCEDURE

A. Orifice Calibration

Calibration of the air-metering orifice was based entirely on drag-coefficient data for solid spheres. The method for computing terminal velocities for spheres of given diameter and specific weight is outlined in Reference 2. It is based on the fact that the drag equation

$$\log C_D = \log \frac{4g\,(\rho - \rho_a)\,D^3\,\rho_a}{3\mu_a^2} - 2 \log Re\ , \qquad (5.1)$$

which is derived from the equation of motion for spheres subjected to gravitational, buoyancy, and drag forces, plots as a straight line with slope of -2 on log C_D vs. log Re coordinates. This equation can be solved when either Re or C_D is set equal to unity since all quantities but C_D and Re are known.

To obtain the terminal velocity for a given drop size, Equation (5.1) is solved for Re by setting $C_D = 1$ and substituting the proper values for D and the other known physical constants. The corresponding straight line, having a negative slope of 2 and passing through the point whose coordinates are the computed Reynolds number and $C_D = 1$, is drawn on a log-plot showing the experimental drag coefficient curve for solid spheres as a function of Reynolds number. Such a plot is shown on page 16 of Reference 11.

The intersection of the straight line with the drag coefficient curve locates the only solution which satisfies both the equation and the experimental drag coefficient curve. The terminal velocity is computed from the value of Re at the point of intersection.

Results for cumene drops are shown plotted in Figure 24, giving terminal velocity as a function of drop diameter.

To relate this information to orifice pressure measurements, test results were obtained giving the diameter of freely-suspended drops as a function of orifice pressure drop. Test data, given in Table VII are plotted in Figure 25.

TABLE VII

ORIFICE PRESSURE DROP VERSUS FREE-DROP DIAMETER

Δp in. Hg	D microns	Δp in. Hg	D microns
25.3	757	11.9	525
23.8	739	9.9	472
21.9	698	7.9	436
19.9	682	5.9	379
17.9	631	3.95	325
15.9	595	1.95	240
13.9	568	1.24	212

For this test, n-butyl benzene was used in place of cumene because of its identical specific gravity (sp. gr. = 0.866) but much slower rate of evaporation. (See Table VI.) The latter was intended to reduce the possible effects of evaporation on drag.

By cross-plotting the information in Figures 24 and 25, the desired result was obtained giving air velocity as a function of orifice pressure drop. This result and the corresponding empirical equation are shown in Figure 26.

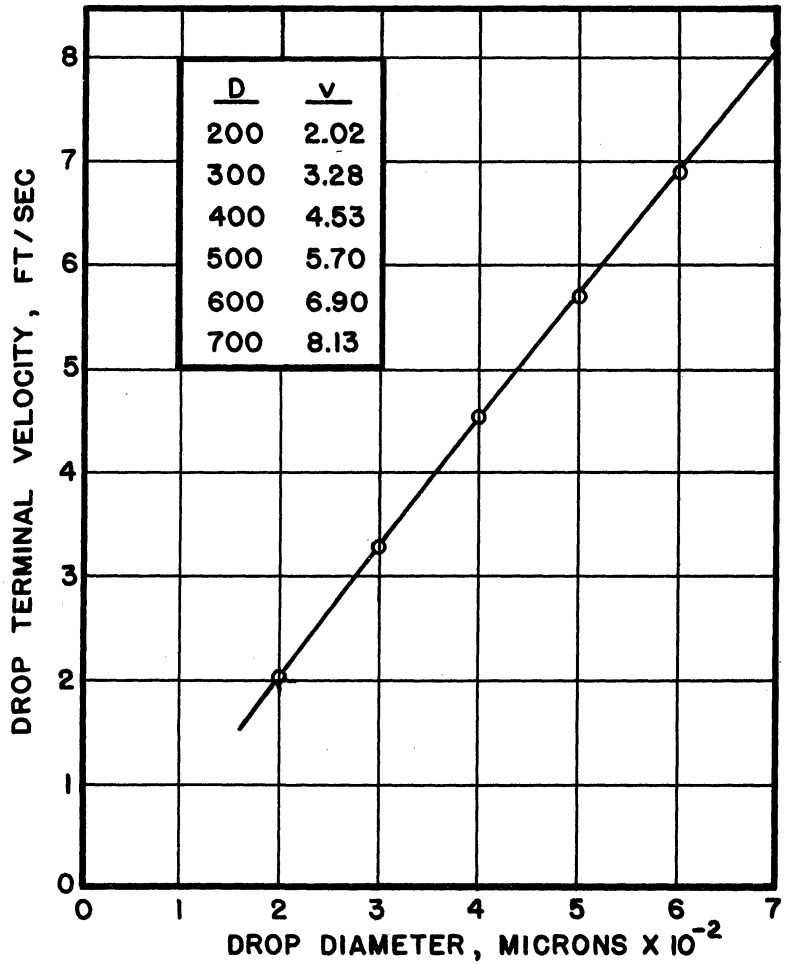

FIG. 24 DROP TERMINAL VELOCITY DETERMINED FROM DRAG COEFFICIENT CURVE, REF.

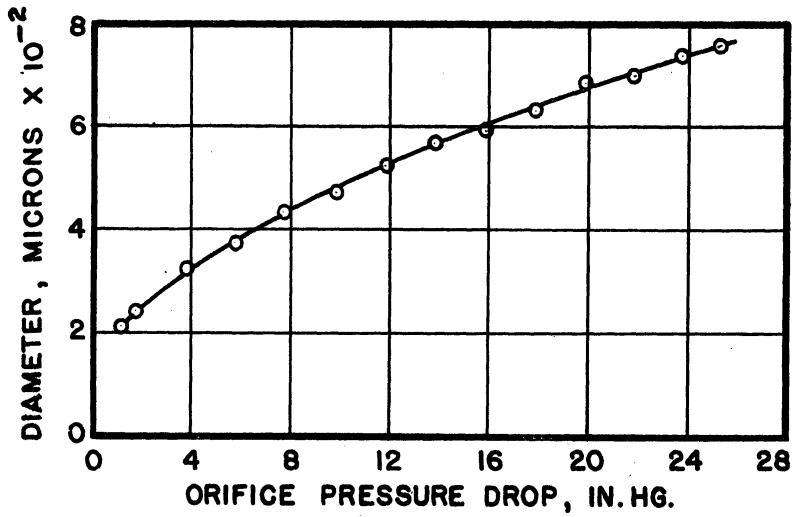

FIG. 25 RELATIONSHIP BETWEEN DROP DIAMETER AND ORIFICE PRESSURE DROP

In addition to providing relative air velocity data, the velocity information was also used for calibrating a hot wire probe. The probe was used for some preliminary velocity measurements and velocity profile explorations. The calibration was based on King's equation (4.1) which states that the square of the hot wire heating current is a linear function of the square-root of the air velocity. Figure 27 shows the linear calibration curve obtained from the experimental data tabulated in Table VIII. The schematic diagram of the hot wire anemometer circuit is given by Figure 28.

TABLE VIII

EXPERIMENTAL DATA FOR HOT-WIRE CALIBRATION

i^2 $(ma)^2$	Δp in. Hg	v ft/sec	$v^{1/2}$ $(ft/sec)^{1/2}$
1.44×10^4	0	0	0
1.56	0.04	0.37	0.61
1.62	0.09	0.52	0.72
1.69	0.18	0.74	0.86
1.73	0.26	0.90	0.95
1.80	0.44	1.16	1.08
1.88	0.88	1.64	1.28
1.96	1.32	2.02	1.42
2.00	1.76	2.32	1.52
2.03	2.20	2.60	1.61
2.10	3.08	3.08	1.71
2.20	3.96	3.50	1.87
2.25	6.0	4.30	2.07
2.31	8.0	4.96	2.23
2.40	10.0	5.55	2.36
2.50	14.0	6.56	2.56
2.60	20.0	7.85	2.80

B. Drop-Size Measurements

Because of the distortion of drop shape caused by the filament suspensions used in the fixed-drop evaporation tests, it was necessary to

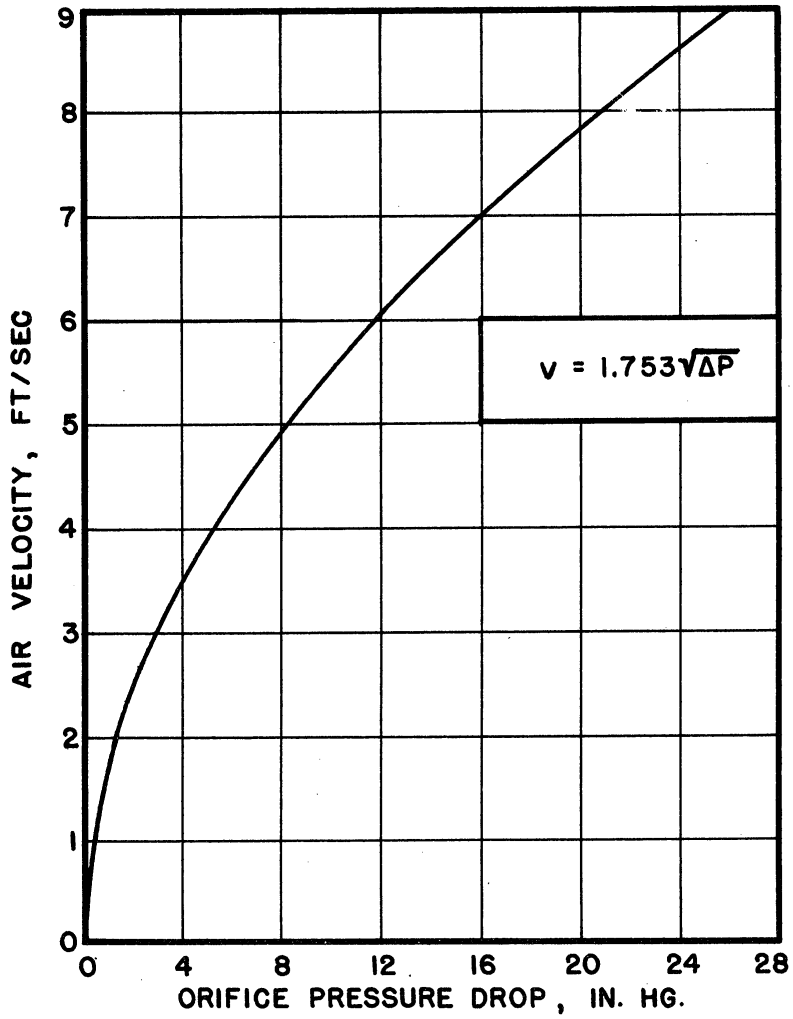

FIG. 26 RELATIONSHIP BETWEEN AIR VELOCITY AND ORIFICE PRESSURE DROP

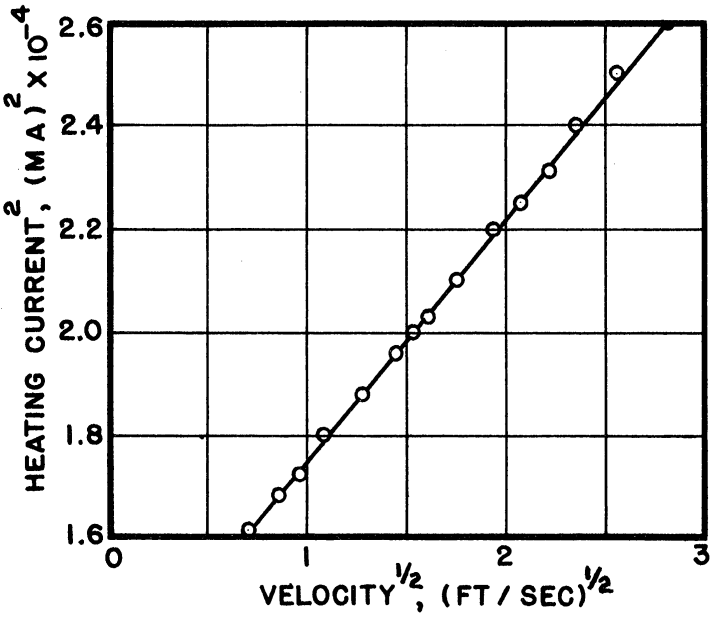

FIG. 27 RELATIONSHIP BETWEEN HOT WIRE HEATING CURRENT AND AIR VELOCITY

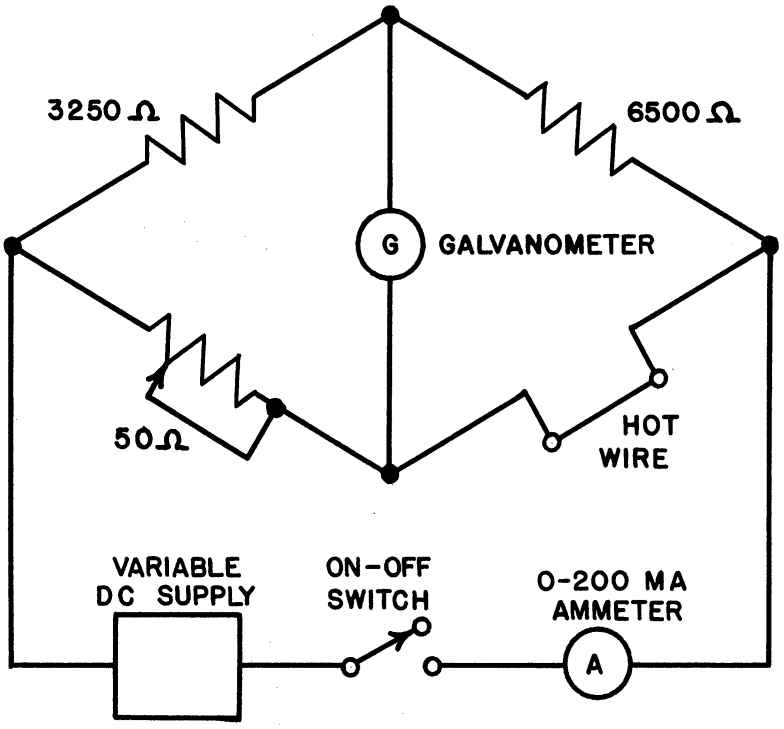

FIG. 28 SCHEMATIC DIAGRAM OF HOT WIRE ANEMOMETER CIRCUIT

determine which of the many possible drop-size measurements would lead to the best approximation of drop volume. By tracing on fine coordinate paper the outlines of several enlarged drop images, covering the range of sizes encountered in these tests, it was possible to determine the volume of each size by graphical integration. These values were compared to the volumes obtained from diameters measured at various positions and inclinations on the image and it was found that the average diameter obtained from the two measurements made at 45 degrees from the horizontal position gave the best results for all sizes. Therefore, all drop-size measurements in this investigation were obtained in this manner.

Magnification factors for each evaporation run were obtained by comparing the photographic image and actual sizes of a fine wire. Since variations in film shrinkage, time of exposure, and film development affect film image size, photographs of the wire were taken at the beginning of every run.

C. Experimental Test Procedure

The equipment, set up and connected as shown in Figure 13 and 14, is ready for a test run. About forty-five minutes before the run is to be made, the amplifier, oscillator, and variable D.C. supply are turned on and allowed to warm up. During this time the camera lens is opened, set to about f/4.5, and the focusing screen inserted into the film magazine compartment. The background light for the drop, after being turned on, is positioned to give the best field of illumination when viewed on the viewing screen in the lens extension tube.

With the air turned on at a relatively low velocity and the ultrasonic supply warmed up, the oscillator is tuned to the approximate

resonant frequency of the transducer tube, approximately 35,000 cps, and the voltage across the tube adjusted to about 20 volts by varying the D.C. supply. A small diameter wire, glued to the end of a fine thread, is lowered into the tube and the oscillator frequency varied until the wire is suddenly "grasped" by the sound field and held in a fixed position. The voltage is again adjusted to about 20 volts and a fine frequency adjustment is made to increase the grasp if possible. When the adjustment is correct the ultrasonic field will hold the wire in position against moderate shifts of the thread suspension.

A glass eye-dropper, drawn to a fine tip, is then filled with a liquid of relatively low volatility, such as kerosene, and the drops are shaken from the dropper into the tube directly above the node previously occupied by the wire. If the majority of the drops fall, the air velocity is increased; if they rise, the velocity is decreased. It will be found that eventually some drops become suspended in the air stream. The air velocity is further adjusted until the drop occupies a position between the two windows in the tube and becomes visible on the viewing and focusing screens. Viewing the image on the focusing screen with a pencil-type microscope, about 20X, the lens is adjusted to bring the image into sharp focus. The filament suspension, mounted in its holder, is then located in the tube so that it is centered in the field of view of the camera and properly focused.

Before each run is made, the following readings and settings are checked:

air temperature,

critical frequency setting,

air velocity setting,

voltage (sound field intensity),

camera focus,

camera speed,

lens opening,

lamp control (variac) setting,

intervalometer setting.

Photographs are then taken of the test number, wire for size determination, and the evaporating drop suspended on the filament, in that order.

For taking the drop pictures, the drop is attached to the filament by means of a fine eye-dropper. The filament is immediately lowered into the tube and the camera and stop-watch started simultaneously. Under the control of the intervalometer, the camera photographs the evaporating drop at fixed time intervals. At the start of the last series of photographs, the stop-watch is stopped, providing a check on the timing of the intervalometer.

The drop temperature for cumene was assumed to be 4.5°F lower than the temperature of the air stream. The value was based on experimental results obtained in this investigation and was found to hold for the small range of air temperatures encountered in these tests.

After development, the film was projected in a microfilm reader where the drop-size measurements were made. These data, together with the corresponding time measurements, are tabulated in Appendix B.

The procedure used for the free-drop tests was similar to the one just described for fixed-drops. However, in the test with free drops no filament suspension is required to support the drop, and the free drops are "falling" at their terminal velocity with respect to the air stream throughout the evaporation process.

CHAPTER VI

DISCUSSION OF RESULTS

The expression for Nu, based upon the heat-transfer processes occurring across an assumed equivalent thermal boundary-layer, was modified by boundary-layer considerations to give,

$$Nu = \alpha \left[2 + f\,(Pr)^{1/3}\,(Re)^{1/2}\right] . \qquad (2.43)$$

In general, the form of this result is in agreement with the expressions for Nu obtained by others, notably Frössling,[5] Equation (1.5); Ranz and Marshall,[26] Equation (1.9); Ingebo,[14] Equation (1.13); and Kinzer and Gunn,[17] Equation (1.16). However, the Equation (2.43) does contain an additional factor α not found in the other expressions. An inspection of Equations (2.42) and (2.17), defining α and the expansion for the ln term in the evaporation equation, shows that the value for α is very nearly equal to unity for low temperature evaporation, i.e., when the expansion given by Equation (2.17) is very closely approximated by the first term alone. In fact, if only the first term of the expansion is considered, α becomes equal to unity and Equation (2.43) reduced to

$$Nu = \left[2 + f\,(Pr)^{1/3}\,(Re)^{1/2}\right] . \qquad (6.1)$$

With an increase in $(T_f - T)$, as for high temperature evaporation or combustion, the other terms of the expansion cannot be neglected, and α becomes an important factor in the expression for Nu. For these cases, instead of using the expansion, it becomes more convenient to use Equation (2.42), giving α in terms of $\ln\left[1 + c\,(T_f - T)/L\right]$ directly.

The term α arises because of the effect of mass transfer on the heat-transfer process. Consider the case of a drop evaporating under the influence of a fixed-temperature difference. If in some manner the evaporated vapor could be collected right at the drop surface, the maximum amount of heat would reach the surface. However, if the vapor were allowed to diffuse away from the drop, the heat reaching the surface would be reduced by the amount required to heat the vapor to the ambient temperature. This heat loss should be indicated by a decrease in the Nusselt number for the process, and it seems quite appropriate that the loss would be goverened by the latent heat of the liquid, the specific heat of the vapor, and the temperature difference between the drop surface and ambient air stream, as given by the factor α.

The term f in the expression for Nu is the only empirical factor appearing in the evaporation equations derived in Chapter II. Therefore, it was necessary to evaluate f from experimental results. Since its appearance was based on a simplified boundary layer, it would be difficult to reduce the factor to more fundamental quantities of the physical system--unless a more thorough and certainly more involved study were made of the actual dynamic and thermal boundary layers. The simplified spherical boundary layers would quite probably have to be discarded in such a study.

In the evaluation of f from the experimental results for evaporation at constant velocity, it was assumed that f was a function of velocity only. This was necessary for solving the integral in Equation (2.24). The assumption can hardly be considered drastic in view of the fact that all of the investigators mentioned above except Kinzer and Gunn indicate that f is a fixed constant for all cases.

The results of this investigation are listed in Table V and show f varying with velocity, the variation being quite small for velocities greater than 4 ft/sec. The general shape of the curve obtained from these data is quite similar in some respects to the one given by Kinzer and Gunn for their factor F in Equation (1.16). Their curve continues to rise for smaller velocities, then quite suddenly drops to almost zero at very low velocities. (Their result is actually plotted as a function of drop diameter for freely-falling drops.)

No sound theoretical reason can be given at this time for the behavior of f. Since f is associated with the formation of the boundary film, the explanation will no doubt come from a closer examination of the theory describing the flow around drops.

A correlation of the evaporation data for fixed drops of cumene evaporating into air streams of constant velocity and no ultrasonic field is given by Figure 55 in Appendix D. The fact that f is not a fixed constant for all cases gives rise to the separate curves for each of the test velocities.

The values for Nu shown in Figure 55 are considerably higher than those reported in the literature. This is also apparent when comparing the expressions for Nu and noting that the minimum value obtained for f in this investigation is almost three times the value reported by Ranz and Marshall.[26] It is quite probable that the agreement would have been closer if some other method of air velocity calibration had been used. By assuming equal drag coefficients for both solid and liquid spheres the resulting calibration no doubt gives velocity measurements that are somewhat low. Any correction would increase the value of the velocity, increase the Reynolds number, decrease f, and shift the curves in Figure 55 to the right.

This would bring the results closer to the values for Nu given in the literature.

When the evaporation process is described in terms of drop diameter and elapsed time of evaporation, the theoretical equation for the process is given by

$$[D^2 - D_o^2] - 2 \int_{D_o}^{D} \frac{D^2}{D_f} \, d(D) = -\frac{8k}{\rho c} \ln \left[1 + \frac{c\,(T_f - T)}{L}\right] t \,, \qquad (2.24)$$

where the dependence of D_f upon D is required for a complete solution. If D/D_f is assumed constant throughout the evaporation process for a single drop, the above equation becomes identically equal to the result obtained by Godsave,[8] that is,

$$D^2 = D_o^2 - \lambda t \,; \qquad (1.10)$$

where λ is given by Equation (2.28).

The experimental results obtained in this investigation indicate that the value of the exponent in the above equation is not constant for all conditions and certainly not equal to two except, possibly, for evaporation into stagnant air. This is also indicated by Ingebo[14] who shows that for Nu > 10, which would correspond to large values of Re, the total vaporization time is given by

$$t_t = C D_o^{1.4} \qquad (6.2)$$

The result predicts the value n = 1.4 for the exponent in Equation (1.10) and corresponds to the value n = 1.47 found in this investigation for maximum velocity. Therefore, the assumption that D/D_f = constant for all cases appears to be incorrect or only an approximation at best.

By basing the relationship between D_f and D upon boundary layer considerations for the evaporation of fixed drops in a constant velocity

air stream, a second solution to Equation (2.24) was obtained and is given by,

$$\left.\begin{aligned}(D_o^{3/2} - D^{3/2}) - \frac{3}{2} C (D_o - D) + 3C^2 (D_o^{1/2} - D^{1/2}) - 3C^3 \ln \left(\frac{D_o^{1/2} + C}{D^{1/2} + C}\right) \\ = \frac{6k}{C\rho c} \ln \left[1 + \frac{c (T_f - T)}{L}\right] t\end{aligned}\right\} \quad (2.51)$$

where

$$C = \frac{2}{f (Pr)^{1/3} (v/\nu)^{1/2}} . \quad (6.2)$$

The equation shows good agreement with experimental results as indicated in Table XXX and illustrated in Figure 56 in Appendix D. It should be pointed out that the experimental checks were made for those runs from which the values of f were evaluated, demonstrating that the equation accurately predicts the "shape" of the evaporation curves. The same degree of accuracy could not be expected to hold for the other tests at similar conditions because of the spread in experimental results for fixed conditions, as shown in Table II.

The effects on evaporation of the various factors involved in the heat transfer and evaporation processes are easily determined from an inspection of Equations (2.8) and (2.43). It is apparent that the variation in f becomes an important factor in establishing the value for Nusselt's number. Also, as the temperature difference between the drop and its surroundings increases, the factor α becomes increasingly more important in evaluating Nusselt's number and should not be neglected for these cases.

The introduction of ultrasonic energy into the evaporation process greatly increased the complexity of the problem by both direct and indirect means.

Figures 6 and 7 show the effect on evaporation of increasing field intensity. In general, as the intensity increased the rate of evaporation also increased. However, the opposite effect was also found at low intensities. While no satisfactory explanation can be found for this effect, it is believed that the increase in evaporation with an increase in field intensity is due to the turbulent-like character of the ultrasonic field. This characteristic causes a break-up of the laminar boundary layer surrounding the drop and increases both the temperature and vapor-concentration gradients next to the drop, thereby increasing the rates of both the heat and mass transfer processes.

A change in ultrasonic frequency appears to have an indirect effect on evaporation through its effect on the "tuning" of the ceramic tube. For a given impressed voltage, the tube will generate its field of maximum intensity at its resonant frequency. As the frequency shifts from this critical value the amplitude of vibration of the tube will diminish, lowering the field intensity and drop evaporation rate. However, Figure 8 shows that for a large shift from the critical frequency the evaporation rate drops below the value given for evaporation at zero field intensity--an effect that certainly was not expected and is hard to explain. The same effect was obtained for the two series of tests taken at different relative air velocities and shown in Figure 8.

An additional indirect effect on evaporation is due to the shift in critical frequency with a change in relative air velocity. Results of

experimental tests are shown in Figure 9. Over the range of velocities used in the evaporation tests, the critical frequency decreases with increasing velocity. This behavior appears to be due to the cooling effect of the air stream on the tube.

A large part of the heat generated within the tube wall by internal friction is given up to the air stream, the rate of heat transfer increasing with increasing velocity. Since resonance of the tube is established when the mean circumference is equal to one wavelength of sound within the ceramic, and since sonic velocity increases with temperature, the resonant frequency must increase with an increase in temperature, i.e., a decrease in relative air velocity.

The evaporation rate of a free-drop evaporating in an ultrasonic field such as used in this investigation would be influenced by all of the factors mentioned above. With reference to Figure 9, consider an evaporating free-drop initially at the critical frequency corresponding to the existing initial velocity. Since the frequency is not changed during the test, the evaporation process takes place from right to left along a horizontal line on Figure 9. In moving from right to left during evaporation, the effect of the ultrasonic field will decrease as the critical frequency gets higher and higher with respect to the set frequency. However, the normal rate of change of diameter increases as the drop size decreases, as shown in Figure 3. The two effects appear to cancel one another, giving the linear evaporation curves shown in Figures 10 and 11.

The results giving the effects of ultrasonic energy on drop evaporation must be considered as preliminary at this time, since it

appears that no other investigation of this topic has been made. The experimental equipment and test procedure were exploratory in nature. Many improvements in both are contemplated.

Many of the difficulties encountered in taking test data arose from the extreme sensitivity of the evaporation process to slight changes in some of the variables associated with the ultrasonic system. The results appear to be especially sensitive to:

(a) Location of the drop with respect to the sound node,

(b) Variations of impressed frequency. The effect of slight variations around the critical value is quite evident in Figure 8.

(c) Variations in ceramic tube temperature. No control was imposed during these tests.

CHAPTER VII

CONCLUSIONS AND RECOMMENDATIONS

A. Conclusions

Experimental results for drops suspended on a fine glass filament in a moving air stream indicate that elapsed time of evaporation is a linear function of D^2 only when evaporation takes place into stagnant air.

For evaporation into a moving air stream the experimental results are closely approximated by a linear function of D^n versus elapsed time. The value of n was found to decrease with an increase of relative air velocity and approached a limiting value between 1.45 and 1.5 for high velocities. The evaporation process is closely approximated by the equation

$$D^n = D_o^n - \lambda t \qquad (3.2)$$

where n is a function of relative air velocity.

The analysis of the heat transfer process during drop evaporation, modified by boundary-layer considerations, led to the following expression for Nusselt's number:

$$Nu = \alpha \left[2 + f\,(Pr)^{1/3}\,(Re)^{1/2}\right], \qquad (2.43)$$

where α is a function of the temperature difference between the drop surface and the surroundings, latent heat of the liquid, and specific heat of the vapor; f is a semi-empirical factor to be determined experimentally.

When expressed in terms of drop diameter, the evaporation equation obtained from the analysis of the heat transfer process is given by

$$\left[D^2 - D_o^2\right] - 2 \int_{D_o}^{D} \left(\frac{D^2}{D_f}\right) dD = -\frac{8k}{\rho c} \ln\left[1 + \frac{c\,(T_f - T)}{L}\right] t \,. \qquad (2.24)$$

For the assumption (D/D_f) = constant, Equation (2.24) becomes equal to the result obtained by Godsave,[8] i.e.,

$$D^2 - D_o^2 = -\lambda t \tag{2.27}$$

where

$$\lambda = \frac{8k}{\rho c}\left(\frac{D_f}{D_f - D}\right) \ln\left[1 + \frac{c\,(T_f - T)}{L}\right] t\,. \tag{2.28}$$

When the expression for (D/D_f) is obtained from boundary layer considerations for evaporation at constant relative air velocity, Equation (2.24) becomes

$$(D_o^{3/2} - D^{3/2}) - \frac{3}{2} C\,(D_o - D) + 3C^2\,(D_o^{1/2} - D^{1/2}) - 3C^3 \ln\left(\frac{D_o^{1/2} + C}{D^{1/2} + C}\right) \tag{2.51}$$

$$= \frac{6k}{C\rho c} \ln\left[1 + \frac{c\,(T_f - T)}{L}\right] t$$

where C is given by Equation (6.2). The agreement between Equation (2.51) and the experimental results is good, as indicated in Figure 56.

The factor α must be considered when evaluating Nusselt's number for drops evaporating in high temperature atmospheres.

The use of equal drag coefficients for liquid and solid spheres in the calibration of relative air velocity apparently has resulted in low values for relative air velocity.

Results obtained with drops evaporating in an ultrasonic field show that the evaporation rate is affected by the field, the effect being dependent on both field intensity and frequency. The combined action of the ultrasonic field and relative air velocity on the evaporation of freely suspended drops is such as to make drop diameter a linear function of elapsed time of evaporation.

A correlation between normal evaporation and evaporation within the ultrasonic field has not yet been established because of the complex nature by which the field effects are dependent upon such parameters as relative air velocity, field frequency and intensity, temperature of the barium titanate tube and location of the drop with respect to the sound node.

The investigation of the effects of ultrasonic energy on evaporation cannot be considered more than exploratory in nature. Only a start has been made on a new technique for studying and possibly controlling evaporation and combustion of liquid fuel drops. Further developments are required to gather additional information on the exact mechanism by which the ultrasonic field affects the evaporation process.

B. Recommendations

1. The equipment described in this dissertation can be used to obtain accurate drag coefficient data for evaporating liquid drops or solid particles. An accurate measure of relative air velocity is required.

2. High intensity ultrasonic energy is capable of breaking up large drops. This phenomenon should be investigated as a possible aid to fuel atomization and evaporation.

3. It appears that high-frequency, high-intensity ultrasonic energy may provide a relatively simple means for obtaining greatly improved mixing in a fuel spray, thereby leading to higher combustion rates. This possibility should be investigated.

4. An investigation should be made concerning the possibility of building similar equipment for operation at high temperatures. Application to single drop combustion studies would, no doubt, lead to many interesting results.

5. A complete check of the evaporation Equation (2.51) is required for a wide range of conditions, either with original data, or with existing data obtained by other investigators and recorded in the literature. Its application to combustion should be checked.

6. The manner in which the evaporation rate is made to fall below the normal rate at certain frequencies was quite unexpected and should be investigated.

APPENDIXES

APPENDIX A

DERIVATION OF THE EXPRESSION FOR DETERMINING EXPONENT n FROM THE EXPERIMENTAL RESULTS

The equation

$$(t_t' - t) = K_1 + K_2 D^n \tag{A-1}$$

in three unknowns K_1, K_2, and n is applied to the experimental curves of drop diameter versus elapsed time of evaporation. Three positions on the curves are required to solve for the three unknowns; these positions are designated by the drop diameters D_x, D_y, and D_z. With reference to Figure 3, the equations for the three positions are given by

$$t_t' - t_x = x = K_1 + K_2 D_x^n \tag{A-2}$$

$$t_t' - t_y = y = K_1 + K_2 D_y^n \tag{A-3}$$

$$t_t' - t_z = z = K_1 + K_2 D_z^n . \tag{A-4}$$

From Equation (A-4) we obtain

$$K_1 = z - K_2 D_z^n . \tag{A-5}$$

This result is substituted in Equations (A-2) and (A-3) to give

$$x = z - K_2 (D_z^n - D_x^n) \tag{A-6}$$

and

$$y = z - K_2 (D_z^n - D_y^n) . \tag{A-7}$$

Solving for K_2 in both of these equations gives

$$K_2 = \frac{z - x}{D_z^n - D_x^n} = \frac{z - y}{D_z^n - D_y^n} \tag{A-8}$$

which reduces to

$$(y - x) D_z^n - (z - x) D_y^n + (z - y) D_x^n = 0 . \tag{A-9}$$

Upon dividing by (y - x),

$$D_z^n - \frac{z - x}{y - x} D_y^n + \frac{z - y}{y - x} D_x^n = 0 . \qquad (A.10)$$

If we let

$$\frac{z - x}{y - x} = 1 + K , \qquad (A.11)$$

then

$$\frac{z - x}{y - x} - \frac{y}{y - x} + \frac{y}{y - x} = \frac{z - y}{y - x} + \frac{y - x}{y - x} = \frac{z - y}{y - x} + 1 , \qquad (A.12)$$

so that

$$\frac{z - y}{y - x} + 1 = 1 + K , \qquad (A.13)$$

or

$$K = \frac{z - y}{y - x} . \qquad (A.14)$$

By substituting Equations (A.11) and (A.14) into Equation (A.10) and dividing through by D_x^n, Equation (A.10) becomes

$$\left(\frac{D_z}{D_x}\right)^n - (1 + K) \left(\frac{D_y}{D_x}\right)^n + K = 0 . \qquad (A.15)$$

This expression is solved for K, giving K in terms of the drop diameters at the three positions and n,

$$K = \frac{(D_z/D_x)^n - (D_y/D_x)^n}{\left(\frac{D_y}{D_x}\right)^n - 1} . \qquad (A.16)$$

If the diameter ratios are selected so that

$$\frac{D_z}{D_x} = \left(\frac{D_y}{D_x}\right)^2 , \qquad (A.17)$$

then substitution gives

$$K = \frac{(D_y/D_x)^{2n} - (D_y/D_x)^n}{(D_y/D_x)^n - 1} \qquad (A.18)$$

so that upon factoring we obtain

$$K = \frac{(D_y/D_x)^n \left[(D_y/D_x)^n - 1\right]}{(D_y/D_x)^n - 1} \qquad (A.19)$$

or

$$K = \left(\frac{D_y}{D_x}\right)^n . \qquad (A.20)$$

This is solved for n by taking the $\log_{10}$ of both sides, giving the result

$$n = \frac{\text{Log } K}{\text{Log } (D_y/D_x)} . \qquad (A.21)$$

If we select

$$D_x = 400 \text{ microns},$$

$$D_z = 1000 \text{ microns},$$

then

$$\frac{D_z}{D_x} = 2.5 \qquad (A.22)$$

and

$$\frac{D_y}{D_x} = \left(\frac{D_z}{D_x}\right)^{1/2} = 1.581 . \qquad (A.23)$$

The diameter at y is then computed to be,

$$D_y = 1.581\ D_x = 632.5 \text{ microns} . \qquad (A.24)$$

Substitution in Equation (A.21) finally leads to the result

$$n = \frac{\text{Log } K}{\text{Log } (1.581)} = \frac{\text{Log } K}{0.199} , \qquad (A.25)$$

where K is given in terms of the measured quantities x, y, and z by Equation (A.14).

Tabulated results from the experimental part of the study are given in Table I.

APPENDIX B

EXPERIMENTAL EVAPORATION CURVES AND DATA

On Figures 29 through 54, the following dimensions apply to the various quantities:

velocity (v)	f/sec,
voltage (V)	volts A.C. (rms),
temperature (T)	°F,
x (measured at 400μ)	constant x seconds,
y (measured at 700μ)	constant x seconds,
z (measured at 1000μ)	constant x seconds,
evaporation constant (λ)	(microns x 10^{-2})^n/sec.

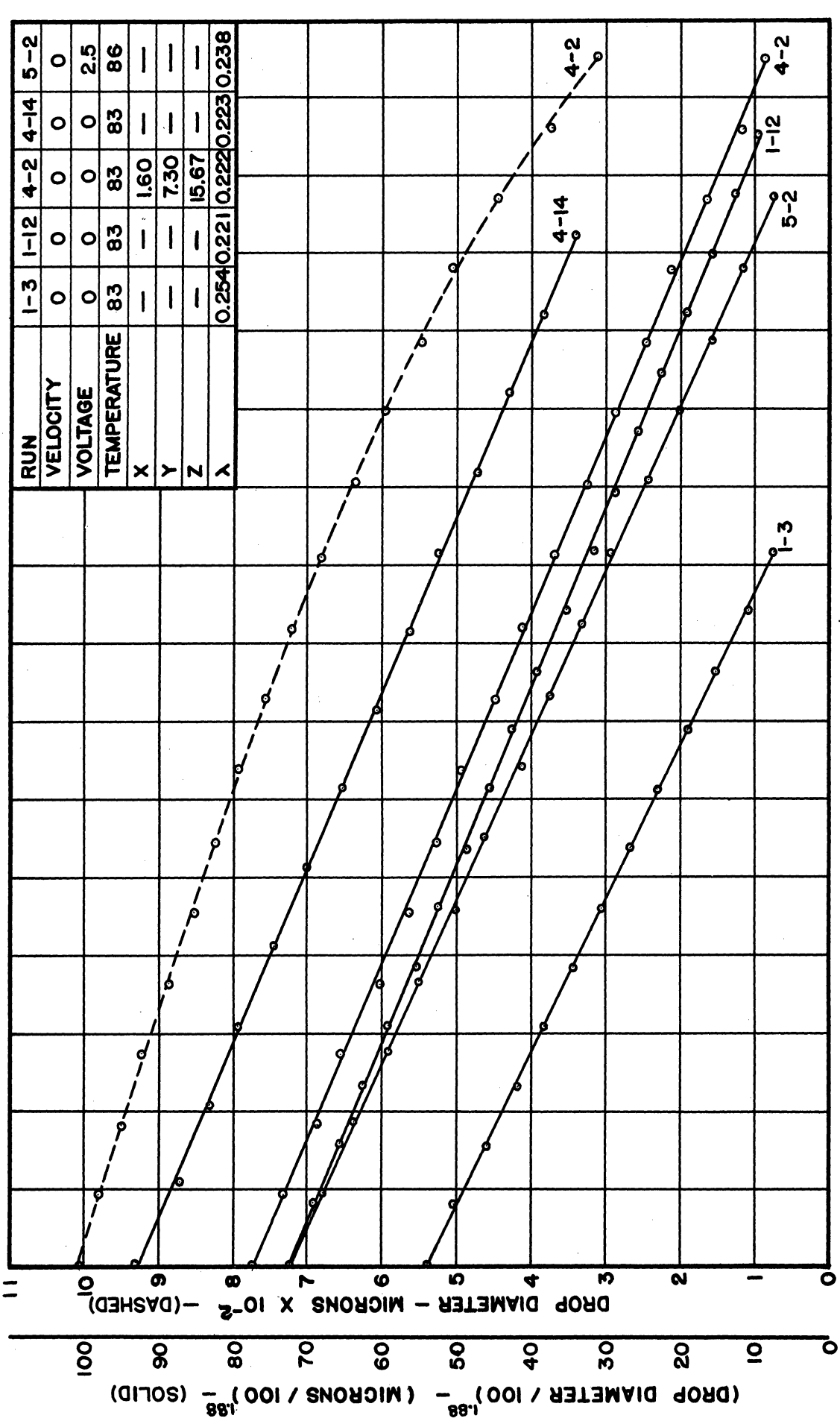

FIG.29 EVAPORATION CURVES FOR FIXED DROPS - CUMENE (v = 0 ft/sec)

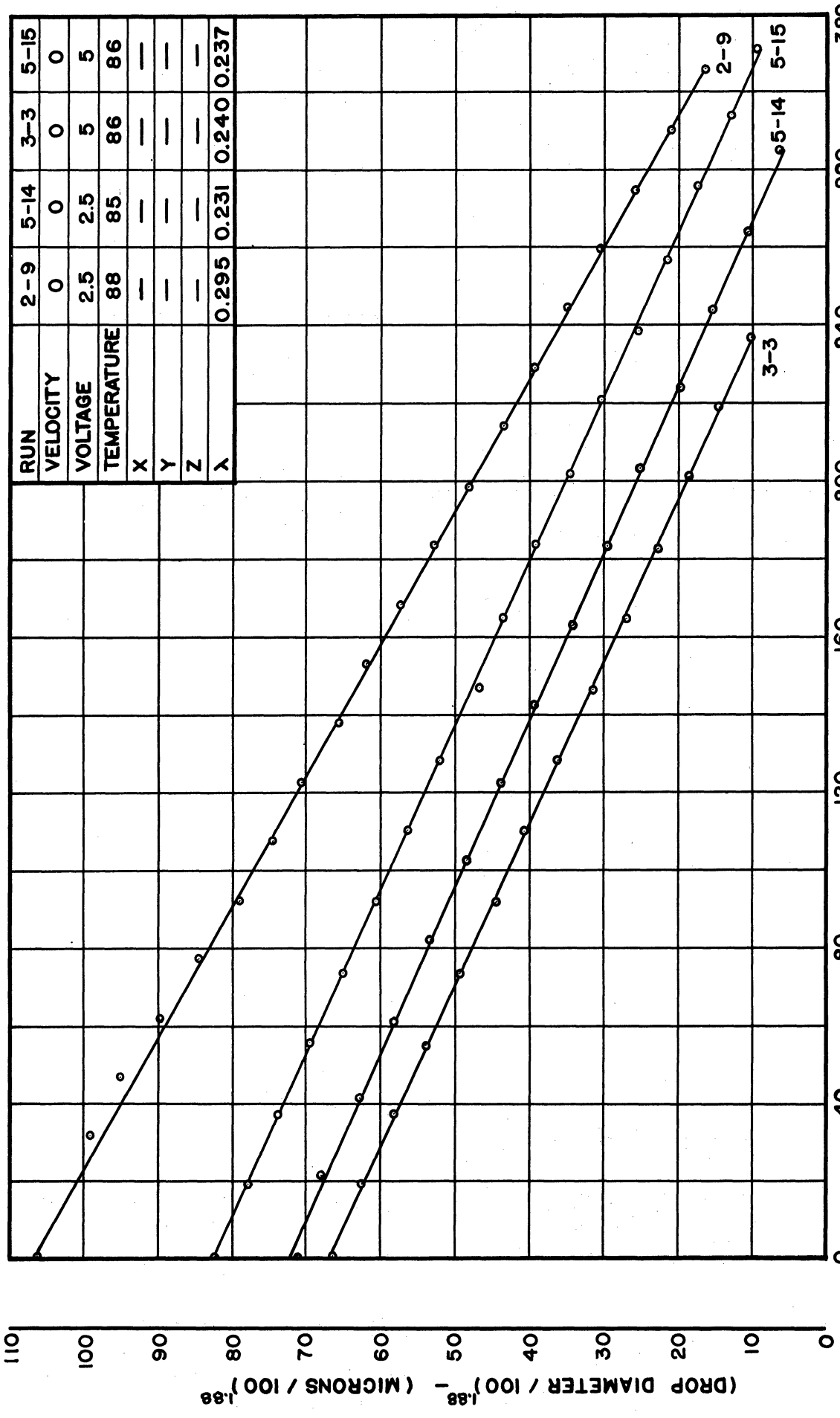

FIG.30 EVAPORATION CURVES FOR FIXED DROPS - CUMENE (v = 0 ft/sec)

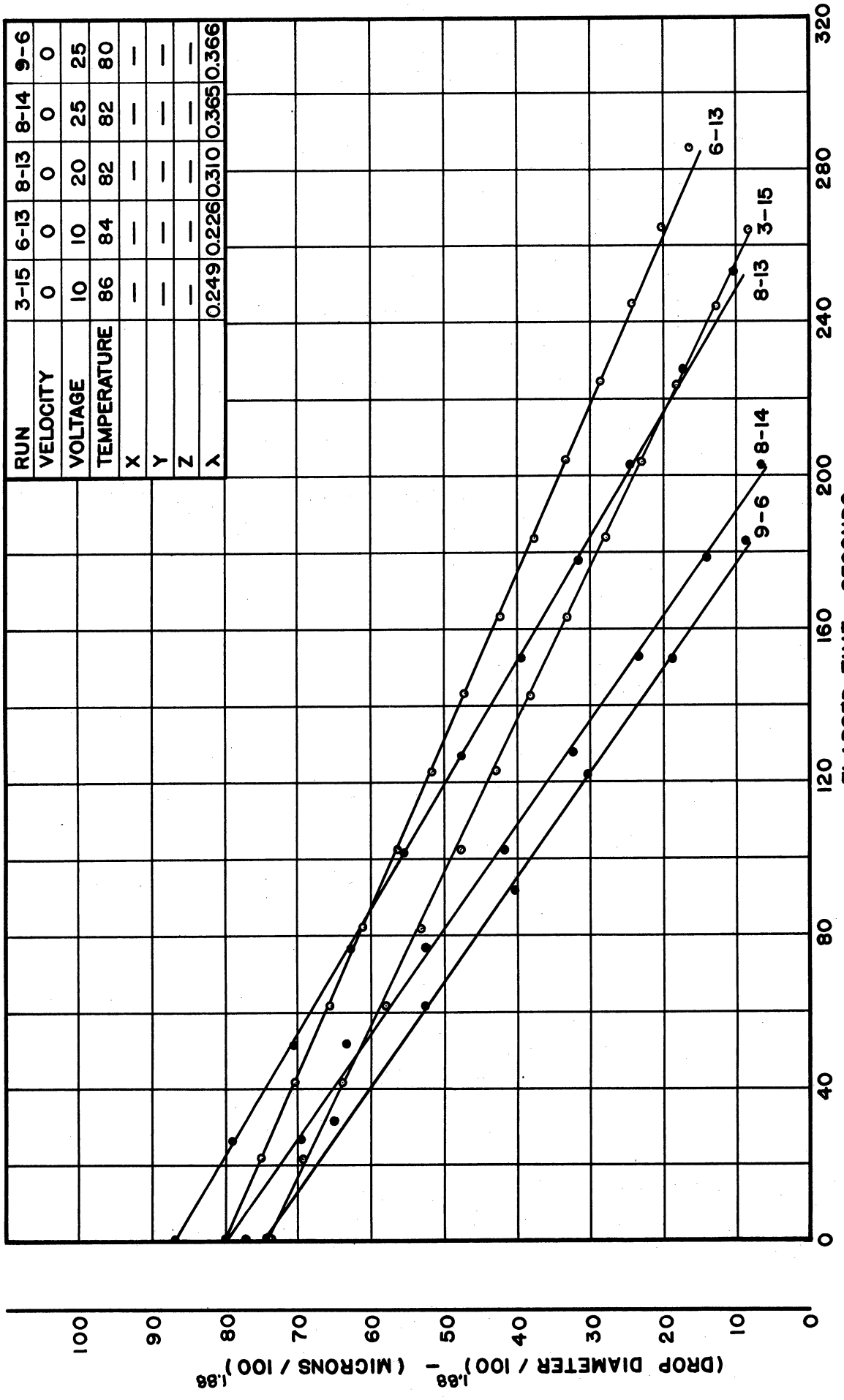

FIG.31 EVAPORATION CURVES FOR FIXED DROPS - CUMENE (v = 0 ft/sec)

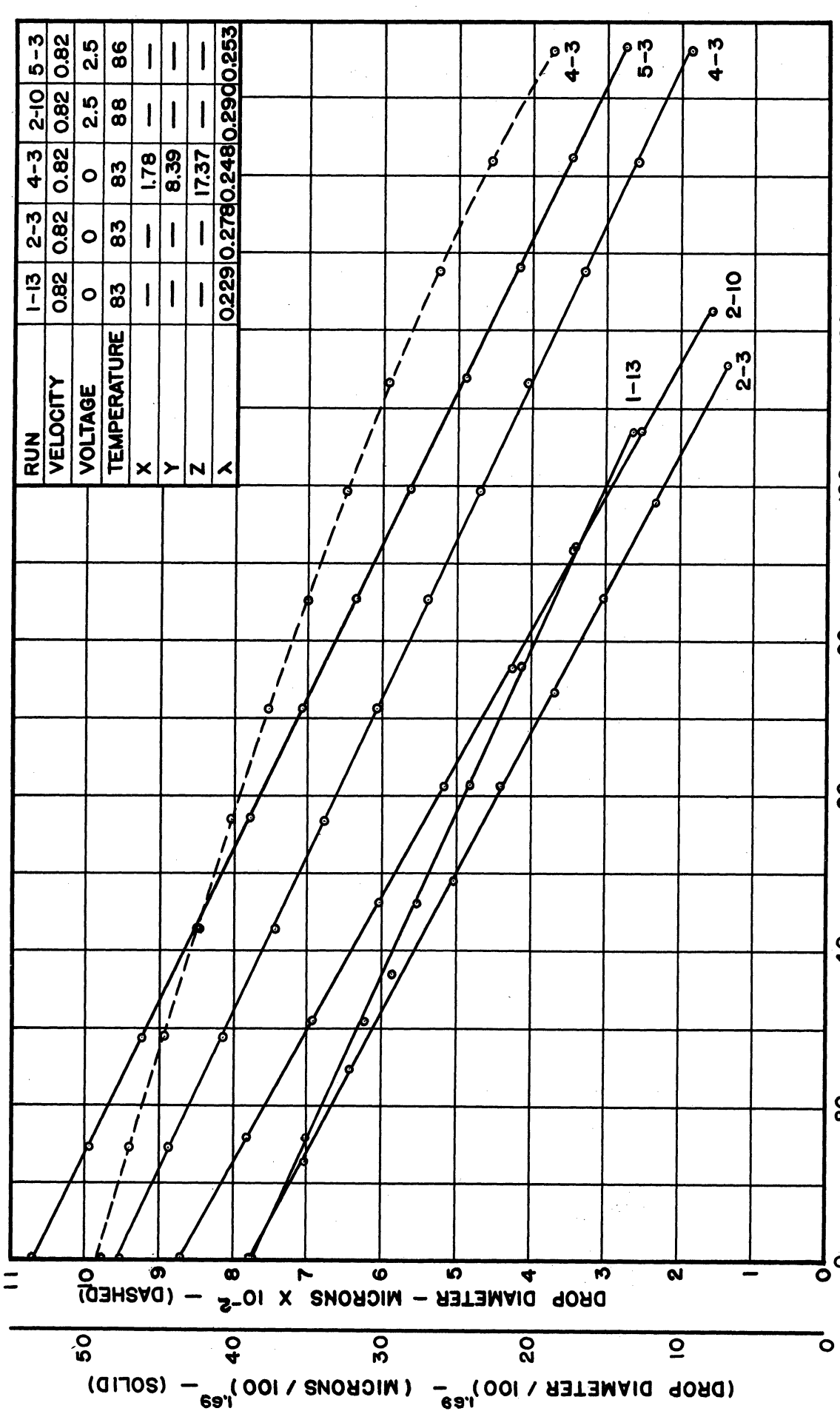

FIG.32 EVAPORATION CURVES FOR FIXED DROPS - CUMENE (v=0.82 ft/sec)

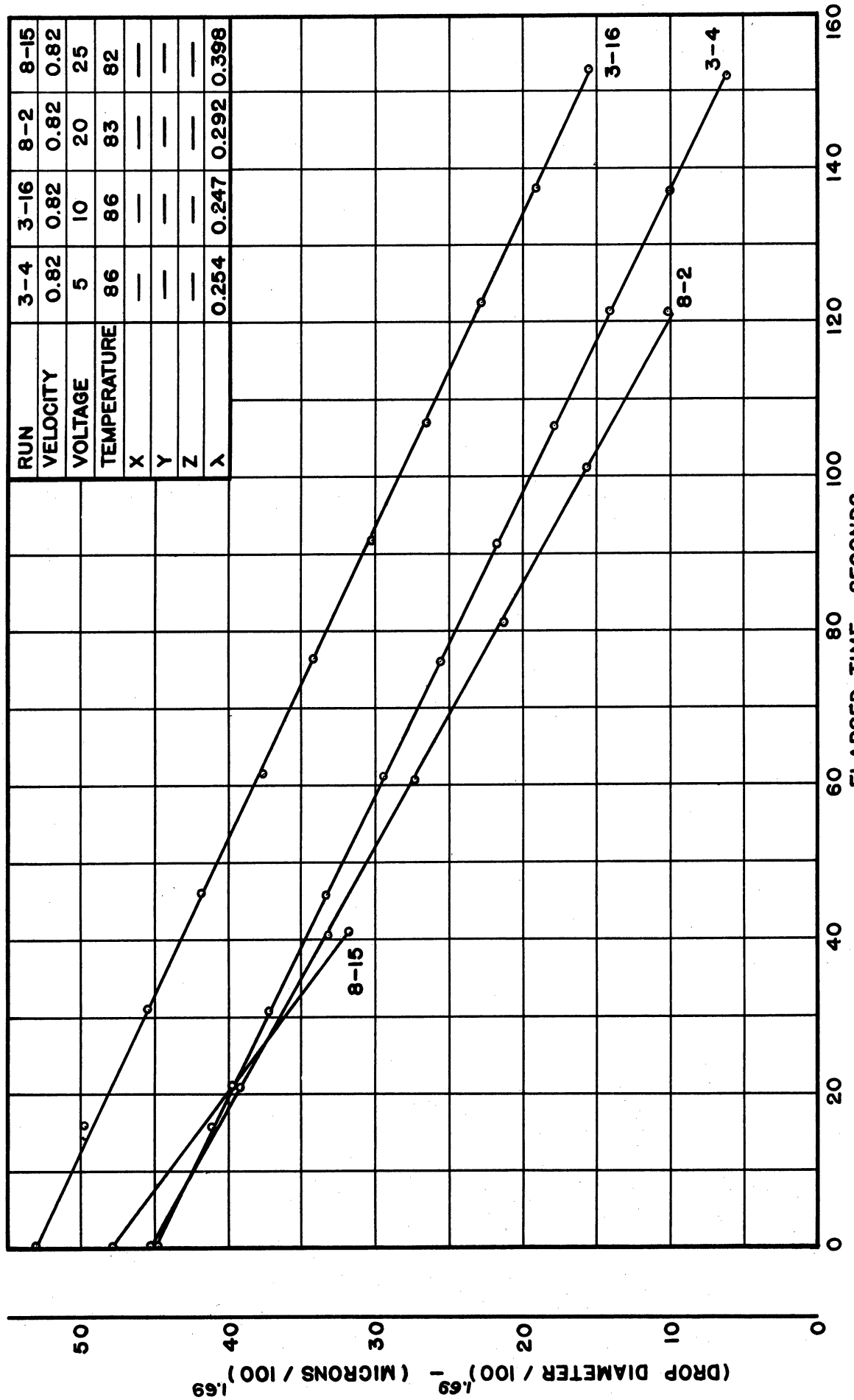

FIG.33 EVAPORATION CURVES FOR FIXED DROPS - CUMENE (v=0.82 ft/sec)

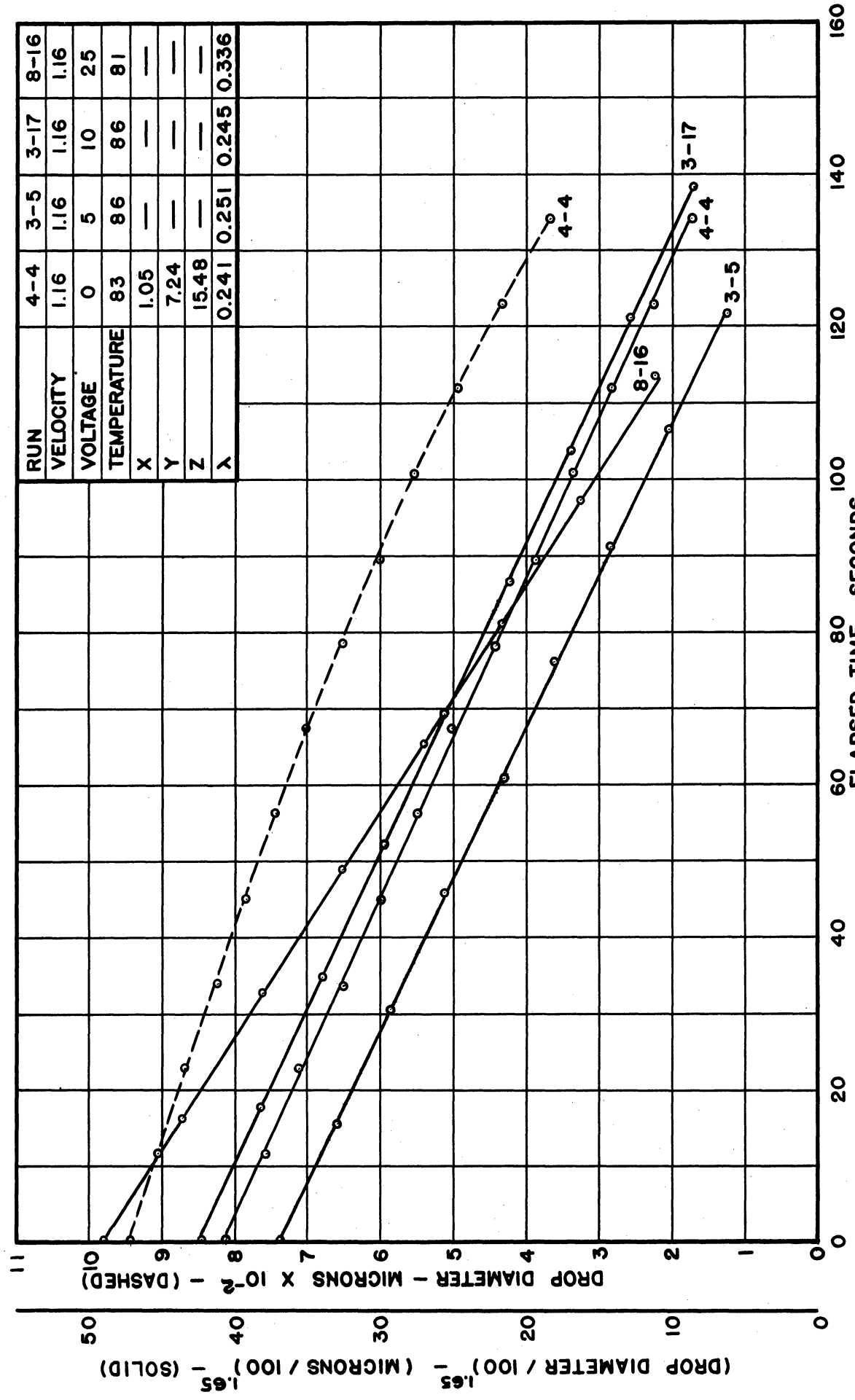

FIG.34 EVAPORATION CURVES FOR FIXED DROPS - CUMENE (v = 1.16 ft/sec)

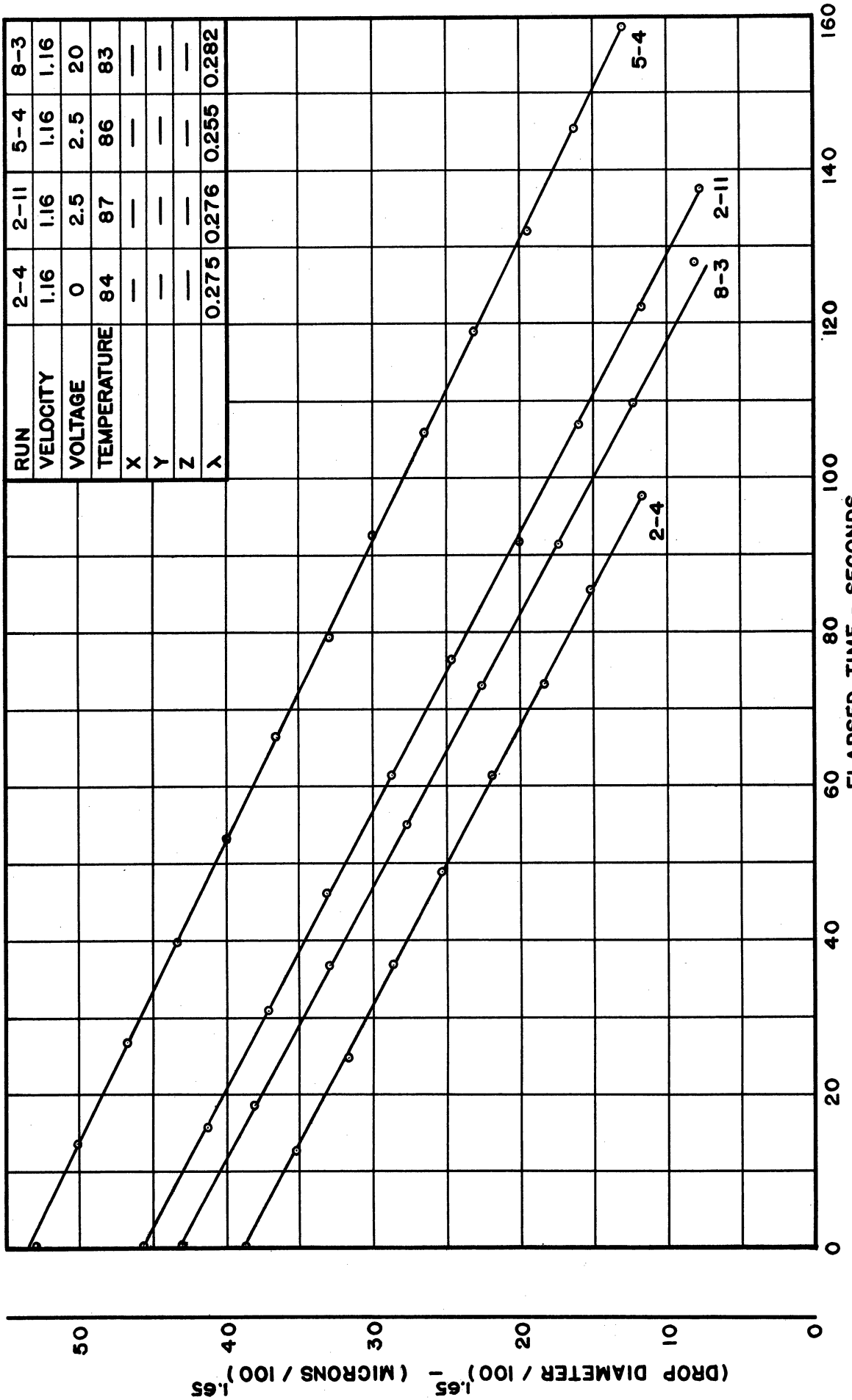

FIG.35 EVAPORATION CURVES FOR FIXED DROPS - CUMENE (v=1.16 ft/sec)

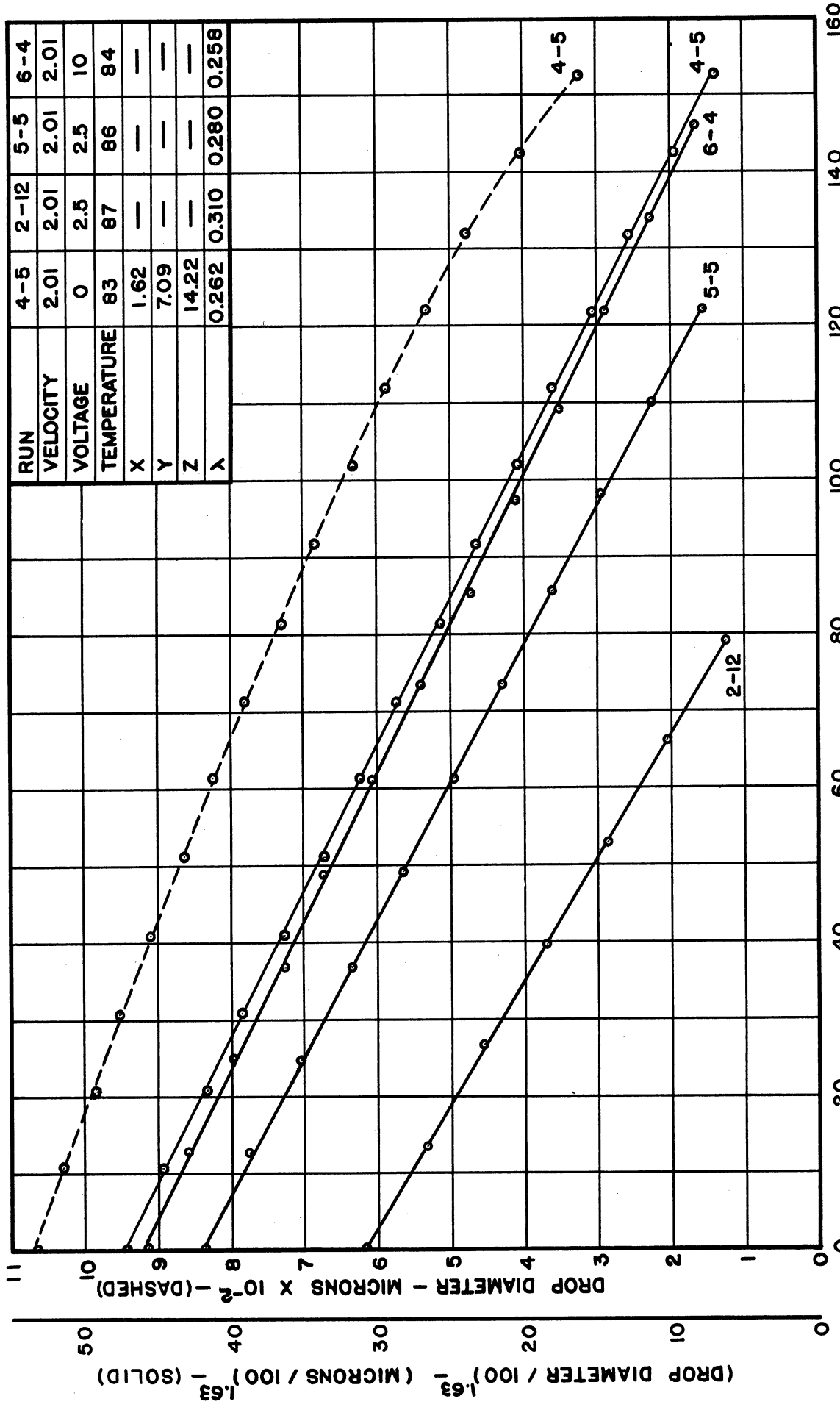

FIG.36 EVAPORATION CURVES FOR FIXED DROPS - CUMENE (v = 2.01 ft/sec)

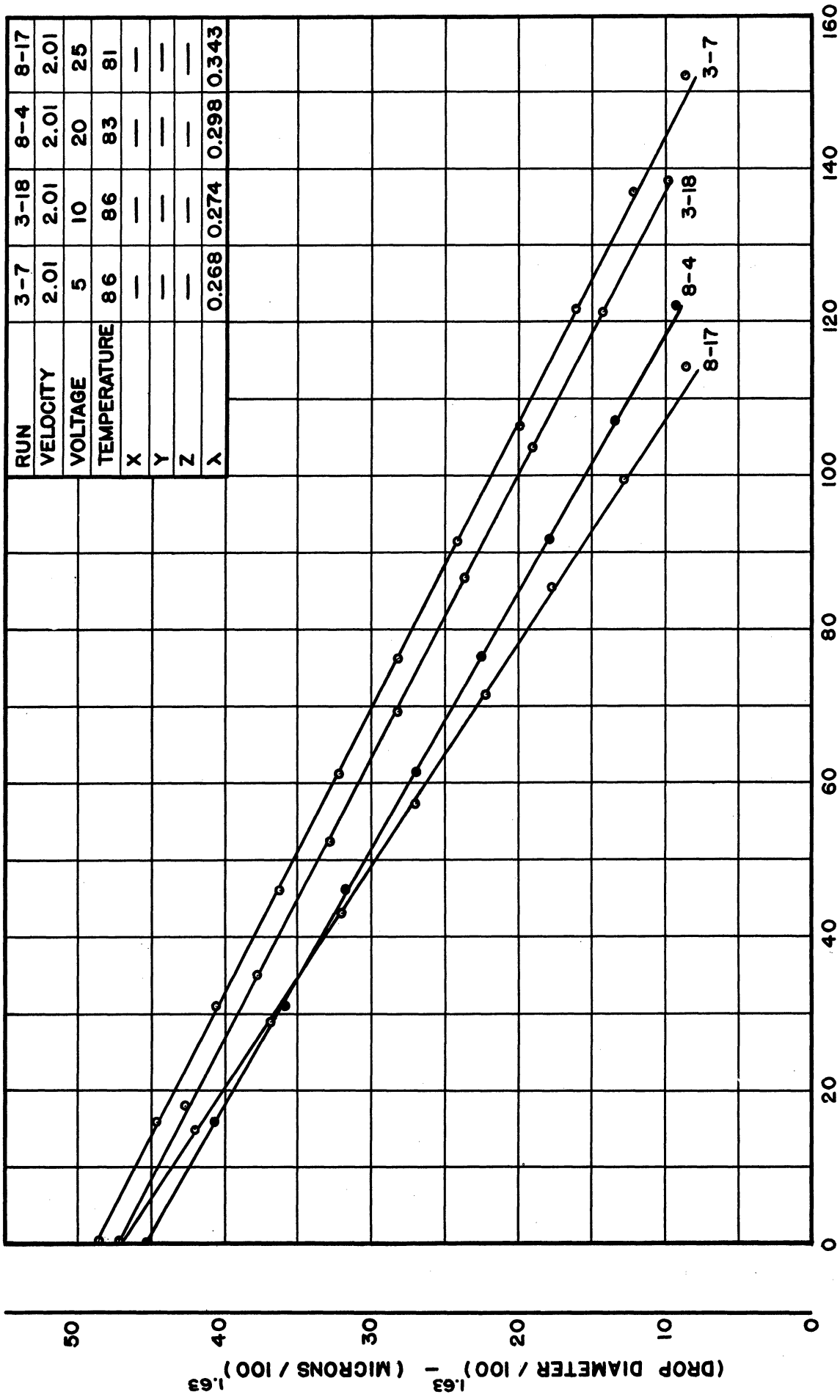

FIG.37 EVAPORATION CURVES FOR FIXED DROPS - CUMENE (v = 2.01 ft/sec)

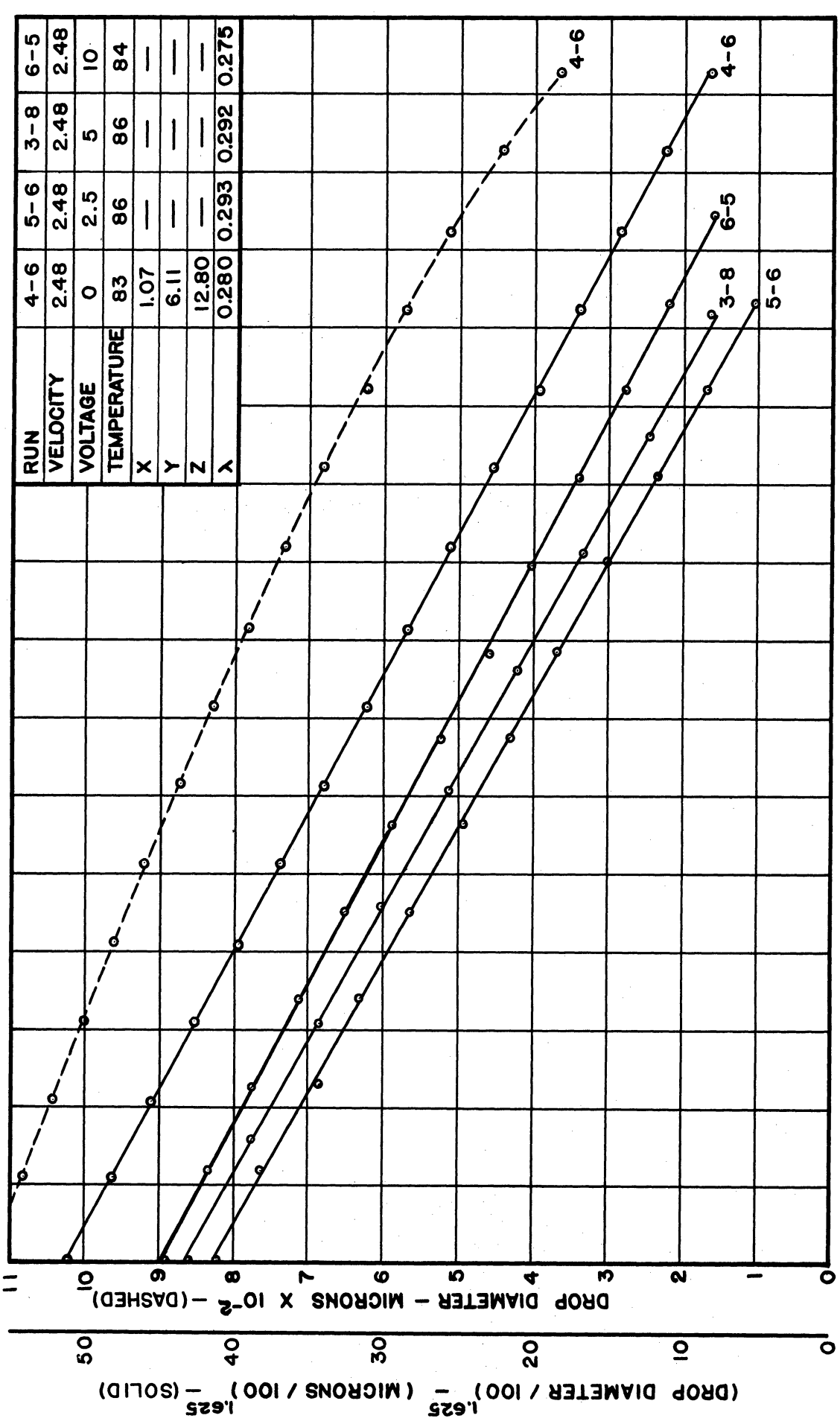

FIG.38 EVAPORATION CURVES FOR FIXED DROPS - CUMENE (v = 2.48 ft/sec)

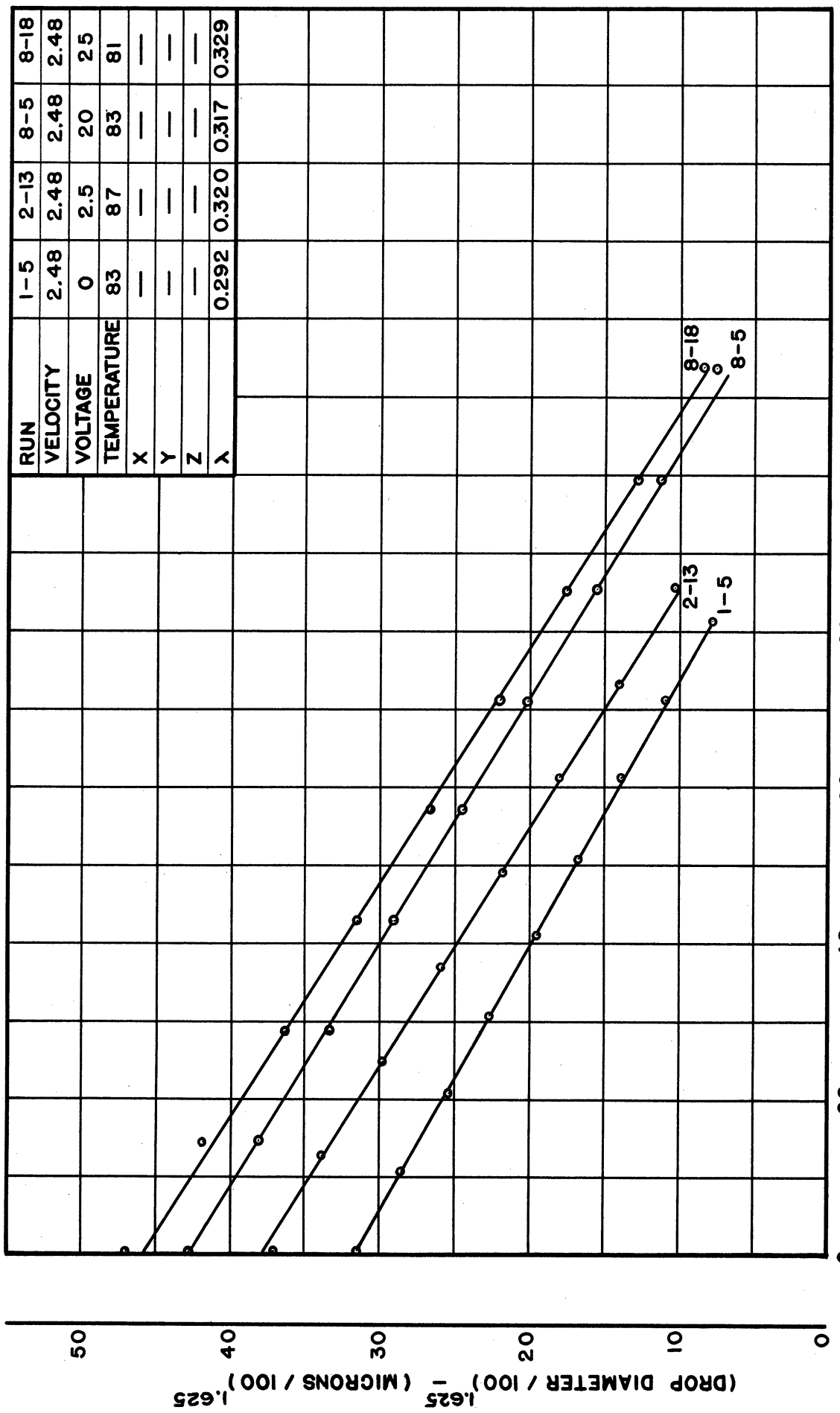

FIG.39 EVAPORATION CURVES FOR FIXED DROPS - CUMENE (v = 2.48 ft / sec)

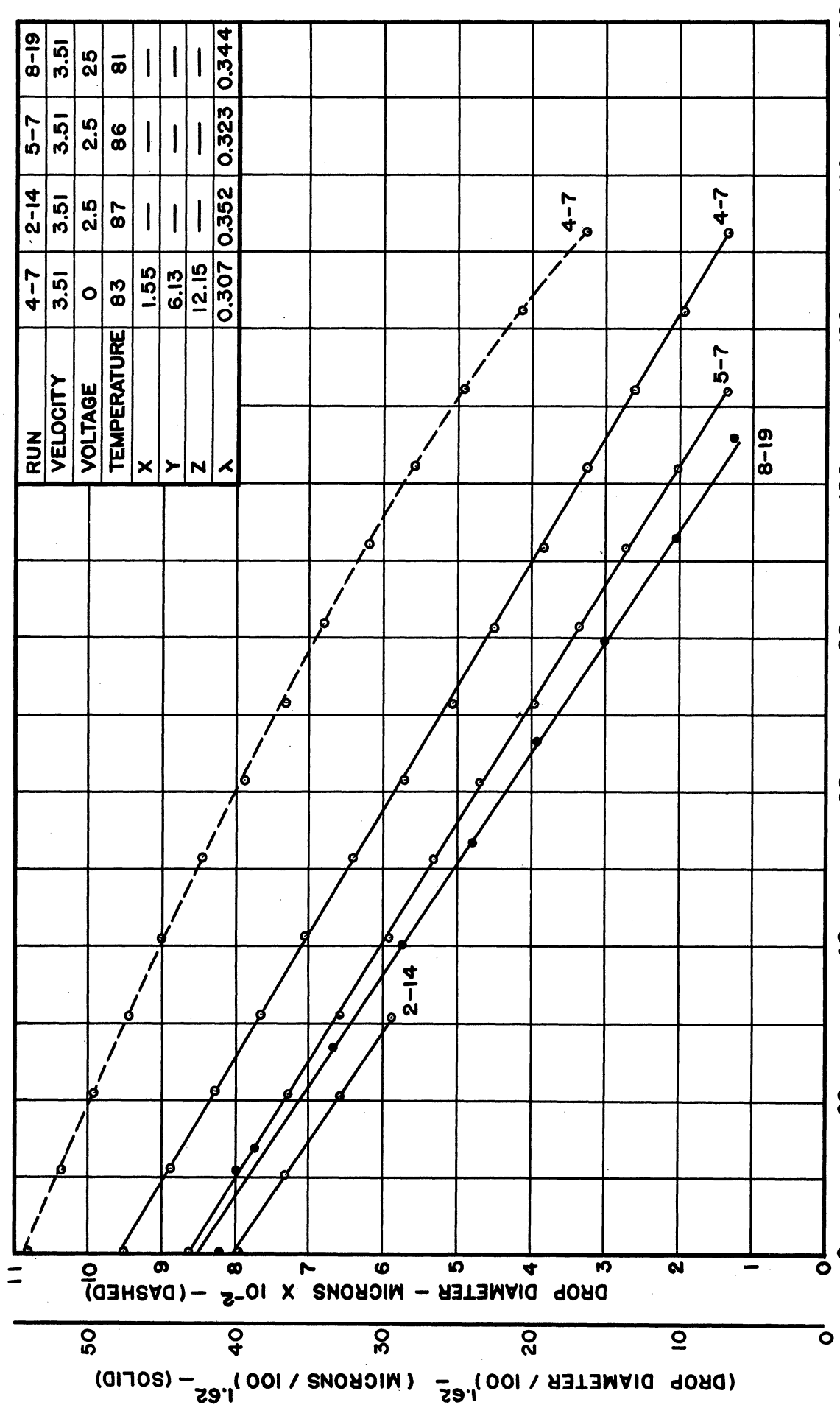

FIG.40 EVAPORATION CURVES FOR FIXED DROPS - CUMENE (v=3.51 ft / sec)

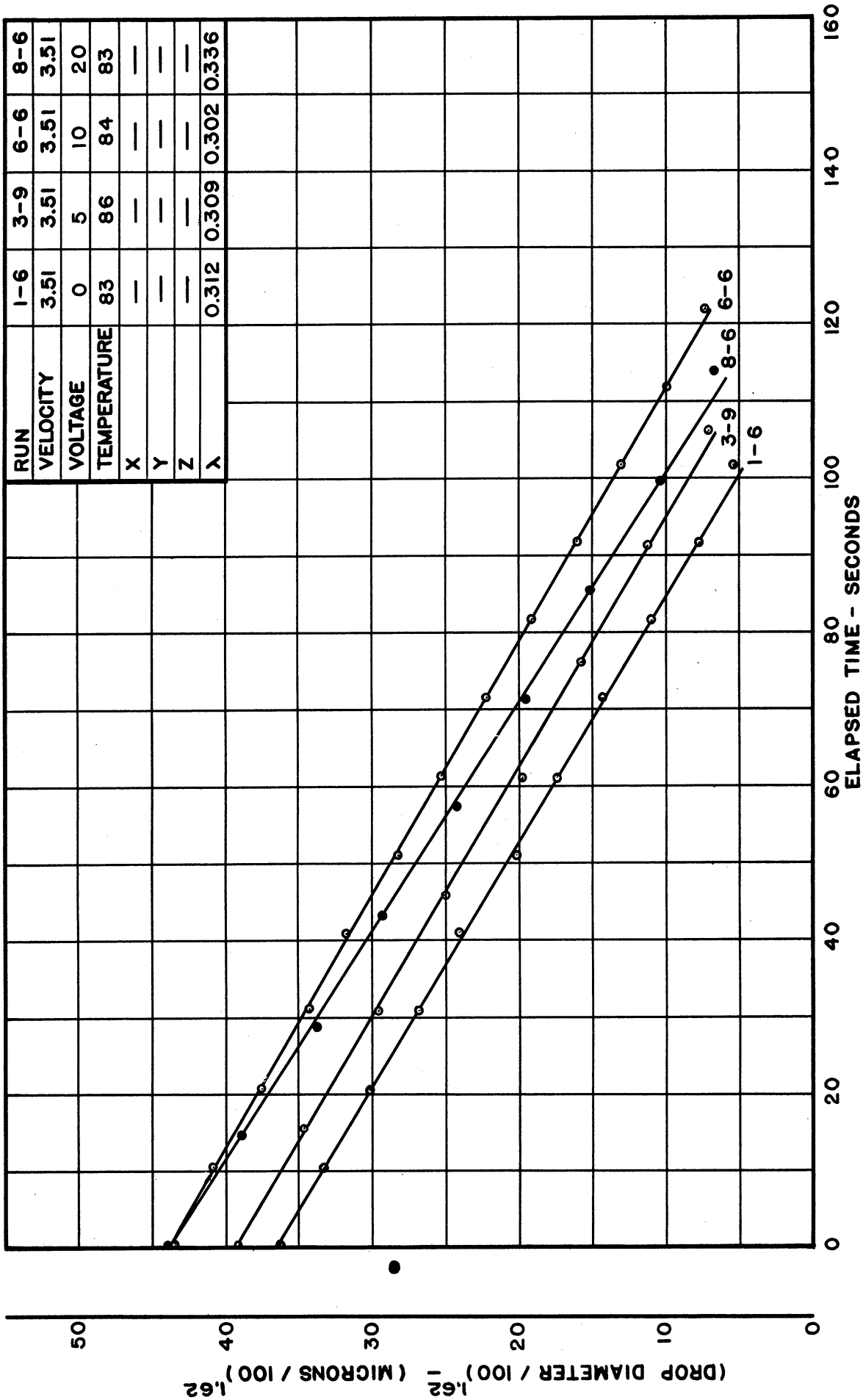

FIG.41 EVAPORATION CURVES FOR FIXED DROPS - CUMENE (v=3.51 ft/sec)

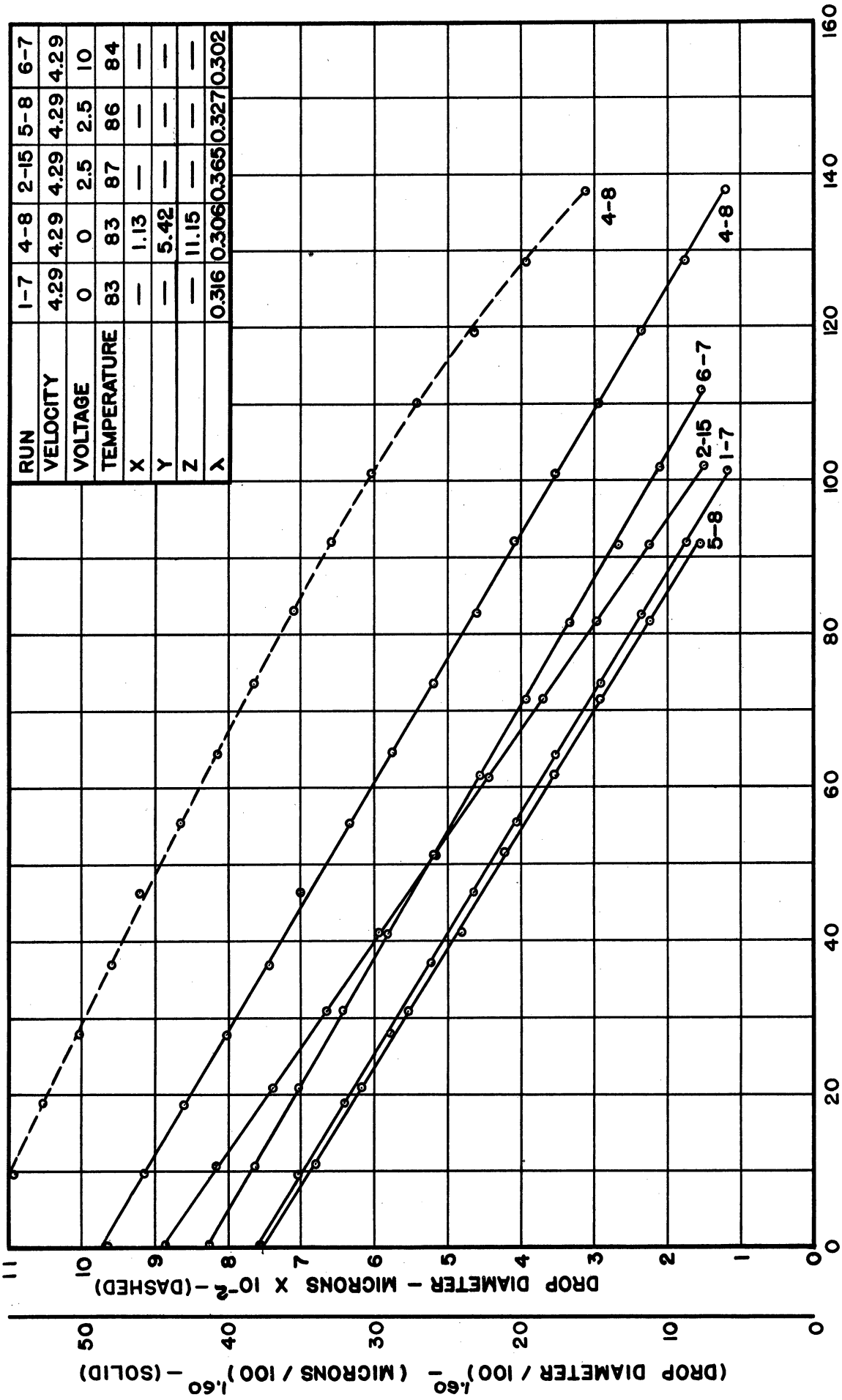

FIG.42 EVAPORATION CURVES FOR FIXED DROPS - CUMENE (v = 4.29 ft/sec)

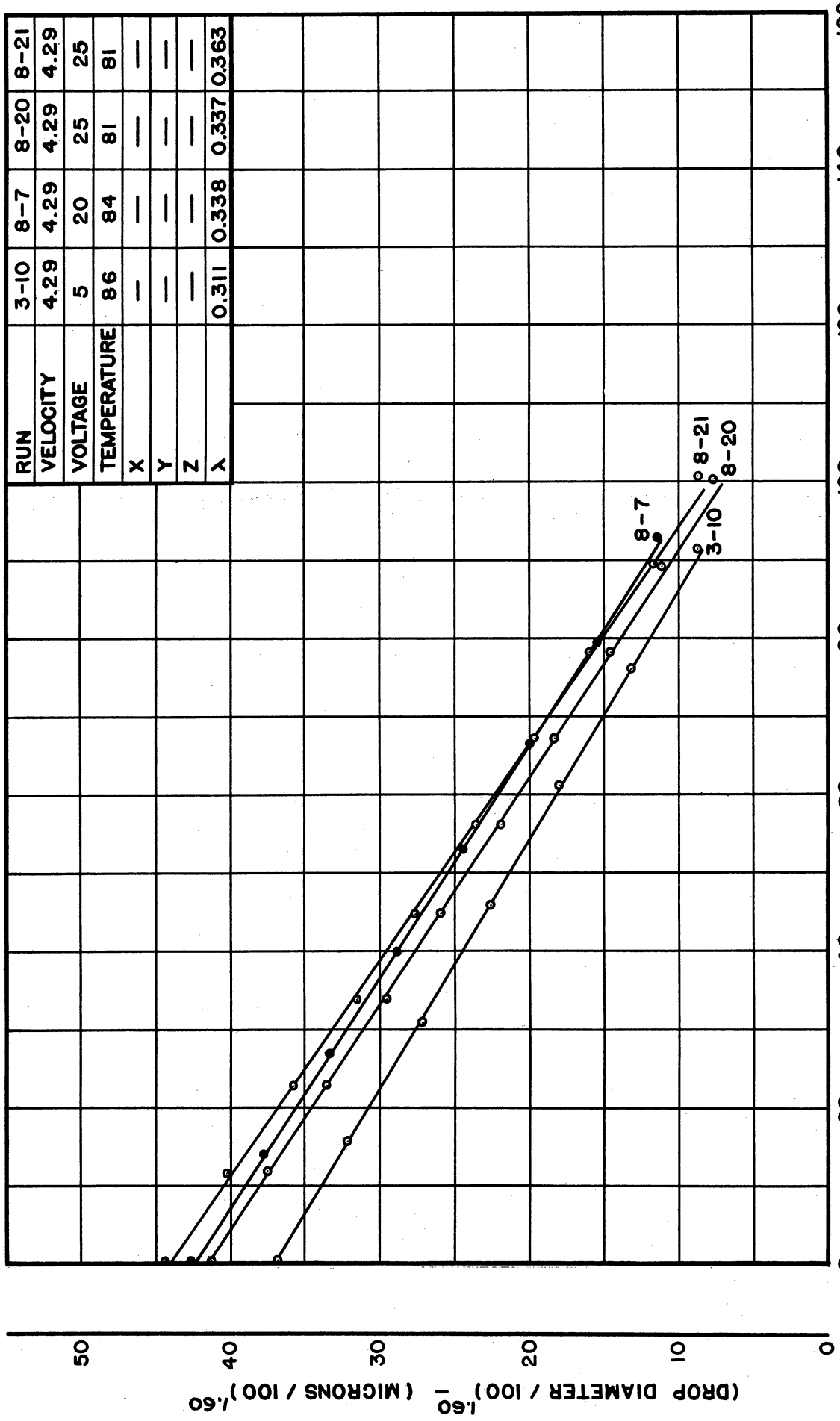

FIG. 43 EVAPORATION CURVES FOR FIXED DROPS - CUMENE (v = 4.29 ft/sec)

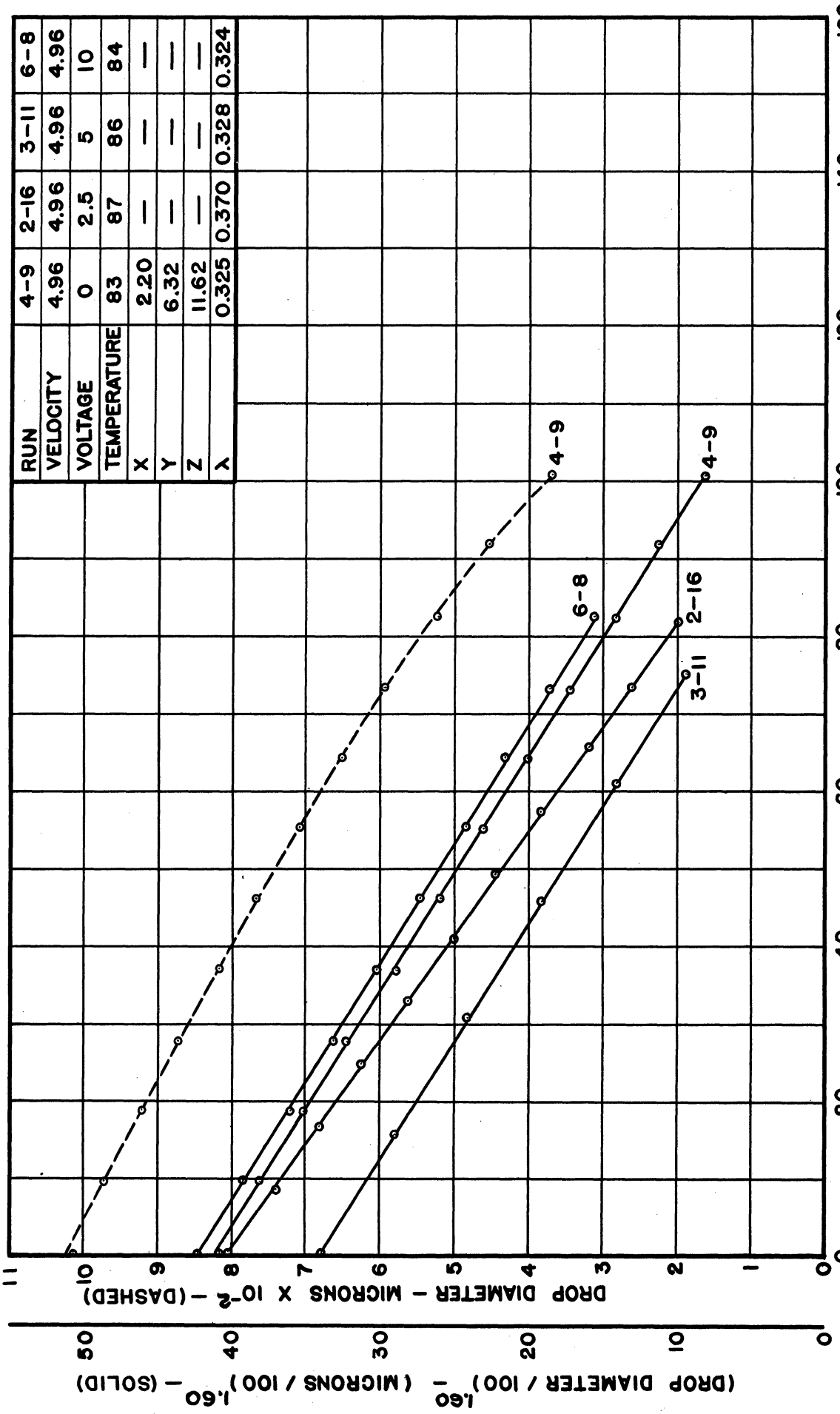

FIG.44 EVAPORATION CURVES FOR FIXED DROPS - CUMENE (v = 4.96 ft/sec)

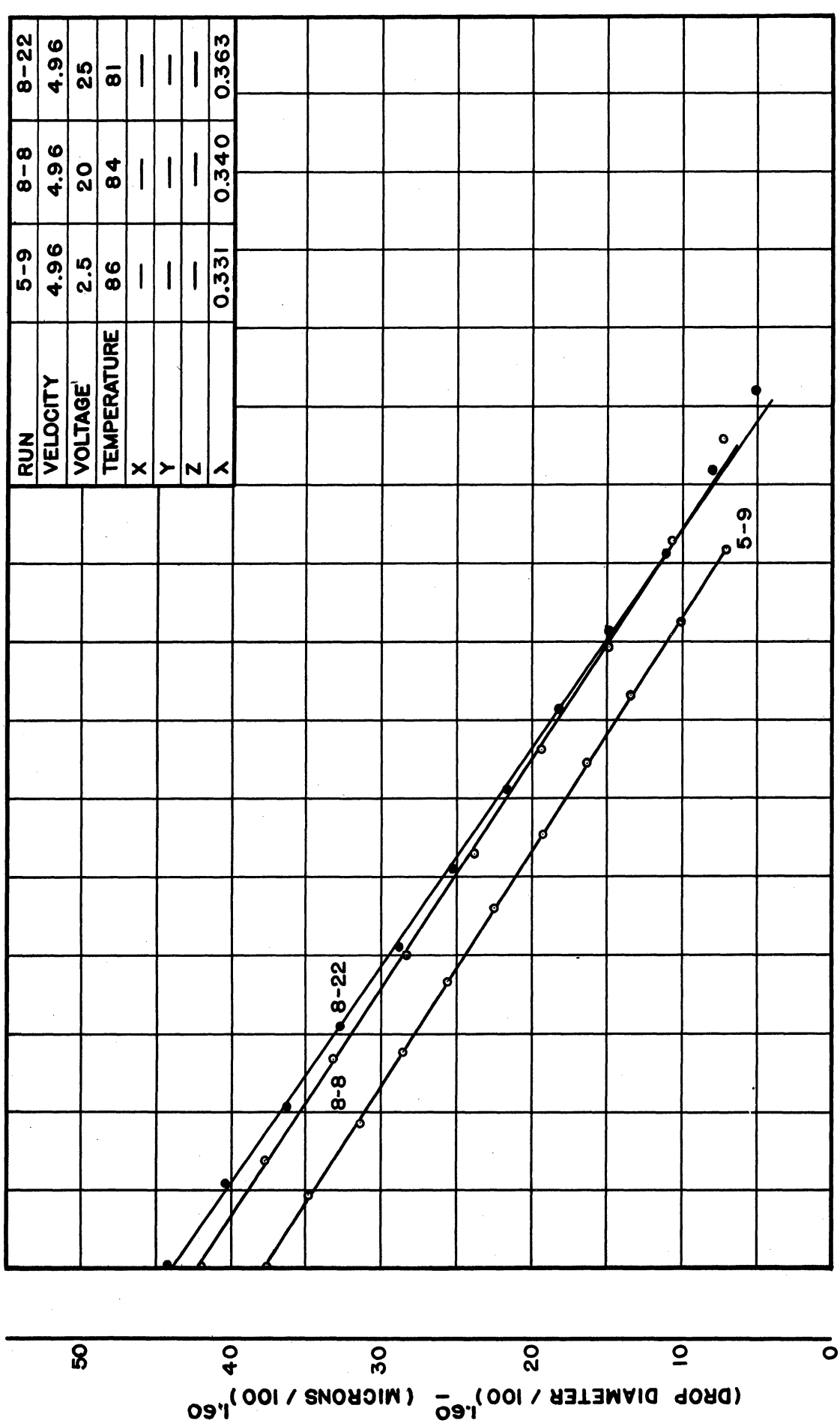

FIG.45 EVAPORATION CURVES FOR FIXED DROPS - CUMENE (v = 4.96 ft/sec)

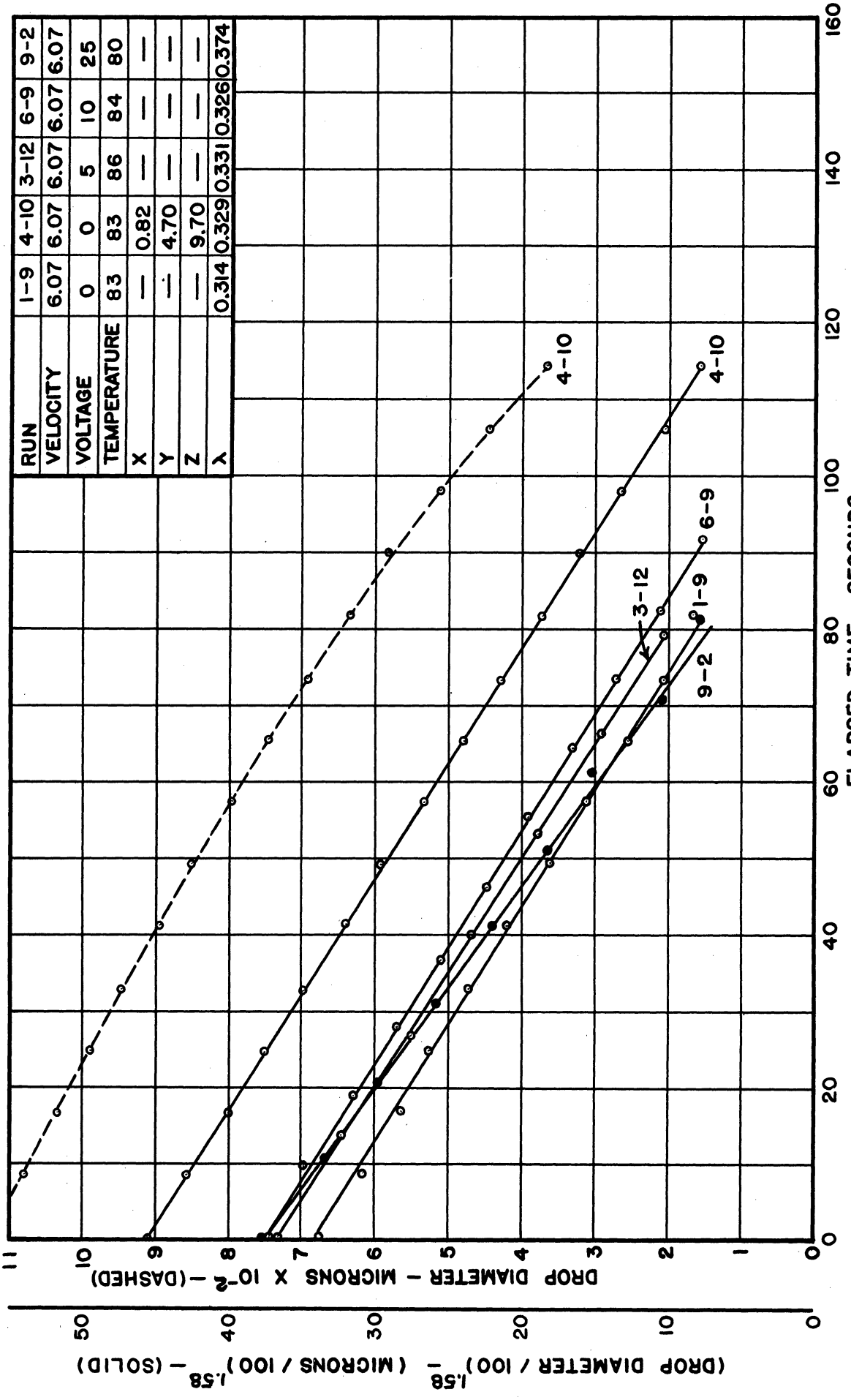

FIG.46 EVAPORATION CURVES FOR FIXED DROPS - CUMENE (v = 6.07 ft/sec)

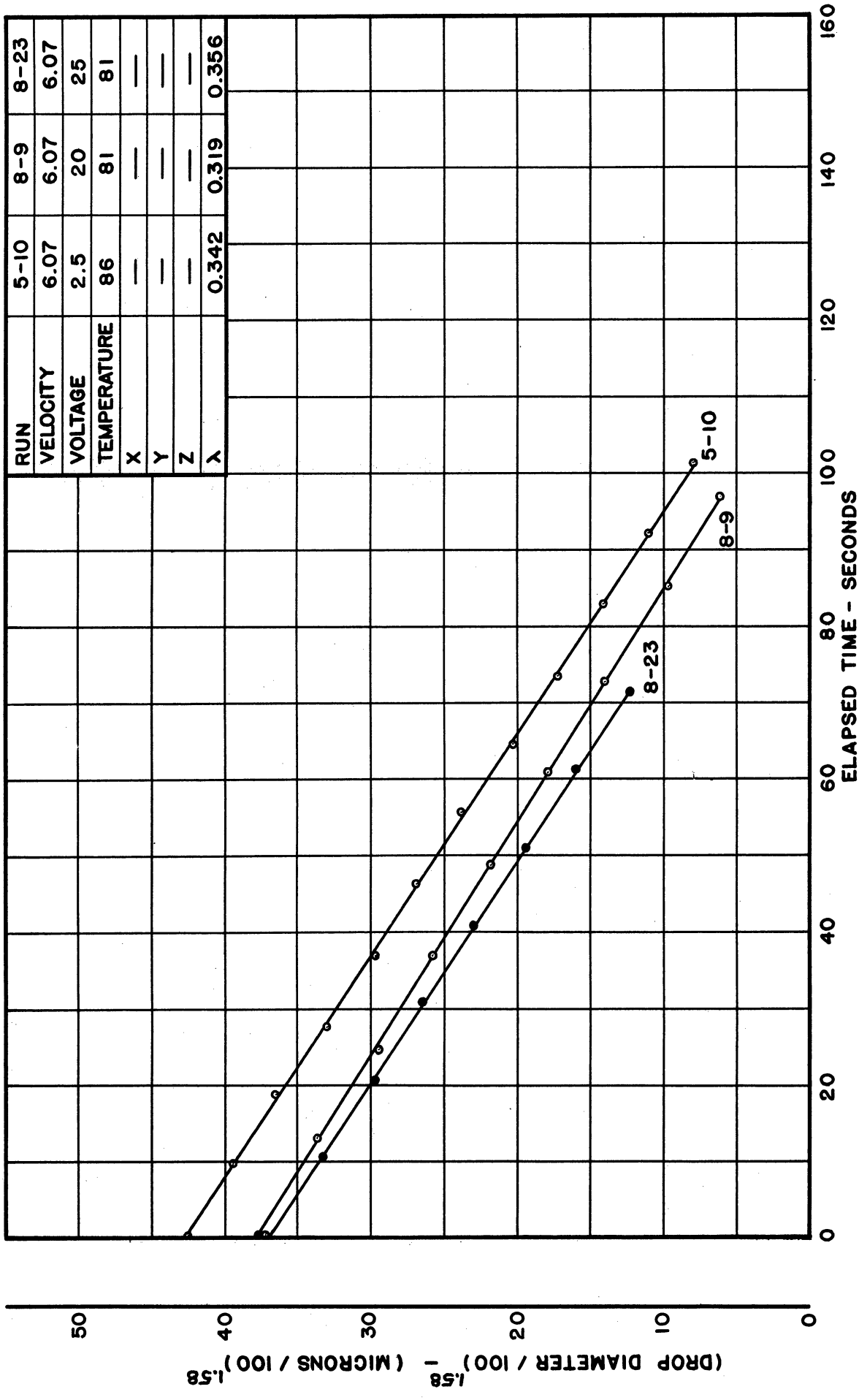

FIG.47 EVAPORATION CURVES FOR FIXED DROPS - CUMENE (v = 6.07 ft/sec)

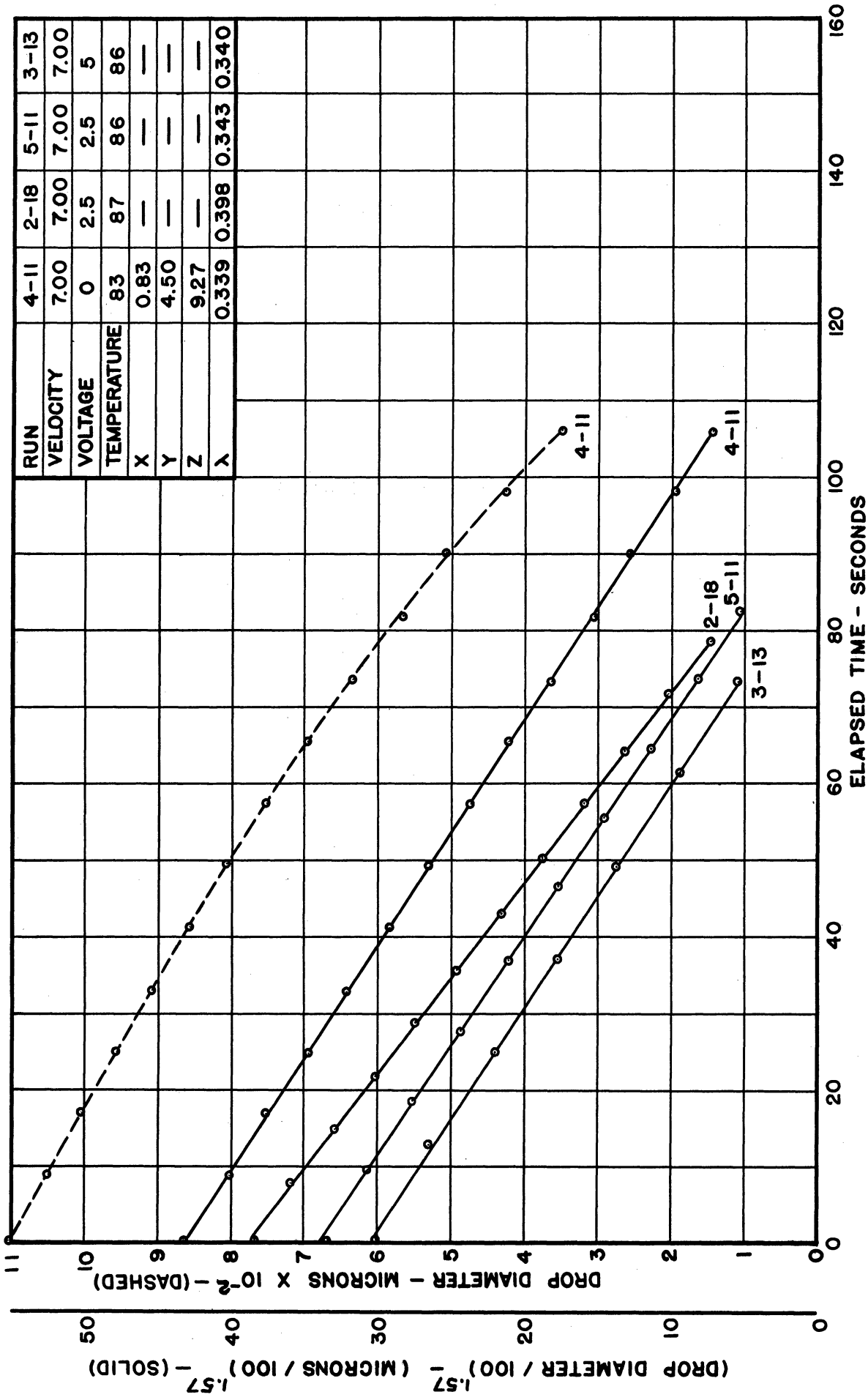

FIG.48 EVAPORATION CURVES FOR FIXED DROPS - CUMENE (v = 7.00 ft/sec)

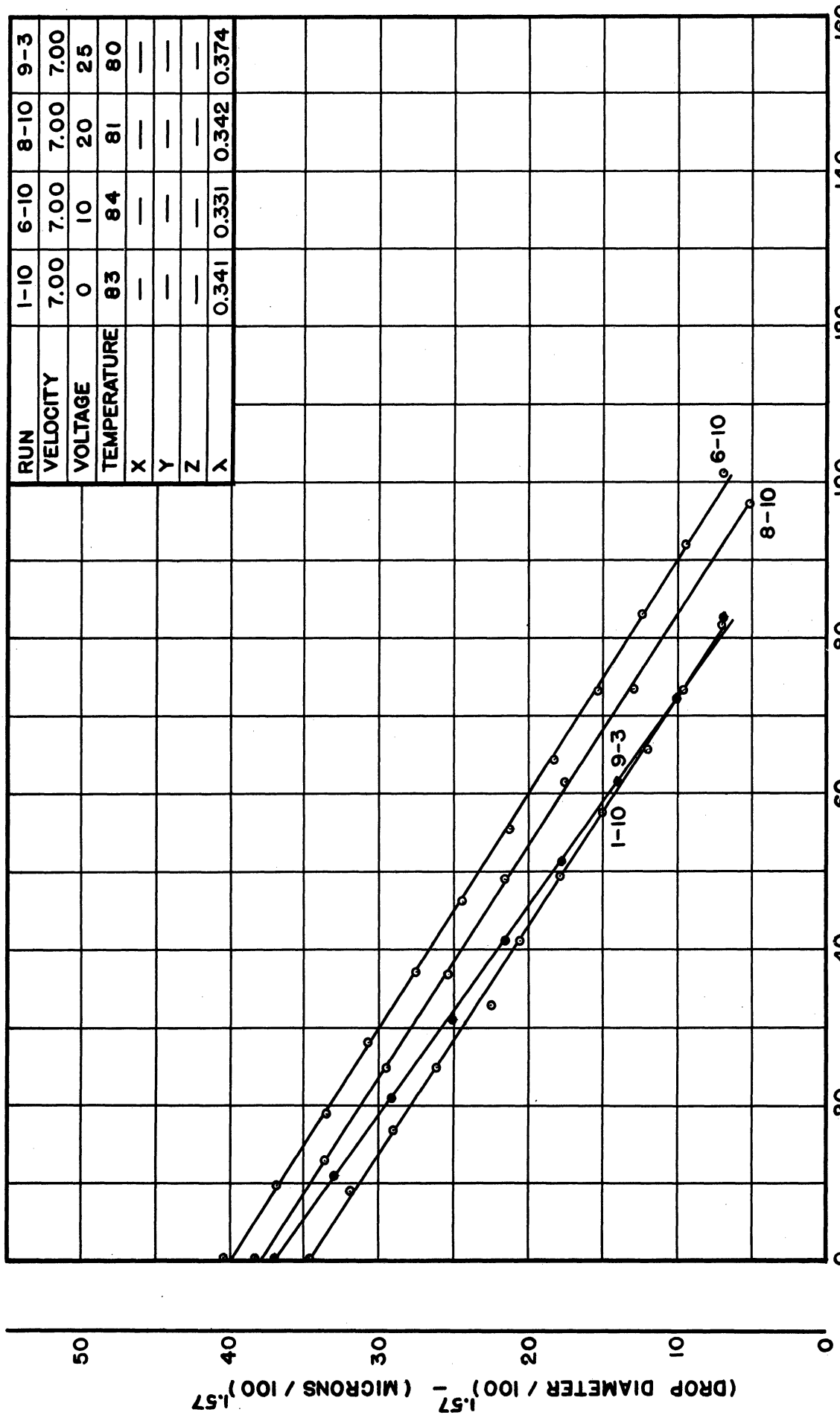

FIG.49 EVAPORATION CURVES FOR FIXED DROPS - CUMENE (v = 7.00 ft/sec)

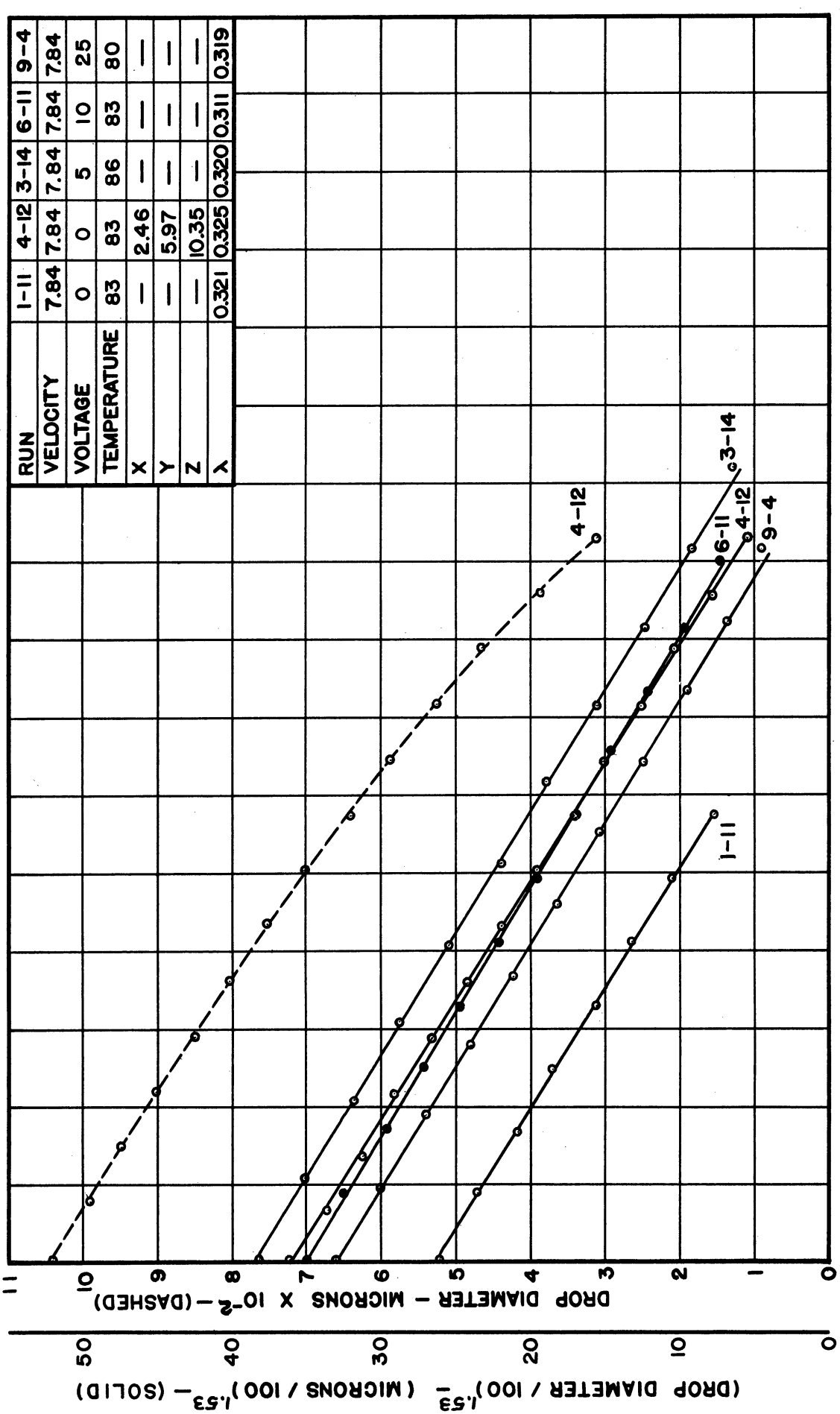

FIG.50 EVAPORATION CURVES FOR FIXED DROPS - CUMENE (v = 7.84 ft/sec)

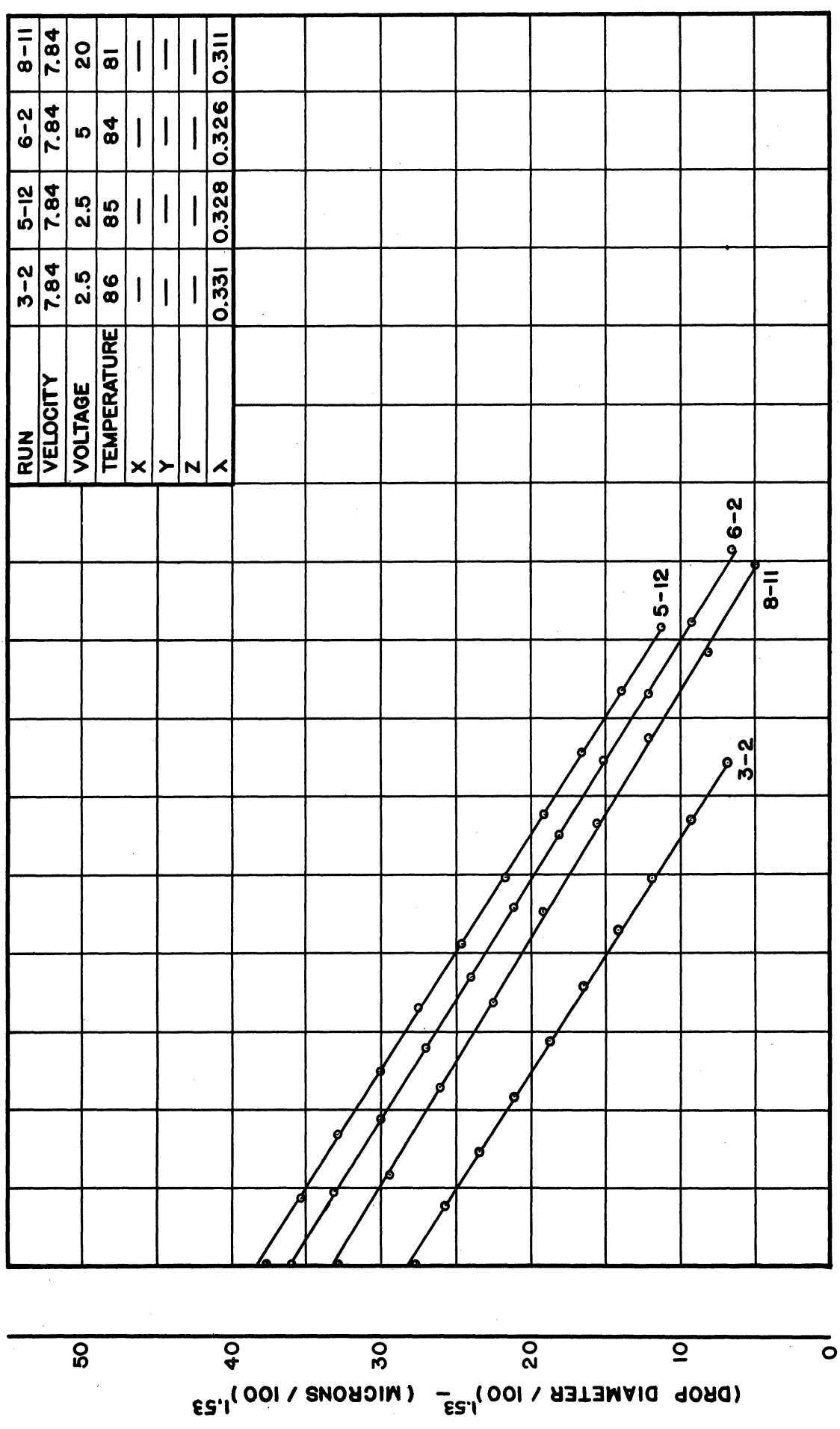

FIG.51 EVAPORATION CURVES FOR FIXED DROPS - CUMENE (v = 7.84 ft/sec)

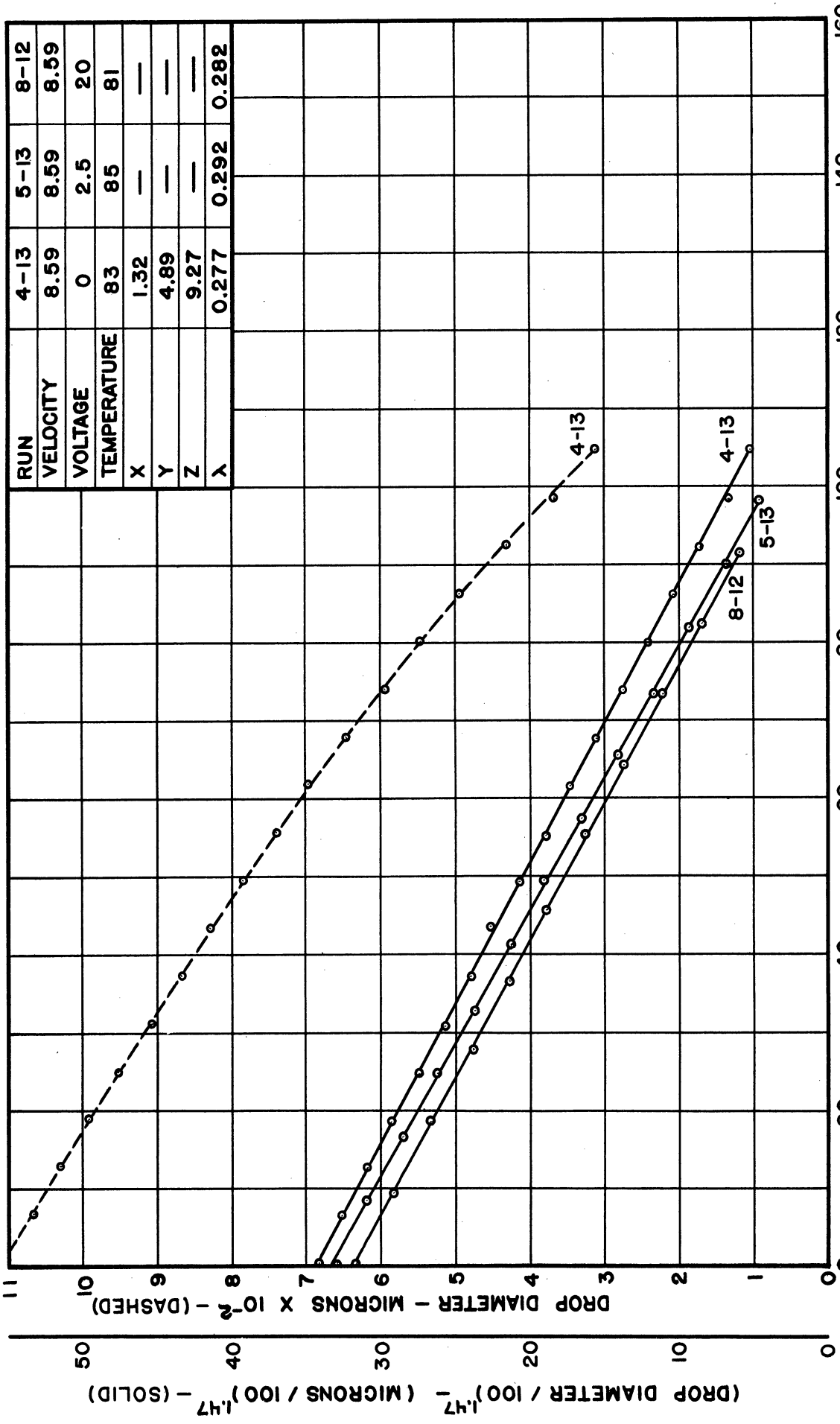

FIG.52 EVAPORATION CURVES FOR FIXED DROPS - CUMENE (v = 8.59 ft/sec)

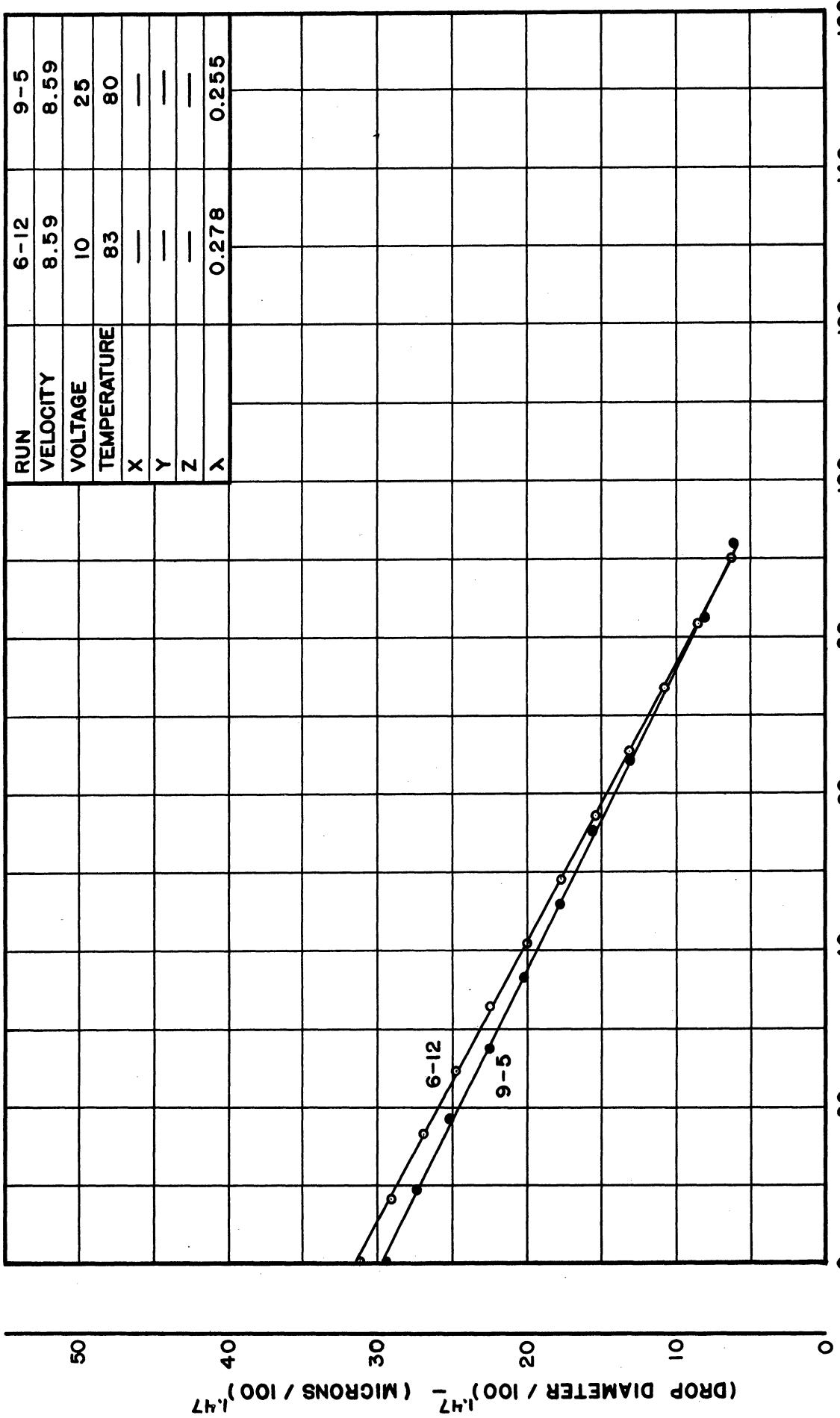

FIG.53 EVAPORATION CURVES FOR FIXED DROPS - CUMENE (v = 8.59 ft/sec)

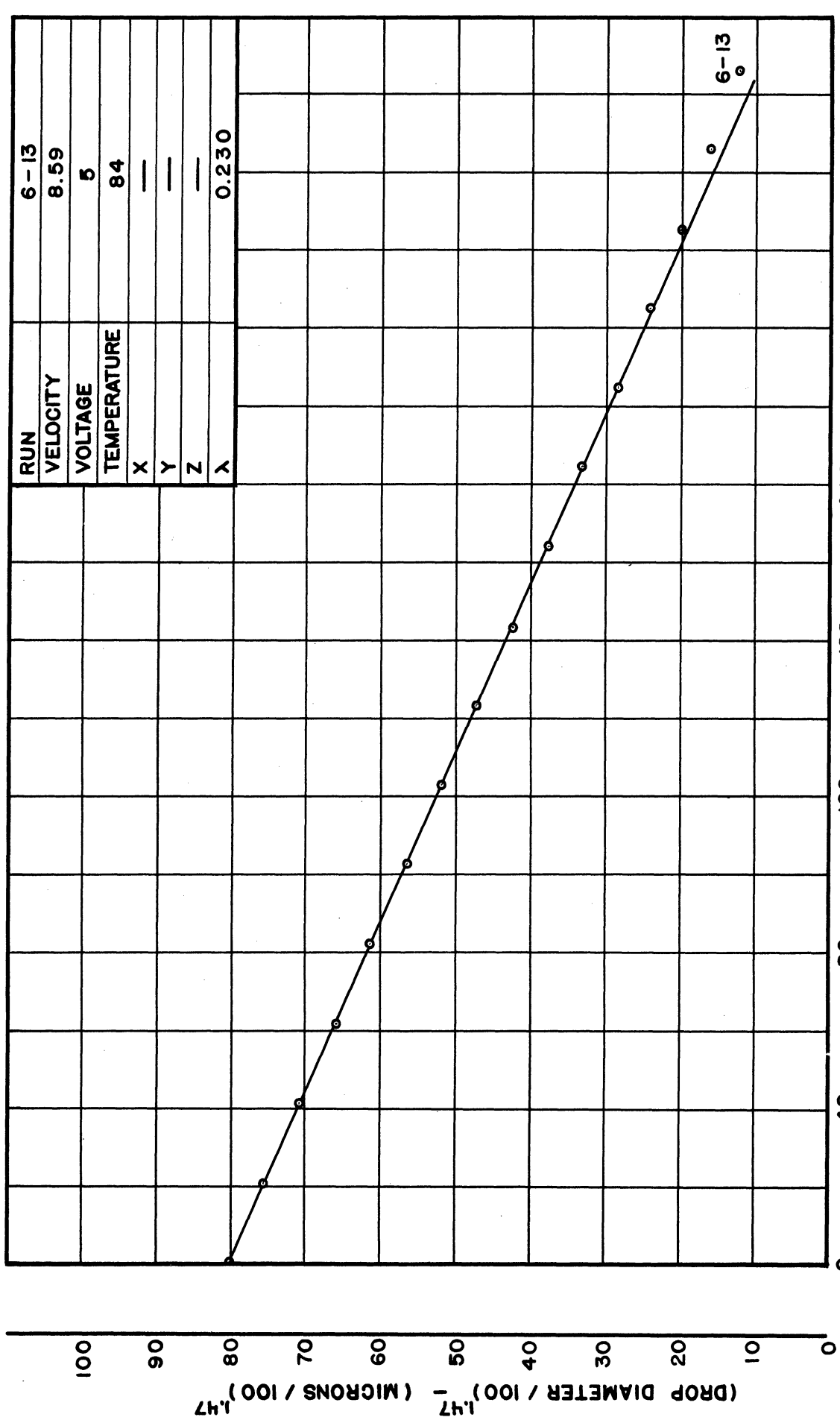

FIG.54 EVAPORATION CURVES FOR FIXED DROPS - CUMENE (v = 8.59 ft/sec)

TABLE IX

EVAPORATION DATA - FIXED CUMENE DROPS

Field voltage = 0 volts

D = Drop diameter (microns)
t = Elapsed time (seconds)

Run 1-3
v = 0.00 fps
T = 83° F.

t	D	$(\frac{D}{100})^{1.88}$
0.0	836	54.0
15.3	805	50.5
30.6	767	46.0
45.9	729	41.9
61.2	695	38.3
76.5	658	34.4
91.8	616	30.7
107.1	575	26.9
122.4	531	23.1
137.7	479	19.0
153.0	425	15.1
168.3	356	10.9
183.6	288	7.3

Run 1-12
v = 0.00 fps
T = 83° F.

t	D	$(\frac{D}{100})^{1.88}$
0.0	978	72.5
15.3	953	69.3
30.6	928	65.9
45.9	904	62.8
61.2	877	59.0
76.5	846	55.3
91.8	821	52.4
107.1	790	48.7
122.4	760	45.4
137.7	733	42.4
153.0	704	39.2
168.3	665	35.2
183.6	628	31.5
198.9	596	28.7
214.2	562	25.7
229.5	522	22.4
244.8	479	19.0
260.1	432	15.6
275.4	384	12.5
290.7	330	9.4

Run 4-2
v = 0.00 fps
T = 83° F.

t	D	$(\frac{D}{100})^{1.88}$
0.0	1008	77.2
18.3	981	73.3
36.6	950	68.8
54.9	924	65.5
73.2	887	60.3
91.5	852	56.1
109.7	824	52.7
128.0	794	49.1
146.3	757	44.9
164.6	722	41.1
182.9	681	36.9
201.2	638	32.6
219.5	598	28.8
237.8	549	24.5
256.1	508	21.2
274.4	445	16.5
292.7	371	11.8
310.9	311	8.4

Run 4-14
v = 0.00 fps
T = 83° F.

t	D	$(\frac{D}{100})^{1.88}$
0.0	1117	93.2
20.4	1079	87.2
40.8	1051	83.3
61.3	1022	79.4
81.7	993	74.7
102.1	960	70.0
122.5	926	65.5
142.9	890	60.8
163.4	852	56.1
183.8	820	52.2
204.2	776	47.0
224.6	739	42.9
245.0	696	38.3
265.5	652	34.0

Run 1-13
v = 0.82 fps
T = 83° F.

t	D	$(\frac{D}{100})^{1.69}$
0.0	871	38.8
15.3	819	35.0
30.6	769	31.2
45.9	714	27.7
61.2	659	24.2
76.5	600	20.7
91.8	536	17.1
107.1	461	13.2

Run 2-3
v = 0.82 fps
T = 84° F.

t	D	$(\frac{D}{100})^{1.69}$
0.0	872	38.9
12.3	823	35.2
24.5	782	32.4
36.8	730	28.7
49.0	674	25.2
61.3	626	22.1
73.5	563	18.5
85.8	499	15.1
98.0	428	11.7

Run 4-3
v = 0.82 fps
T = 83° F.

t	D	$(\frac{D}{100})^{1.69}$
0.0	982	47.6
14.2	946	44.5
28.5	897	40.8
42.7	851	37.3
57.0	804	34.0
71.2	756	30.5
85.4	703	27.0
99.7	650	23.6
113.9	594	20.3
128.2	525	16.5
142.4	455	12.9
156.6	371	9.2
170.9	280	5.7

Run 2-4
v = 1.16 fps
T = 84° F.

t	D	$(\frac{D}{100})^{1.65}$
0.0	916	38.7
12.3	868	35.2
24.5	814	31.8
36.8	765	28.7
49.0	710	25.4
61.3	650	22.0
73.5	583	18.4
85.8	520	15.1
98.0	446	11.8

TABLE X

EVAPORATION DATA - FIXED CUMENE DROPS

Field Voltage = 0 volts

D = Drop diameter (microns)
t = Elapsed time (seconds)

Run 4-4
v = 1.16 fps
T = 83° F.

t	D	$(\frac{D}{100})^{1.65}$
0.0	945	40.7
11.2	909	38.0
22.5	871	35.7
33.7	826	32.6
44.9	787	30.0
56.2	746	27.5
67.4	704	25.1
78.6	653	22.1
89.8	603	19.4
101.1	554	16.8
112.3	497	14.1
123.5	432	11.2
134.8	369	8.6

Run 4-5
v = 2.01 fps
T = 83° F.

t	D	$(\frac{D}{100})^{1.63}$
0.0	1066	47.4
10.2	1031	44.8
20.4	988	41.8
30.7	953	39.4
40.9	910	36.5
51.1	866	33.8
61.3	827	31.2
71.5	782	28.6
81.8	731	25.6
92.0	689	23.2
102.2	635	20.4
112.4	589	18.0
122.6	531	15.2
132.9	476	12.7
143.1	401	9.6
153.3	323	6.8

Run 1-5
v = 2.48 fps
T = 83° F.

t	D	$(\frac{D}{100})^{1.625}$
0.0	837	31.5
10.2	785	28.5
20.4	731	25.4
30.6	681	22.6
40.8	623	19.5
51.0	565	16.6
61.2	504	13.8
71.4	435	10.9
81.6	351	7.7
91.8	280	5.3

Run 4-6
v = 2.48 fps
T = 83° F.

t	D	$(\frac{D}{100})^{1.625}$
0.0	1123	51.1
10.2	1085	48.2
20.5	1047	45.6
30.7	1007	42.8
40.9	964	39.8
51.2	922	37.0
61.4	876	34.0
71.6	830	31.1
81.8	785	28.5
92.1	735	25.6
102.3	683	22.8
112.5	626	19.7
122.8	571	17.0
133.0	515	14.3
143.2	443	11.2
153.5	369	8.3

Run 1-6
v = 3.51 fps
T = 83° F.

t	D	$(\frac{D}{100})^{1.62}$
0.0	919	36.3
10.2	871	33.3
20.4	817	30.0
30.6	763	26.9
40.8	712	24.0
51.0	639	20.1
61.2	584	17.5
71.4	518	14.4
81.6	441	11.0
91.8	356	7.8
102.0	276	5.2

Run 4-7
v = 3.51 fps
T = 83° F.

t	D	$(\frac{D}{100})^{1.62}$
0.0	1084	47.4
10.2	1039	44.3
20.5	994	41.3
30.7	946	38.1
41.0	901	35.2
51.2	848	32.0
61.4	790	28.5
71.7	735	25.3
81.9	682	22.5
92.2	620	19.2
102.4	559	16.2
112.6	491	13.2
122.9	412	9.9
133.1	329	6.9

Run 1-7
v = 4.29 fps
T = 83° F.

t	D	$(\frac{D}{100})^{1.60}$
0.0	968	37.8
9.2	925	35.1
18.4	871	32.0
27.6	819	28.9
36.8	768	26.0
46.0	714	23.2
55.2	656	20.2
64.4	598	17.5
73.6	532	14.5
82.8	464	11.7
92.0	386	8.7
101.2	301	5.8

Run 4-8
v = 4.29 fps
T = 83° F.

t	D	$(\frac{D}{100})^{1.60}$
0.0	1130	48.3
9.2	1091	45.8
18.5	1051	43.0
27.7	1004	40.1
36.9	961	37.2
46.2	922	35.0
55.4	868	31.8
64.6	817	28.8
73.8	767	26.0
83.1	710	23.0
92.3	658	20.4
101.5	601	17.6
110.8	542	14.9
120.0	467	11.8
129.2	393	8.9
138.5	311	6.1

TABLE XI

EVAPORATION DATA - FIXED CUMENE DROPS

Field Voltage = 0 volts

D = Drop diameter (microns)
t = Elapsed time (seconds)

Run 4-9
v = 4.96 fps
T = 83° F.

t	D	$(\frac{D}{100})^{1.60}$
0.0	1015	40.8
9.2	971	38.0
18.4	922	35.0
27.7	873	32.1
36.9	818	28.8
46.1	767	26.0
55.3	710	23.0
64.5	651	20.0
73.8	593	17.2
83.0	522	14.1
92.2	452	11.2
101.4	369	8.1

Run 1-9
v = 6.07 fps
T = 83° F.

t	D	$(\frac{D}{100})^{1.58}$
0.0	925	33.6
8.2	874	30.7
16.4	825	28.0
24.6	791	26.2
32.8	737	23.5
41.0	685	20.9
49.2	622	18.0
57.4	569	15.6
65.6	499	12.7
73.8	441	10.4
82.0	379	8.2
90.2	341	6.9

Run 4-10
v = 6.07 fps
T = 83° F.

t	D	$(\frac{D}{100})^{1.58}$
0.0	1121	45.6
8.2	1081	43.0
16.4	1037	40.0
24.7	993	37.6
32.9	950	35.0
41.1	897	32.0
49.3	852	29.6
57.5	800	26.7
65.8	748	24.0
74.0	697	21.5
82.2	635	18.6
90.4	584	16.2
98.6	511	13.2
106.9	445	10.3
115.1	369	7.9

Run 1-10
v = 7.00 fps
T = 83° F.

t	D	$(\frac{D}{100})^{1.57}$
0.0	956	34.6
8.2	906	31.9
16.4	855	29.1
24.6	798	26.1
32.8	726	22.5
41.0	686	20.5
49.2	626	17.8
57.4	560	15.0
65.6	490	12.1
73.8	423	9.6
82.0	345	7.0
90.2	280	5.0

Run 4-11
v = 7.00 fps
T = 83° F.

t	D	$(\frac{D}{100})^{1.57}$
0.0	1102	43.3
8.2	1052	40.1
16.4	1008	37.6
24.6	958	34.7
32.8	910	32.1
41.0	859	29.2
49.2	808	26.5
57.4	751	23.7
65.6	697	21.1
73.8	636	18.2
82.0	568	15.2
90.2	509	12.9
98.4	428	9.8
106.6	350	7.1

Run 1-11
v = 7.84 fps
T = 83° F.

t	D	$(\frac{D}{100})^{1.53}$
0.0	843	26.1
8.2	788	23.5
16.4	728	20.8
24.6	673	18.5
32.8	603	15.6
41.0	538	13.1
49.2	465	10.5
57.4	380	7.7

Run 4-12
v = 7.84 fps
T = 83° F.

t	D	$(\frac{D}{100})^{1.53}$
0.0	1042	36.1
7.2	994	33.6
14.4	951	31.3
21.6	905	29.1
28.8	853	26.6
36.0	804	24.3
43.1	754	22.0
50.3	702	19.7
57.5	643	17.2
64.7	589	15.1
71.9	527	12.7
79.1	466	10.5
86.3	389	8.0
93.5	312	5.7

Run 4-13
v = 8.59 fps
T = 83° F.

t	D	$(\frac{D}{100})^{1.47}$
0.0	1108	34.2
6.2	1067	32.6
12.4	1033	31.0
18.6	994	29.3
24.8	954	27.5
31.0	910	25.7
37.1	869	24.0
43.3	831	22.6
49.5	787	20.7
55.7	742	19.0
61.9	699	17.4
68.1	650	15.6
74.3	596	13.8
80.5	549	12.2
86.7	496	10.5
92.9	432	8.6
99.0	369	6.8
105.2	312	5.3

TABLE XII

EVAPORATION DATA - FIXED CUMENE DROPS

Field voltage = 2.5 volts

D = Drop diameter (microns)
t = Elapsed time (seconds)

Run 2-9 v = 0.00 fps T = 87° F.			Run 5-2 v = 0.00 fps T = 86° F.			Run 5-14 v = 0.00 fps T = 85° F.		
t	D	$(\frac{D}{100})^{1.88}$	t	D	$(\frac{D}{100})^{1.88}$	t	D	$(\frac{D}{100})^{1.88}$
0.0	1200	106.5	0.0	979	72.8	0.0	968	71.3
15.3	--	--	18.4	947	68.1	20.4	942	68.0
30.7	1155	99.2	36.8	916	64.1	40.9	904	62.8
46.0	1124	95.0	55.1	877	59.2	61.3	868	58.0
61.3	1094	89.8	73.5	844	55.2	81.7	828	53.1
76.7	1060	84.6	91.9	806	50.4	102.2	788	48.4
92.0	1021	79.0	110.3	769	46.2	122.6	748	43.9
107.3	993	74.8	128.7	725	41.4	143.0	704	39.2
122.7	965	70.8	147.0	689	37.4	163.4	655	34.2
138.0	924	65.4	165.4	645	33.2	183.9	605	29.5
153.3	898	62.0	183.8	602	29.2	204.3	555	25.1
168.7	861	57.2	202.2	547	24.5	224.7	492	20.0
184.0	827	52.9	220.6	493	20.1	245.2	430	15.5
199.3	787	48.2	238.9	434	15.8	265.6	357	10.9
214.7	745	43.7	257.3	370	11.7	286.0	272	6.6
230.0	708	39.5	275.7	288	7.3			
245.3	662	35.0						
260.7	618	30.7						
276.0	566	26.0						
291.3	507	21.1						
306.7	449	16.8						
322.0	387	12.8						

TABLE XIII

EVAPORATION DATA - FIXED CUMENE DROPS

Field Voltage = 2.5 volts

D = Drop diameter (microns)
t = Elapsed time (seconds)

Run 5-3 v = 0.82 fps T = 86° F.			Run 2-10 v = 0.82 fps T = 88° F.			Run 2-11 v = 1.16 fps T = 87° F.			Run 5-4 v = 1.16 fps T = 86° F.		
t	D	$(\frac{D}{100})^{1.69}$	t	D	$(\frac{D}{100})^{1.69}$	t	D	$(\frac{D}{100})^{1.65}$	t	D	$(\frac{D}{100})^{1.65}$
0.0	1055	53.6	0.0	932	43.6	0.0	1015	45.8	0.0	1112	53.0
14.3	1010	49.9	15.3	875	39.1	15.3	954	41.3	13.3	1075	50.1
28.5	967	46.2	30.7	814	34.7	30.7	894	37.1	26.5	1028	46.9
42.8	919	42.4	46.0	751	30.2	46.0	834	33.1	39.8	982	43.4
57.1	874	39.0	61.3	687	25.9	61.3	767	28.8	53.1	934	40.0
71.4	828	35.5	76.7	613	21.4	76.7	697	24.6	66.4	886	36.7
85.6	775	31.9	92.0	536	17.1	92.0	615	20.0	79.6	833	33.0
99.9	721	28.2	107.3	447	12.6	107.3	536	16.0	92.9	785	30.0
114.2	665	24.5	122.7	341	7.9	122.7	447	11.8	106.2	728	26.5
128.4	603	20.9				138.0	346	7.8	119.4	671	23.1
142.7	542	17.4							132.7	606	19.5
156.9	471	13.8							146.0	544	16.4
171.2	395	10.2							159.2	473	13.0
185.5	312	6.9							172.5	388	9.3
									185.8	303	6.2

Run 2-12 v = 2.01 fps T = 87° F.			Run 5-5 v = 2.01 fps T = 86° F.			Run 2-13 v = 2.48 fps T = 87° F.			Run 5-6 v = 2.48 fps T = 86° F.		
t	D	$(\frac{D}{100})^{1.63}$	t	D	$(\frac{D}{100})^{1.63}$	t	D	$(\frac{D}{100})^{1.625}$	t	D	$(\frac{D}{100})^{1.625}$
0.0	820	30.8	0.0	989	41.9	0.0	924	37.1	0.0	987	41.2
13.3	750	26.6	12.3	942	38.8	12.3	872	33.9	11.2	942	38.3
26.5	680	22.8	24.5	889	35.2	24.5	808	29.8	22.5	883	34.4
39.8	600	18.5	36.8	834	31.8	36.8	741	25.9	33.7	838	31.6
53.0	513	14.4	49.1	777	28.3	49.0	667	21.8	45.0	780	28.2
66.3	417	10.2	61.4	717	24.7	61.3	591	18.0	56.2	721	24.8
79.5	311	6.3	73.6	659	21.5	73.5	510	14.1	67.4	661	21.6
			85.9	590	18.1	85.8	417	10.2	78.7	601	18.5
			98.2	520	14.7				89.9	534	15.2
			110.4	439	11.1				101.2	458	11.8
			122.7	350	7.7				112.4	373	8.5
									123.6	277	5.2

TABLE XIV

EVAPORATION DATA - FIXED CUMENE DROPS

Field Voltage = 2.5 volts

D = Drop diameter (microns)
t = Elapsed time (seconds)

Run 2-14 v = 3.51 fps T = 87° F.			Run 5-7 v = 3.51 fps T = 86° F.			Run 2-15 v = 4.29 fps T = 87° F.			Run 5-8 v = 4.29 fps T = 86° F.		
t	D	$(\frac{D}{100})^{1.62}$	t	D	$(\frac{D}{100})^{1.62}$	t	D	$(\frac{D}{100})^{1.60}$	t	D	$(\frac{D}{100})^{1.60}$
0.0	972	39.9	0.0	1023	43.3	0.0	1062	44.0	0.0	966	37.7
10.2	922	36.7	10.2	974	40.0	10.2	1013	40.6	10.2	909	34.1
20.4	868	33.0	20.4	921	36.5	20.4	954	36.9	20.4	858	31.0
30.6	808	29.5	30.7	866	33.0	30.6	891	33.1	30.7	799	27.7
			40.9	810	29.6	40.8	829	29.5	40.9	732	24.1
			51.1	759	26.6	51.0	764	25.9	51.1	673	21.1
			61.3	701	23.5	61.2	690	22.0	61.3	602	17.7
			71.5	633	19.9	71.4	617	18.4	71.5	532	14.5
			81.8	572	16.9	81.6	536	14.7	81.8	453	11.2
			92.0	500	13.6	91.8	447	11.0	92.0	360	7.7
			102.2	418	10.2	102.0	350	7.4			
			112.4	331	6.9						

Run 2-16 v = 4.96 fps T = 87° F.			Run 5-9 v = 4.96 fps T = 86° F.			Run 5-10 v = 6.07 fps T = 86° F.			Run 2-18 v = 7.00 fps T = 87° F.		
t	D	$(\frac{D}{100})^{1.60}$	t	D	$(\frac{D}{100})^{1.60}$	t	D	$(\frac{D}{100})^{1.58}$	t	D	$(\frac{D}{100})^{1.57}$
0.0	1006	40.2	0.0	964	37.5	0.0	1075	42.5	0.0	1021	38.3
8.2	957	37.0	9.2	920	34.8	9.2	1023	39.5	7.2	979	35.9
16.4	910	34.2	18.4	863	31.4	18.4	974	36.5	14.3	924	32.9
24.6	861	31.3	27.6	812	28.5	27.6	916	33.0	21.5	877	30.1
32.8	803	28.1	36.8	758	25.5	36.8	858	29.8	28.6	823	27.4
41.0	747	24.9	46.1	700	22.5	46.1	803	26.8	35.8	770	24.6
49.2	691	22.1	55.3	635	19.3	55.3	743	23.8	42.9	710	21.6
57.4	631	19.1	64.5	573	16.3	64.5	674	20.4	50.1	649	18.8
65.6	565	15.9	73.7	504	13.3	73.7	605	17.2	57.2	584	16.0
73.8	498	13.0	82.9	422	10.0	82.9	535	14.1	64.4	519	13.2
82.0	419	9.9	92.1	338	7.0	92.1	455	11.0	71.5	443	10.3
						101.3	373	8.0	78.7	359	7.4

TABLE XV

EVAPORATION DATA - FIXED CUMENE DROPS

Field voltage = 2.5 volts

D = Drop diameter (microns)
t = Elapsed time (seconds)

Run 5-11 v = 7.00 fps T = 86° F.			Run 3-2 v = 7.84 fps T = 86° F.			Run 5-12 v = 7.84 fps T = 85° F.			Run 5-13 v = 8.59 fps T = 85° F.		
t	D	$(\frac{D}{100})^{1.57}$	t	D	$(\frac{D}{100})^{1.53}$	t	D	$(\frac{D}{100})^{1.53}$	t	D	$(\frac{D}{100})^{1.47}$
0.0	941	33.8	0.0	877	27.6	0.0	1070	37.6	0.0	1076	32.8
9.2	885	30.7	7.1	835	25.7	8.2	1032	35.4	8.2	1030	30.9
18.4	828	27.6	14.2	787	23.5	16.4	982	33.0	16.4	977	28.5
27.7	762	24.3	21.4	735	21.1	24.6	926	30.1	24.6	922	26.1
36.9	694	21.0	28.5	680	18.8	32.8	871	27.5	32.8	861	23.7
46.1	621	17.6	35.6	625	16.5	41.1	813	24.7	41.0	803	21.4
55.3	552	14.6	42.7	564	14.1	49.3	748	21.7	49.2	745	19.1
64.5	472	11.4	49.8	501	11.8	57.5	689	19.1	57.4	676	16.6
73.8	381	8.2	57.0	433	9.4	65.7	628	16.6	65.6	610	14.2
83.0	288	5.3	64.1	354	6.9	73.9	560	13.9	73.8	537	11.8
						82.1	487	11.2	82.0	459	9.4
						90.3	401	8.4	90.2	373	6.9
						98.5	315	5.8	98.4	290	4.8

TABLE XVI

EVAPORATION DATA - FIXED CUMENE DROPS

Field voltage = 5 volts

D = Drop diameter (microns)
t = Elapsed time (seconds)

Run 3-3
v = 0.00 fps
T = 86° F.

t	D	$(\frac{D}{100})^{1.88}$
0.0	933	66.4
18.3	903	62.6
36.6	867	58.1
54.9	833	53.9
73.2	794	49.1
91.5	752	44.4
109.8	716	40.5
128.1	673	36.1
146.4	625	31.3
164.7	578	27.0
183.0	529	22.9
201.3	473	18.6
219.6	415	14.5
237.9	341	10.0

Run 5-15
v = 0.00 fps
T = 86° F.

t	D	$(\frac{D}{100})^{1.88}$
0.0	1048	82.8
18.4	1017	78.0
36.8	989	74.0
55.3	954	69.5
73.7	921	65.0
92.1	889	60.7
110.5	855	56.4
128.9	818	52.0
147.4	-	--
165.8	744	43.7
184.2	702	39.1
202.6	659	34.7
221.0	615	30.4
239.5	563	25.7
257.9	511	21.5
276.3	456	17.4
294.7	392	13.0
313.1	329	9.4
331.6	269	6.4

Run 3-4
v = 0.82 fps
T = 86° F.

t	D	$(\frac{D}{100})^{1.69}$
0.0	951	44.9
15.3	901	41.1
30.5	851	37.2
45.8	798	33.4
61.0	740	29.5
76.3	681	25.6
91.5	619	21.7
106.8	552	17.9
122.0	476	14.0
137.3	392	10.1
152.5	304	6.5

Run 3-5
v = 1.16 fps
T = 86° F.

t	D	$(\frac{D}{100})^{1.65}$
0.0	890	36.9
15.3	833	33.0
30.5	774	29.3
45.8	715	25.6
61.0	645	21.6
76.3	578	18.1
91.5	498	14.2
106.8	407	10.2
122.0	304	6.2

Run 3-7
v = 2.01 fps
T = 86° F.

t	D	$(\frac{D}{100})^{1.63}$
0.0	1084	48.7
15.3	1031	44.8
30.5	970	40.7
45.8	908	36.3
61.0	844	32.3
76.3	775	28.1
91.5	704	24.1
106.8	627	19.9
122.0	551	16.1
137.3	462	12.1
152.5	373	8.6
167.8	323	6.7

Run 3-8
v = 2.48 fps
T = 86° F.

t	D	$(\frac{D}{100})^{1.625}$
0.0	1014	43.0
15.3	952	39.0
30.5	882	34.3
45.8	813	30.1
61.0	736	25.6
76.3	653	21.1
91.5	566	16.7
106.8	473	12.4
122.0	367	8.3

Run 3-9
v = 3.51 fps
T = 86° F.

t	D	$(\frac{D}{100})^{1.62}$
0.0	962	39.1
15.3	891	34.7
30.5	810	29.6
45.8	731	25.0
61.0	632	19.9
76.3	548	15.8
91.5	443	11.2
106.8	333	7.0

Run 3-10
v = 4.29 fps
T = 86° F.

t	D	$(\frac{D}{100})^{1.60}$
0.0	952	36.9
15.3	874	32.1
30.5	790	27.3
45.8	699	22.5
61.0	609	18.0
76.3	503	13.2
91.5	386	8.7

TABLE XVII

EVAPORATION DATA - FIXED CUMENE DROPS

Field voltage = 5 volts

D = Drop diameter (microns)
t = Elapsed time (seconds)

Run 3-11
v = 4.96 fps
T = 86° F.

t	D	$(\frac{D}{100})^{1.60}$
0.0	906	34.0
15.3	823	29.2
30.5	731	24.2
45.8	632	19.1
61.0	525	14.1
76.3	408	9.5

Run 3-12
v = 6.07 fps
T = 86° F.

t	D	$(\frac{D}{100})^{1.53}$
0.0	975	36.6
13.3	901	32.2
26.5	816	27.5
39.8	733	23.3
53.1	639	18.7
66.4	543	14.5
79.6	434	10.2
92.9	332	6.6

Run 3-13
v = 7.00 fps
T = 86° F.

t	D	$(\frac{D}{100})^{1.57}$
0.0	872	30.0
12.3	805	26.5
24.5	717	22.0
36.8	623	17.7
49.0	527	13.6
61.3	416	9.4
73.5	291	5.4

Run 3-14
v = 7.84 fps
T = 86° F.

t	D	$(\frac{D}{100})^{1.53}$
0.0	1081	38.2
10.2	1023	35.1
20.4	958	31.8
30.6	899	28.8
40.8	830	25.5
51.1	755	22.0
61.3	683	18.9
71.5	601	15.6
81.7	519	12.4
91.9	423	9.1
102.1	332	6.3

Run 6-2
v = 7.84 fps
T = 84° F.

t	D	$(\frac{D}{100})^{1.53}$
0.0	1041	36.0
9.2	984	33.1
18.3	926	30.1
27.5	863	27.0
36.6	800	24.1
45.8	734	21.1
55.0	666	18.1
64.1	592	15.2
73.3	513	12.2
82.4	428	9.2
91.6	339	6.5

Run 6-3
v = 8.59 fps
T = 84° F.

t	D	$(\frac{D}{100})^{1.47}$
0.0	1051	31.8
8.2	1003	29.6
16.3	946	27.2
24.5	895	25.1
32.6	836	22.6
40.8	778	20.4
48.9	715	18.0
57.1	650	15.6
65.2	584	13.4
73.4	514	11.1
81.5	435	8.7
89.7	351	6.3

TABLE XVIII

EVAPORATION DATA - FIXED CUMENE DROPS

Field voltage = 10 volts

D = Drop diameter (microns)
t = Elapsed time (seconds)

Run 3-15
v = 0.00 fps
T = 86° F.

t	D	$(\frac{D}{100})^{1.88}$
0.0	987	73.9
20.4	956	69.7
40.8	916	64.1
61.3	869	58.1
81.7	830	53.3
102.1	783	48.0
122.5	739	43.0
142.9	693	38.2
163.4	642	33.1
183.8	587	27.9
204.2	530	23.0
224.6	467	18.1
245.0	389	12.8
265.5	307	8.2

Run 6-13
v = 0.00 fps
T = 84° F.

t	D	$(\frac{D}{100})^{1.88}$
0.0	1027	80.0
20.5	998	75.4
40.9	962	70.7
61.4	926	65.7
81.8	891	61.2
102.3	855	56.5
122.7	816	51.9
143.2	779	47.2
163.6	734	42.5
184.1	691	37.9
204.5	647	33.4
225.0	598	28.8
245.4	547	24.5
265.9	495	20.2
286.3	443	16.4
306.8	386	12.7
327.2	352	10.7

Run 3-16
v = 0.82 fps
T = 86° F.

t	D	$(\frac{D}{100})^{1.69}$
0.0	1049	53.1
15.3	1011	49.9
30.6	959	45.5
45.9	912	41.9
61.2	857	37.7
76.6	809	34.1
91.9	752	30.2
107.2	696	26.5
122.5	639	22.9
137.8	573	19.1
153.1	505	15.5
168.4	429	11.7
183.7	350	8.3

Run 3-17
v = 1.16 fps
T = 86° F.

t	D	$(\frac{D}{100})^{1.65}$
0.0	970	42.3
17.4	913	38.4
34.7	849	34.0
52.1	781	29.7
69.4	716	25.6
86.8	635	21.1
104.1	556	17.0
121.5	469	12.8
138.8	366	8.5

Run 6-4
v = 2.01 fps
T = 84° F.

t	D	$(\frac{D}{100})^{1.63}$
0.0	1041	45.7
12.2	1005	43.0
24.4	957	39.8
36.6	908	36.3
48.8	863	33.7
61.1	811	30.3
73.3	755	27.0
85.5	696	23.6
97.7	639	20.5
109.9	579	17.5
122.1	513	14.4
134.3	443	11.3
146.5	367	8.3
158.7	303	6.1

Run 3-18
v = 2.01 fps
T = 86° F.

t	D	$(\frac{D}{100})^{1.68}$
0.0	1067	47.4
17.4	1002	42.9
34.7	929	37.8
52.1	851	32.9
69.4	776	28.2
86.8	696	23.6
104.1	609	19.0
121.5	512	14.3
138.8	402	9.7

Run 6-5
v = 2.48 fps
T = 84° F.

t	D	$(\frac{D}{100})^{1.625}$
0.0	1036	44.6
11.2	995	41.9
22.4	950	38.8
33.7	901	35.7
44.9	855	32.8
56.1	801	29.5
67.3	748	26.3
78.5	690	23.0
89.8	633	20.1
101.0	571	17.0
112.2	506	14.0
123.4	437	11.0
134.6	361	8.0
145.9	298	5.9

Run 6-6
v = 3.51 fps
T = 84° F.

t	D	$(\frac{D}{100})^{1.62}$
0.0	1027	43.5
10.2	989	40.8
20.4	938	37.5
30.6	889	34.3
40.8	842	31.7
51.1	786	28.2
61.3	733	25.2
71.5	677	22.1
81.7	618	19.1
91.9	554	16.0
102.1	488	13.0
112.3	412	9.9
122.5	340	7.3
132.7	282	5.4

TABLE XIX

EVAPORATION DATA - FIXED CUMENE DROPS

Field voltage = 10 volts

D = Drop diameter (microns)
t = Elapsed time (seconds)

Run 6-7 v = 4.29 fps T = 84° F.			Run 6-8 v = 4.96 fps T = 84° F.			Run 6-9 v = 6.07 fps T = 84° F.			Run 6-10 v = 7.00 fps T = 84° F.		
t	D	$(\frac{D}{100})^{1.60}$	t	D	$(\frac{D}{100})^{1.60}$	t	D	$(\frac{D}{100})^{1.58}$	t	D	$(\frac{D}{100})^{1.57}$
0.0	1023	41.4	0.0	1040	42.3	0.0	986	37.1	0.0	1057	40.4
10.2	977	38.2	9.2	994	39.4	9.2	946	34.8	9.2	993	36.8
20.4	924	35.1	18.4	944	36.2	18.4	886	31.3	18.4	938	33.5
30.6	874	32.1	27.6	894	33.2	27.6	832	28.5	27.6	883	30.6
40.8	820	29.1	36.8	843	30.3	36.8	775	25.5	36.8	823	27.4
51.0	762	25.8	46.0	791	27.4	46.0	712	22.3	46.1	763	24.4
61.2	707	22.9	55.1	735	24.3	55.2	655	19.5	55.3	700	21.1
71.4	645	19.7	64.3	683	21.6	64.4	592	16.6	64.5	635	18.2
81.6	579	16.6	73.5	621	18.6	73.6	519	13.5	73.7	567	15.2
91.8	506	13.4	82.7	559	15.7	82.8	443	10.5	82.9	495	12.4
102.0	436	10.5	91.9	495	12.9	92.0	361	7.6	92.1	417	9.4
112.2	356	7.6	101.1	424	10.1	101.2	292	5.5	101.3	343	6.9
122.4	298	5.7	110.3	353	7.5				110.5	305	5.8
			119.5	299	5.7						

Run 6-11 v = 7.84 fps T = 83° F.			Run 6-12 v = 8.59 fps T = 83° F.		
t	D	$(\frac{D}{100})^{1.53}$	t	D	$(\frac{D}{100})^{1.47}$
0.0	1021	35.0	0.0	1037	31.0
8.2	973	32.6	8.2	989	29.0
16.4	919	29.7	16.4	938	26.8
24.6	867	27.2	24.6	883	24.6
32.8	812	24.7	32.8	828	22.4
41.0	758	22.1	41.0	767	19.9
49.1	698	19.6	49.2	707	17.7
57.3	639	17.0	57.4	645	15.5
65.5	578	14.6	65.6	577	13.2
73.7	511	12.1	73.8	506	10.8
81.9	439	9.6	82.0	431	8.6
90.1	369	7.4	90.2	355	6.4
98.3	323	6.0	98.4	305	5.1

TABLE XX

EVAPORATION DATA - FIXED CUMENE DROPS

Field voltage = 20 volts

D = Drop diameter (microns)
t = Elapsed time (seconds)

Run 8-13
v = 0.00 fps
T = 82° F.

t	D	$(\frac{D}{100})^{1.88}$
0.0	1075	87.0
25.5	1022	79.1
51.0	966	70.8
76.4	906	62.7
101.9	848	55.6
127.4	781	47.8
152.9	709	39.7
178.4	630	31.7
203.8	548	24.4
229.3	455	17.2
254.8	348	10.4

Run 8-2
v = 0.82 fps
T = 83° F.

t	D	$(\frac{D}{100})^{1.69}$
0.0	956	45.3
20.3	878	39.2
40.6	795	33.2
60.9	709	27.4
81.2	613	21.4
101.5	508	15.6
121.8	394	10.1
142.1	323	7.3

Run 8-3
v = 1.16 fps
T = 83° F.

t	D	$(\frac{D}{100})^{1.65}$
0.0	978	43.0
18.3	909	38.1
36.7	831	33.0
55.0	750	27.7
73.4	663	22.6
91.7	568	17.5
110.0	459	12.4
128.4	356	8.1
146.7	319	6.8

Run 8-4
v = 2.01 fps
T = 83° F.

t	D	$(\frac{D}{100})^{1.63}$
0.0	1040	45.3
15.3	971	40.8
30.6	902	36.0
45.9	831	31.7
61.2	753	26.9
76.5	674	22.5
91.7	588	17.9
107.0	493	13.5
122.3	395	9.4
137.6	338	7.3

Run 8-5
v = 2.48 fps
T = 83° F.

t	D	$(\frac{D}{100})^{1.625}$
0.0	1006	42.8
14.3	941	38.3
28.5	870	33.5
42.8	799	29.3
57.1	718	24.5
71.4	633	20.1
85.6	543	15.6
99.9	445	11.3
114.2	348	7.6
128.4	308	6.2

Run 8-6
v = 3.51 fps
T = 83° F.

t	D	$(\frac{D}{100})^{1.62}$
0.0	1028	43.7
14.3	959	38.9
28.6	879	33.8
42.9	806	29.4
57.2	717	24.3
71.5	628	19.5
85.7	534	15.1
100.0	428	10.5
114.3	327	6.8

Run 8-7
v = 4.29 fps
T = 84° F.

t	D	$(\frac{D}{100})^{1.60}$
0.0	1043	42.7
13.3	969	37.8
26.5	898	33.4
39.8	819	28.9
53.1	739	24.5
66.4	649	19.9
79.6	556	15.5
92.9	456	11.4

Run 8-8
v = 4.96 fps
T = 83° F.

t	D	$(\frac{D}{100})^{1.60}$
0.0	1034	42.0
13.3	967	37.7
26.5	894	33.2
39.8	809	28.3
53.1	725	23.8
66.4	638	19.4
79.6	540	14.8
92.9	438	10.6
106.2	343	7.2
119.4	315	6.3

TABLE XXI

EVAPORATION DATA - FIXED CUMENE DROPS

Field voltage = 20 volts

D = Drop diameter (microns)
t = Elapsed time (seconds)

Run 8-9 v = 6.07 fps T = 81° F.			Run 8-10 v = 7.00 fps T = 81° F.			Run 8-11 v = 7.84 fps T = 81° F.			Run 8-12 v = 8.59 fps T = 81° F.		
t	D	$(\frac{D}{100})^{1.58}$	t	D	$(\frac{D}{100})^{1.57}$	t	D	$(\frac{D}{100})^{1.53}$	t	D	$(\frac{D}{100})^{1.47}$
0.0	988	37.1	0.0	1013	37.8	0.0	980	32.9	0.0	1044	31.6
12.2	926	33.7	12.2	938	33.6	11.2	915	29.6	9.2	988	29.1
24.4	853	29.5	24.4	862	29.5	22.5	846	26.2	18.4	931	26.6
36.5	781	25.8	36.6	783	25.3	33.7	767	22.5	27.6	869	23.9
48.7	704	21.9	48.8	701	21.4	45.0	688	19.1	36.8	803	21.4
60.9	619	17.8	61.1	619	17.5	56.2	602	15.6	46.0	738	18.9
73.1	532	14.0	73.3	513	13.0	67.4	513	12.2	55.1	669	16.3
85.3	422	9.7	85.5	-	--	78.7	394	8.1	64.3	598	13.9
97.4	314	6.1	97.7	283	5.1	89.9	286	5.0	73.5	524	11.4
									82.7	433	8.6
									91.9	342	6.1

TABLE XXII

EVAPORATION DATA - FIXED CUMENE DROPS

Field Voltage = 25 volts

D = Drop diameter (microns)
t = Elapsed time (seconds)

Run 8-14
v = 0.00 fps
T = 82° F.

t	D	$(\frac{D}{100})^{1.88}$
0.0	1009	77.2
25.5	956	69.7
51.1	909	63.4
76.6	821	52.5
102.2	730	41.9
127.7	639	32.5
153.2	538	23.6
178.8	406	14.0
204.3	278	6.8

Run 9-6
v = 0.00 fps
T = 80° F.

t	D	$(\frac{D}{100})^{1.88}$
0.0	983	42.9
30.5	921	65.0
61.1	826	52.8
91.6	716	40.3
122.2	612	30.3
152.7	475	18.8
183.2	316	8.7
213.8	261	6.1

Run 8-15
v = 0.82 fps
T = 82° F.

t	D	$(\frac{D}{100})^{1.69}$
0.0	988	47.9
20.4	882	39.7
40.9	774	31.8

Run 8-16
v = 1.16 fps
T = 81° F.

t	D	$(\frac{D}{100})^{1.65}$
0.0	1059	49.0
16.3	985	43.6
32.6	909	38.1
48.9	828	32.7
65.2	738	27.0
81.6	644	21.6
97.9	543	15.3
114.2	431	11.2
130.5	303	6.2

Run 8-17
v = 2.01 fps
T = 81° F.

t	D	$(\frac{D}{100})^{1.63}$
0.0	1063	47.1
14.3	991	42.0
28.5	915	36.9
42.8	838	32.0
57.1	754	27.0
71.4	669	22.1
85.6	581	17.6
99.9	481	12.9
114.2	374	8.6

Run 8-18
v = 2.48 fps
T = 81° F.

t	D	$(\frac{D}{100})^{1.625}$
0.0	1071	47.0
14.3	997	41.9
28.5	915	36.4
42.8	838	31.6
57.1	756	26.8
71.4	671	22.1
85.6	584	17.6
99.9	483	12.9
114.2	374	8.5

Run 8-19
v = 3.51 fps
T = 81° F.

t	D	$(\frac{D}{100})^{1.62}$
0.0	993	41.2
13.3	955	38.7
26.6	874	33.5
39.9	796	28.8
53.2	713	24.1
66.5	631	19.8
79.8	534	15.1
93.1	423	10.3
106.4	313	6.3

Run 8-20
v = 4.29 fps
T = 81° F.

t	D	$(\frac{D}{100})^{1.60}$
0.0	1025	41.3
11.2	966	37.7
22.4	899	33.6
33.7	831	29.6
44.9	763	25.9
56.1	688	21.9
67.3	616	18.4
78.5	535	14.6
89.8	449	11.1
101.0	356	7.6

TABLE XXIII

EVAPORATION DATA - FIXED CUMENE DROPS

Field voltage = 25 volts

D = Drop diameter (microns)
t = Elapsed time (seconds)

Run 8-21
v = 4.29 fps
T = 81° F.

t	D	$(\frac{D}{100})^{1.60}$
0.0	1072	44.4
11.2	1006	40.1
22.5	936	35.8
33.7	866	31.6
45.0	797	27.6
56.2	722	23.6
67.4	644	19.7
78.7	566	16.0
89.9	476	12.1
101.2	383	8.6
112.4	272	5.0

Run 8-22
v = 4.96 fps
T = 81° F.

t	D	$(\frac{D}{100})^{1.60}$
0.0	1066	44.1
10.2	1008	40.4
20.4	943	36.2
30.6	882	32.7
40.8	816	28.7
51.0	753	25.3
61.2	684	21.7
71.4	613	18.2
81.6	538	14.8
91.8	450	11.1
102.0	369	8.1
112.2	275	5.0

Run 8-23
v = 6.07 fps
T = 81° F.

t	D	$(\frac{D}{100})^{1.58}$
0.0	991	37.6
10.2	928	33.8
20.4	860	29.9
30.6	794	26.5
40.8	724	22.9
51.0	653	19.4
61.2	576	15.9
71.4	490	12.3

Run 9-2
v = 6.07 fps
T = 80° F.

t	D	$(\frac{D}{100})^{1.58}$
0.0	992	37.6
10.2	929	33.8
20.3	856	29.7
30.5	783	25.8
40.7	705	21.9
50.9	625	18.1
61.0	548	14.7
71.2	439	10.3
81.4	368	7.8
91.5	274	4.9

Run 9-3
v = 7.00 fps
T = 80° F.

t	D	$(\frac{D}{100})^{1.57}$
0.0	996	37.0
10.2	929	33.0
20.4	856	29.1
30.6	779	25.0
40.8	705	21.5
51.1	625	17.8
61.3	535	13.9
71.5	434	10.0
81.7	341	6.9

Run 9-4
v = 7.84 fps
T = 80° F.

t	D	$(\frac{D}{100})^{1.53}$
0.0	987	33.1
9.2	926	30.1
18.4	864	27.1
27.5	798	24.0
36.7	736	21.2
45.9	667	18.1
55.1	594	15.3
64.3	519	12.4
73.4	433	9.4
82.6	347	6.7
91.8	269	4.5

Run 9-5
v = 8.59 fps
T = 80° F.

t	D	$(\frac{D}{100})^{1.47}$
0.0	995	29.3
9.2	947	27.2
18.4	894	25.0
27.6	831	22.5
36.8	772	20.2
46.1	710	17.9
55.3	650	15.7
64.5	577	13.2
73.7	502	10.7
82.9	415	8.1
92.1	344	6.1
101.3	293	4.9

TABLE XXIV

EVAPORATION DATA FOR SOME PURE LIQUIDS--FREE DROPS

2,4-Dimethylpentane		Ethyl n-Valerate		Ethyl Alcohol	
Time Sec.	Diameter μ	Time Sec.	Diameter μ	Time Sec.	Diameter μ
0	704	0	1280	0	988
4.25	431	28.5	985	9	851
4.69	410	57.5	740	23	588
7.31	231	87.5	426	32	431

n-Octane		Pyridine		Cumene	
Time Sec.	Diameter μ	Time Sec.	Diameter μ	Time Sec.	Diameter μ
0	1050	0	1050	0	1220
9	862	7.5	945	13	1080
19	630	17.0	798	28	977
29	410	27.2	640	42	840
37	210	37.5	493	57	725
		47.0	315	72	588
		47.5	294	89	461
				102	325
				118	168

Tert-Amyl Alcohol		n-Butyl Alcohol			
Time Sec.	Diameter μ	Time Sec.	Diameter μ	Time Sec	Diameter μ
0	1000	0	1178	61.3	654
3.18	986	3.4	1167	64.4	622
6.43	938	6.8	1145	67.6	589
11.80	861	9.1	1135	71.7	567
15.43	787	12.2	1080	73.6	534
19.06	722	15.8	1058	87.2	425
22.68	659	22.2	980	90.1	392
26.30	606	24.9	948	93.4	371
29.93	529	27.8	926	104.6	283
33.74	468	37.8	840	106.1	261
37.49	417	40.9	818	107.3	240
41.24	356	44.0	774		
45.18	270	47.2	764		
47.37	240	48.3	752		

TABLE XXV

EVAPORATION DATA FOR SOME PURE LIQUIDS--FREE DROPS

n-Decane		Methyl n-Hexyl Ketone		Tert-Butylbenzene	
Time Sec	Diameter μ	Time Sec	Diameter μ	Time Sec	Diameter μ
0	1143	0	1010	0	1196
57.7	970	67	910	35.4	1040
146.5	637	245	495	65.4	882
207.5	445	306	344	95.4	745
266.5	253	366	239	125.4	640
				155.4	462
				185.4	304

n-Butylbenzene		2-Heptanone	
Time Sec	Diameter μ	Time Sec	Diameter μ
0	1174	0	1210
45.3	1052	12	1120
105.3	942	28	1010
165.9	800	42	936
226.3	648	58	820
287.3	517	73	693
346.0	365	88	609
406.3	223	103	514
408.5	202	118	410
		133	273

TABLE XXVI

EVAPORATION DATA FOR FREE DROPS OF ACETOPHENONE AND KEROSENE

Acetophenone

Time Min-Sec	Diameter μ	Time Min-Sec	Diameter μ
0-0	987	14-44.3	317
0-45.0	932	15-45.2	264
1-46.5	901	16-45.2	214
4-46.4	794	17-45.0	155
6-45.6	708	18-15.1	138
8-46.2	611	19-47.5	103
10-53.2	517	20-16.1	94
12-46.1	409	20-46.0	91

Kerosene

Time Min-Sec	Diameter μ	Time Min-Sec	Diameter μ
0-0	862	43-20	490
2-20	795	46-20	480
4-20	745	49-20	480
6-20	730	52-20	480
8-20	700	55-20	485
10-20	675	58-20	468
13-20	633	63-20	446
16-20	630	68-20	440
19-20	610	73-20	425
22-20	590	78-20	414
25-20	560	85-20	403
28-20	545	93-20	382
31-20	540	98-20	370
34-20	530	103-20	360
37-20	512	108-20	360
40-20	495	113-20	327

APPENDIX C

PHYSICAL PROPERTIES AND CONSTANTS

TABLE XXVII

PROPERTIES OF AIR (83°F)

Property	Symbol	Value	Units
Thermal Conductivity	k_a	4.28×10^{-6}	B/sec ft F
Specific Heat	c_a	0.24	B/lb F
Specific Density	ρ_a	0.073	lb/ft^3
Absolute Viscosity	μ_a	125×10^{-7}	lb/ft sec
Kinematic Viscosity	ν_a	17.1×10^{-5}	ft^2/sec

TABLE XXVIII

PROPERTIES OF CUMENE

Property	State	Symbol	Value	Units	°F
Thermal Conductivity	Vapor	k_v	2.22×10^{-6}	B/sec ft F	81
Specific Heat	Vapor	c	0.30	B/lb F	81
Specific Density	Liquid	ρ	55.2	lb/ft^3	60
Absolute Viscosity	Vapor	μ_v	40.3×10^{-7}	lb/ft sec	80
Latent Heat	---	L	160	B/lb	78.5

TABLE XXIX

AVERAGE PROPERTIES OF AIR-VAPOR MIXTURE
(Cumene)

Property	Symbol	Value	Units
Thermal Conductivity	k	3.25×10^{-6}	B/sec ft F
Specific Heat	c_m	0.27	B/lb F
Absolute Viscosity	μ_m	82.6×10^{-7}	lb/ft sec
Prandtl Number	Pr	0.69	--

EVAPORATION EQUATION CONSTANTS

1. $$\alpha = \frac{L}{c_v (T_f - T)} \ln \left[1 + \frac{c_v (T_f - T)}{L}\right]$$

$$= \frac{160}{0.3 (83 - 78.5)} \ln \left[1 + \frac{0.3 (83 - 78.5)}{160}\right]$$

$$\alpha = 0.9956 \text{ (dimensionless)} .$$

2. $$\beta = \frac{\pi k}{c} \ln \left[1 + \frac{c (T_f - T)}{L}\right]$$

$$= \frac{\pi (3.25 \times 10^{-6})}{0.3} \ln \left[1 + \frac{0.3 (83 - 78.5)}{160}\right]$$

$$\beta = 2.86 \times 10^{-7} \text{ (lb/ft sec)}$$

3. $$C = \frac{2}{f (Pr)^{1/3} (\frac{V}{\nu})^{1/2}} = \frac{2}{f (0.69)^{1/3} (\frac{v}{17.1 \times 10^{-5}})^{1/2}}$$

$$C = \frac{2.958}{f v^{1/2}}$$

APPENDIX D

CORRELATED RESULTS AND CHECK OF EVAPORATION EQUATION 2.51 FOR FIXED DROPS OF CUMENE, NO ULTRASONIC FIELD

TABLE XXX

DATA FOR EXPERIMENTAL CHECK OF EVAPORATION EQUATION 2.51

Run	V (fps)	Diam. μ	D_o	1000	800	600	400
4-3	0.82	t_m (sec)	0	--	58.0	111.6	152.2
		t_c (sec)	0	--	58.6	111.5	154.4
4-5	2.01	t_m (sec)	0	17.8	67.0	109.8	143.9
		t_c (sec)	0	18.2	67.3	109.5	144.1
4-8	4.29	t_m (sec)	0	28.5	67.8	101.8	128.7
		t_c (sec)	0	28.5	67.8	101.8	129.7
4-11	7.00	t_m (sec)	0	17.3	50.1	78.4	101.7
		t_c (sec)	0	17.7	50.2	78.4	101.7
4-13	8.59	t_m (sec)	0	17.3	47.2	74.2	96.8
		t_c (sec)	0	17.9	48.0	74.2	95.9

t_m = measured elapsed time of evaporation, experimental results.

t_c = computed elapsed time of evaporation Equation 3.12.

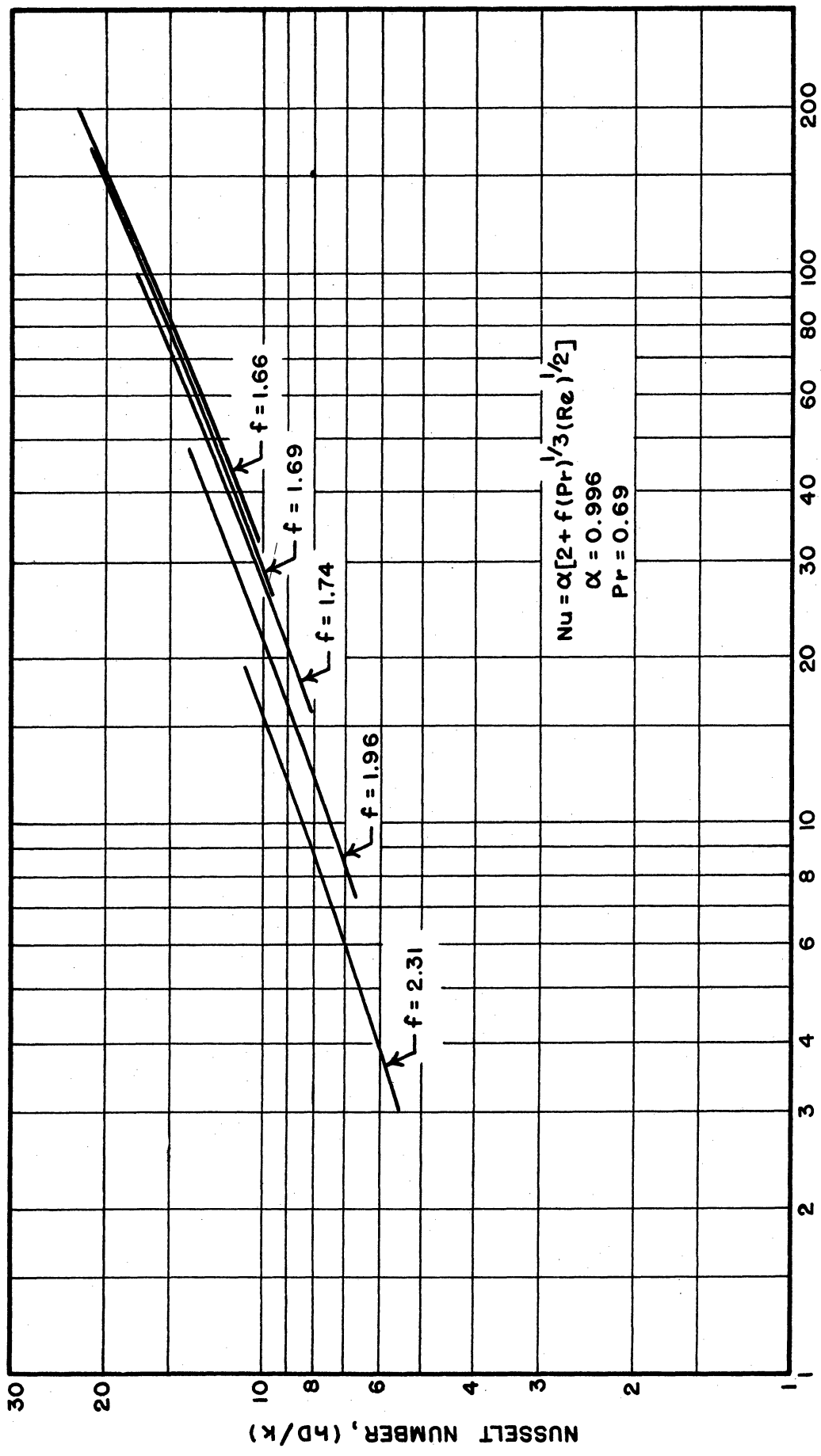

FIG.55 HEAT TRANSFER DATA FOR EVAPORATING FIXED-DROPS OF CUMENE — NO ULTRASONIC FIELD

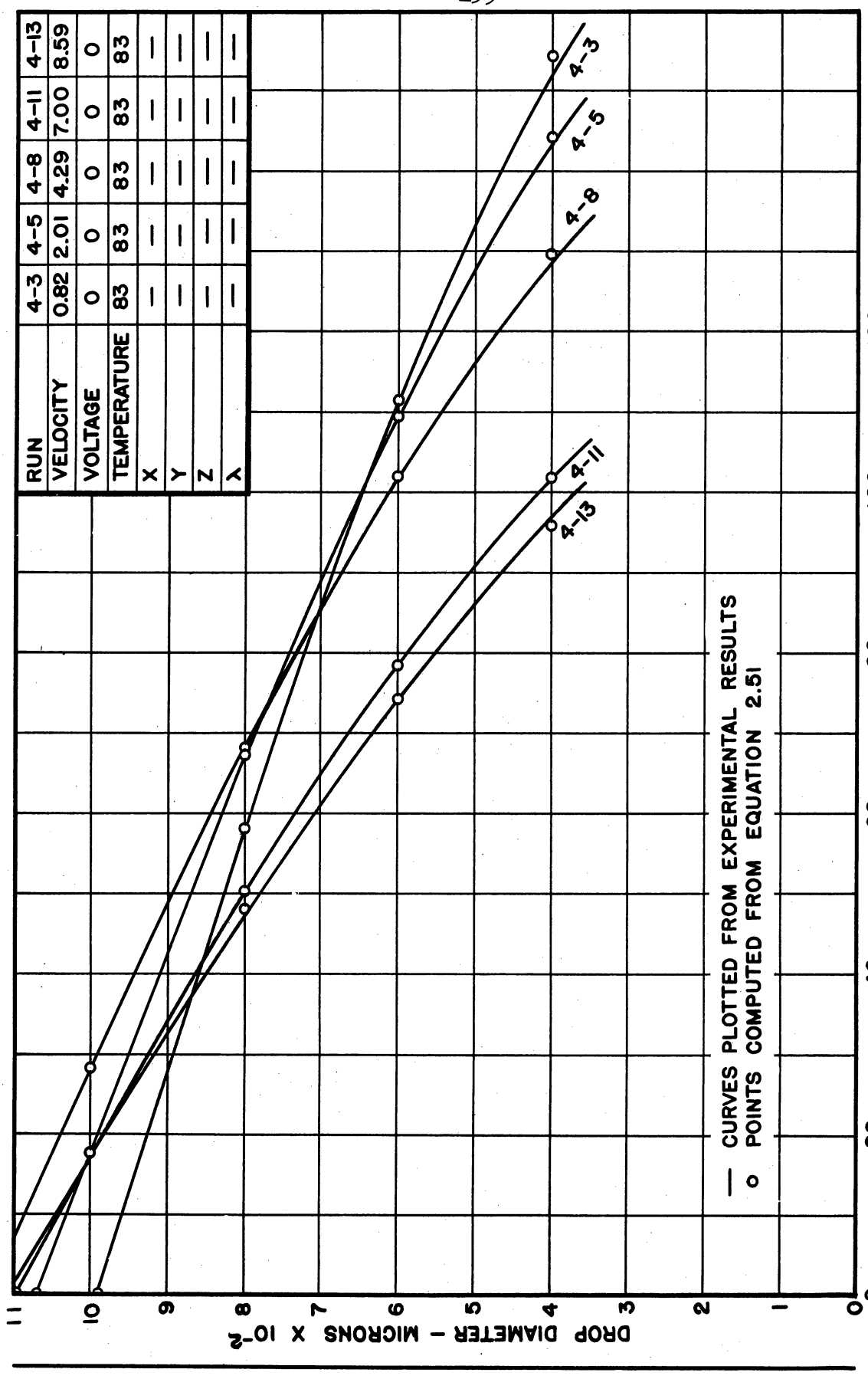

FIG. 56 EXPERIMENTAL CHECK OF EVAPORATION EQUATION 2.51

BIBLIOGRAPHY

1. Bolt, J. A., and Mirsky, W., Some Aspects of the Evaporation Rates of Liquid-Fuel Drops in a Standing Wave Ultrasonic Field, Univ. of Mich. Eng. Res. Inst., Project 2253-3, July, 1955.

2. Brown, G. G., et al. Unit Operations., New York: John Wiley and Sons, Inc., 1950.

3. Eckert, E. R. G., Introduction to the Transfer of Heat and Mass., New York: McGraw-Hill, 1950.

4. Fledderman, R. G., and Hanson, A. R., The Effects of Turbulence and Wind Speed on the Rate of Evaporation of a Fuel Spray, U.S. Navy, Bureau of Ordnance, Report CM667, 1951.

5. Frössling, N., "Uber die Verdunstung fallender Tropfen." Gerlands Beiträge d. Geophysik, 52, 170 (1938).

6. Fuchs, N., Concerning the Velocity of Evaporation of Small Droplets in a Gas Atmosphere, NACA TM-1160 (1947).

7. Godsave, G. A. E., The Combustion of Drops in a Fuel Spray, NGTE (England), Memorandum M95, 1950.

8. Godsave, G. A. E., The Burning of Single Drops of Fuel, NGTE (England): Part I, "The Temperature Distribution and Heat Transfer in the Pre-Flame Region," Report R66 (1950); Part II, "Experimental Results," Report R87 (1951); Part III, "Comparison of Experimental and Theoretical Burning Rates and Discussion of the Mechanism of the Combustion Process," Report R88 (1952); Part IV, "The Flow of Heat and Carbon Residue Formation in Drops of Fuel," Report R125 (1952).

9. Godsave, G. A. E., "Studies of the Combustion of Drops in a Fuel Spray--the Burning of Single Drops of Fuel." Fourth International Symposium on Combustion, Baltimore: Williams and Wilkins, 1953.

10. Gohrbandt, W., The Evaporation of Spheres in a Hot Air Stream, NGTE (England), Memorandum M110 (1951).

11. Goldstein, S., Modern Developments in Fluid Dynamics, 2 vols., England: Oxford University Press, 1938.

12. Graves, C. C., Burning Rates of Single Fuel Drops and their Application to Turbojet Combustion Processes, NACA RM-E53E22, 1953.

13. Hall, A. R., and Diedericksen, J., "An Experimental Study of the Burning of Single Drops of Fuel in Air at Pressures up to Twenty Atmospheres." Fourth International Symposium on Combustion, Baltimore: Williams and Wilkins, 1953.

14. Ingebo, R. D., Vaporization Rates and Heat-Transfer Coefficients for Pure Liquid Drops. NACA TN-2368 (1951).

15. Ingebo, R. D., Study of Pressure Effects on Vaporization Rate of Drops in Gas Streams. NACA TN-2850 (1953).

16. King, L. V., "On the Convection of Heat from Small Cylinders in a Stream of Fluid: Determination of the Convection Constants of Small Platinum Wires with Applications to Hot-Wire Anemometry." Phil. Trans. Roy. Soc. A, 214, 373 (1914).

17. Kinzer, G. D., and Gunn, R., "The Evaporation, Temperature and Thermal Relaxation-Time of Freely-Falling Waterdrops." Journal of Meteorology, 8, 71 (1951).

18. Kobayasi, K., "The Evaporation Velocity of Single Droplets of Liquids." The Engineer's Digest, 15, 463 (1954).

19. Kobayasi, K., "The Combustion of Single Droplets of Fuel." The Engineer's Digest, 16, 17 (1955).

20. Langmuir, I., "The Evaporation of Small Spheres." Phys. Rev. 2, 12, 368 (1918).

21. Langstroth, G. O., et al., "The Evaporation of Droplets in Still Air." Canadian Journal of Research, A 28, 580 (1950).

22. Maisel, D. S., and Sherwood, T. K., "Evaporation of Liquids into Turbulent Gas Streams." Chem. Eng. Prog., 46, 131 (1950).

23. Maxwell, J. B., Data Book on Hydrocarbons, New York: D. Van Nostrand Co., Inc., 1950.

24. Maxwell, J. C., "Diffusion," Scientific Papers, Vol. II, Cambridge University Press, 1890.

25. McAdams, W. H., Heat Transmission. 2nd Edition, New York: McGraw-Hill Book Company., Inc., 1942.

26. Ranz, W. E., and Marshall, W. R., "Evaporation from Drops, Part I," Chem. Eng. Prog., 48, 141 (1952); Part II, ibid., p. 173.

27. Rossini, F. D., Selected Values of Physical and Thermodynamic Properties of Hydrocarbons and Related Compounds. Pittsburgh: Carnegie Press, 1953.

28. Saad, M. A., "Evaporation and Combustion of Single Fuel Droplets in a Hot Atmosphere," Ph.D. Dissertation, Mech. and Ind. Eng. Dept., Univ. of Mich., 1956.

29. Simpson, H. C., "Combustion of Droplets of Heavy Liquid Fuels," Sc.D. Dissertation, Chem. Eng. Dept., M.I.T., 1954.

30. Spalding, D. B., "Combustion of Liquid Fuel in a Gas Stream, Part I" Fuel, 29, 2 (1950); Part II, ibid., p. 25.

31. Spalding, D. B., "The Combustion of Liquid Fuels" Fourth International Symposium on Combustion, Baltimore: Williams and Wilkins, 1953.

32. Topps, J.E.C., An Experimental Study of the Evaporation and Combustion of Falling Droplets. NGTE (England), Memorandum M105 (1951).